2002

Interdiffusion phenomena at partially miscible polymer interfaces

Erin Lynne Jablonski
Iowa State University

INFORMATION TO USERS

This manuscript has been reproduced from the microfilm master. UMI films the text directly from the original or copy submitted. Thus, some thesis and dissertation copies are in typewriter face, while others may be from any type of computer printer.

The quality of this reproduction is dependent upon the quality of the copy submitted. Broken or indistinct print, colored or poor quality illustrations and photographs, print bleedthrough, substandard margins, and improper alignment can adversely affect reproduction.

In the unlikely event that the author did not send UMI a complete manuscript and there are missing pages, these will be noted. Also, if unauthorized copyright material had to be removed, a note will indicate the deletion.

Oversize materials (e.g., maps, drawings, charts) are reproduced by sectioning the original, beginning at the upper left-hand corner and continuing from left to right in equal sections with small overlaps.

ProQuest Information and Learning
300 North Zeeb Road, Ann Arbor, MI 48106-1346 USA
800-521-0600

Interdiffusion phenomena at partially miscible polymer interfaces

by

Erin Lynne Jablonski

A dissertation submitted to the graduate faculty
in partial fulfillment of the requirements for the degree of
DOCTOR OF PHILOSOPHY

Major: Chemical Engineering

Program of Study Committee:
Balaji Narasimhan, Major Professor
Ashraf Bastawros
Vikram Dalal
Surya Mallapragada
Richard Seagrave

Iowa State University
Ames, Iowa
2002

ProQuest Information and Learning Company
300 North Zeeb Road
P.O. Box 1346
Ann Arbor, MI 48106-1346

Graduate College

Iowa State University

This is to certify that the doctoral dissertation of

Erin Lynne Jablonski

has met the dissertation requirements of Iowa State University

Signature was redacted for privacy.

Major Professor

Signature was redacted for privacy.

For the Major Program

TABLE OF CONTENTS

LIST OF FIGURES

LIST OF TABLES

LIST OF SYMBOLS AND NOMENCLATURE

a	statistical segment length of a monomer
AFM	atomic force microscopy
D_M	mutual diffusion coefficient
D^*_{PS}	tracer-diffusion coefficient of polystyrene
D^*_{PBS}	tracer-diffusion coefficient of poly(styrene-*r*-bromo-styrene)
f	volume fraction of brominated units in PBS copolymer
G_C	fracture energy
M_n	number average molecular weight
M_w	weight average molecular weight
N	degree of polymerization
PBS	statistically random copolymer, poly(styrene-*r*-4-bromo-styrene)
PDI	polydispersity index
PS	polystyrene
RBS	Rutherford backscattering spectroscopy
R_g	radius of gyration
SAXS	small angle x-ray scattering
t	time
T	temperature
T_g	glass transition temperature
t_r	reptation time
UCST	upper critical solution temperature
w_I	interfacial width
$w_{I,\infty}$	equilibrium interfacial width
x	mole fraction of brominated units in PBS copolymer
XR	X-ray reflectivity
q	scattering vector
z	spatial position
β	absorption
δ	dispersion
ρ_e	electron density
ρ_{abs}	absorption coefficient
σ	roughness
χ	Flory-Huggins interaction parameter
χ_S	interaction parameter at spinodal
$\chi_{S\text{-}BrS}$	PS-PBS monomer-monomer interaction parameter
ϕ	volume fraction of PBS

ACKNOWLEDGEMENTS

I am very grateful to my major professor, Balaji Narasimhan, for providing guidance, carefully critiquing my work, being patient with my sporadic work habits, allowing me freedom with this project, and for not giving up on me when things didn't go as well as planned. Balaji deserves enormous appreciation for all his efforts to move this project forward and for convincing me to continue with it for my doctoral dissertation.

Dr. Russell Gorga provided the complementary work for this dissertation. I feel very fortunate to have had the opportunity to work with Russell for the duration of this project.

Throughout this project many people have assisted in different aspects of the experimentation. Dr. Robert Pfeffer assisted with much of the RBS work as well as provided advice throughout the beginning of the project. I feel immense gratitude to have worked with such an expert; he remains a dear friend and has always offered me a unique perspective on life. At Argonne National Laboratory I have had the pleasure of working with Douglas Robinson, Didier Wermeille, Jin Wang, and Andrew Richter for the XR studies, all of whom have been extremely helpful and knowledgeable. I have had two undergraduates work with me on this project. Carmen Fornarotto made simplifying modifications to synthesis and bilayer preparation that were greatly appreciated. Melissa Gregory followed and took the initiative to prepare better surfaces and bilayers and was always fun to work with. Melissa helped Russell and I in all aspects of experimental work and really deserves our gratitude; she has become a great friend as well. Wolf-Hartmut Schulte and Chris Wetteland also assisted with the RBS studies.

For his contribution to my experience at Iowa State, I must thank Dr. Charles Glatz. He has been a true academic mentor and I am grateful for all of our insightful discussions. I am also appreciative of the career mentoring provided by Dr. Theodore Madey at Rutgers, who, among other things, advised me to take a postdoctoral research position at NIST. I would also like to thank my committee members for taking the time to review my work.

I want to thank the people I've met in graduate school, both at Rutgers and ISU, who have become close friends: Omar convinced me there was a light at the end of the tunnel; Brandon pointed out the humor in things, and Jen helped abate the stress by taking me to yoga and being a good listener. Thank you to all the members of Balaji's and Surya's groups, especially Matt, Amy, and Mike, and to everyone that has made this a fun and memorable experience.

The National Science Foundation provided financial support for this project and myself (graduate fellowship and grant #: CTS-9984022). This work was also supported by Union Carbide Corporation and Rutgers University Research Council. This material is based upon work supported under a National Science Foundation Graduate Fellowship.

ABSTRACT

This research is focused on understanding the effect of miscibility on interdiffusion phenomena in bilayers of polystyrene (PS) and the statistically random copolymer, poly (styrene-*r*-4-bromostyrene) (PBS). Miscibility in such systems can be quantified by $N^{\bullet}\chi$, where $N^{\bullet}$ is an effective degree of polymerization and χ the Flory-Huggins interaction parameter. In the PS/PBS system, miscibility decreases as $N^{\bullet}\chi$ increases; specifically, systems having $N^{\bullet}\chi > 2$ (but less than some limiting value) are considered partially miscible, while those with $N^{\bullet}\chi < 2$ are miscible. The extent of interdiffusion of the two components at a bilayer interface is ultimately determined by the miscibility of the system, which controls interfacial width and fracture strength. A description of the effect of miscibility on interdiffusion phenomena, interfacial width, phase behavior, and fracture energy and a relationship between these properties has not been elucidated, thus limiting optimal design of polymer interfaces for technologically relevant applications. This work highlights the effect of miscibility on interdiffusion dynamics and interfacial behavior, employing both experimental and modeling tools.

Rutherford backscattering spectroscopy (RBS) was used to quantify interdiffusion in the PS/PBS bilayers. PBS volume fraction versus depth profiles were obtained from the evolution of the bromine peak in the RBS spectra of these bilayers as a function of annealing time. From these profiles, mutual diffusion coefficients were calculated. The results indicate that the extent of interdiffusion increases with temperature (T) and decreases with increasing volume fraction of brominated units in the PBS copolymer (f) and increasing $N^{\bullet}$. In miscible PS/PBS systems, interdiffusion of the bilayers results in a single layer of constant composition. In bilayers with PS and PBS having a disparity in N, the interface is observed

to move toward the faster diffusing (lower N) component, in agreement with the fast-mode theory of mobility. In partially miscible PS/PBS layers, interdiffusion is observed to occur until binodal conditions that agree with predicted phase diagrams are reached, thus showing that miscibility effects limit the extent of interdiffusion and determine the equilibrium compositions of the bilayers. Also in partially miscible bilayers, it is shown that the square-gradient modification to the diffusion equation derived from the Flory-Huggins expression for free energy accurately describes the concentration versus depth profiles.

Interfacial widths (w_i) in PS/PBS bilayers were measured with X-ray reflectivity (XR) and are in qualitative agreement with the results of RBS, providing further insight into the interfacial concentration profile. It was observed in miscible systems that features corresponding to a bilayer configuration disappeared after short diffusion times, indicating complete interdiffusion, while partially miscible and immiscible systems retained bilayers features for even the longest annealing times, indicating interdiffusion to binodal conditions or minimal interdiffusion, respectively. Little interpenetration was observed in immiscible systems ($N^{*}\chi >> 2$, $w_i \sim 10$Å), while interfaces were much broader near binodal conditions ($N^{*}\chi \sim 2$, $w_i > 100$Å). Implications of the miscibility dependence of the mutual diffusion coefficient and interfacial width are discussed both in the context of theoretical arguments as well as for strengthening partially miscible polymer interfaces.

CHAPTER 1

INTRODUCTION

Interdiffusion and the morphology of polymer-polymer interfaces control the structure and properties of a wide range of sophisticated materials through their effect on interphase bonding (microscopically) and fracture energy (macroscopically). Therefore, knowledge of the parameters controlling interdiffusion, interfacial width, and composition at polymer interfaces is a necessary step in the optimal design of polymer composites, electronic devices, high performance nano-composites, and co-extruded and injection-molded products [1-5]. Many polymer/polymer interfaces are partially miscible, i.e., they have an interaction parameter χ approaching the spinodal interaction parameter, χ_s, where phase separation occurs; the resulting adhesion in these systems can be severely limited [6]. Hence, multiphase polymeric materials tailored to possess properties of strength, elasticity, and adhesion are considerably affected by their interfacial characteristics. A detailed understanding of interfacial molecular phenomena and of the parametric dependence of the driving force for interdiffusion in partially miscible polymer systems can have significant impact on the design of the materials mentioned above.

A polymer composite is a multiphase material composed of at least two polymers working together to produce composite properties that are different from the properties of the constituent polymers; polymers can be blended such that the advantageous properties of one polymer will compensate for the deficient properties of the other [7, 8]. Polymer blend materials are cost-effective and can be tailored to particular applications [9]. Desirable mechanical properties, such as high fracture toughness, can be achieved in multiphase

materials with sufficient interdiffusion across the phase boundaries [10]. Thus, making these interfaces compatible has become a focus of intense research. For example, it is common to use block copolymers to reinforce interfaces [11]. As shown in Fig. 1.1, these block copolymers can be used to bridge interfaces between two distinctly different polymers. In the same way, triblock copolymers can be used to reinforce an interface by forming 'hairpins'. Random copolymers can be used to strengthen interfaces by promoting adhesion between phases, and as surfactants they stabilize microstructure [11].

It is also possible to tailor the macroscopic surface properties of a polymer through manipulation of the underlying microscopic structure and chemistry. In some applications there is a desire for good adhesion and strong interactions between substrate and polymer; for other applications it is desirable to produce a surface that is relatively inert and not easily wetted by another material [12]. Preferential segregation due to surface free energy effects becomes an important design parameter for many polymeric materials; the surface composition of a polymer is often very different from that of the bulk due to these effects, making polymers well suited to such surface-active applications as adhesives, lubricants, stabilizers, and coatings [13]. In copolymers, the surface composition and the resulting macroscopic properties can be manipulated through the chemical nature of the homopolymers and molecular architecture of the copolymer chain.

The interfacial and surface properties of polymers are extremely important in the design of materials for biological applications. For example, polymer overlayers are used as protective coatings and to control the wettability and biocompatibility of these materials [14]. Bioadhesion, the interfacial interaction between a biological substrate and a synthetic

polymer [5], is important for applications such as immobilizing a polymer carrier for targeted drug delivery.

In co-extrusion and injection molding applications, the time allowed for interdiffusion is very short, typically on the order of minutes. In such processes, this time limit can result in inadequate bonding between materials, later leading to failure [14]. In melt processing operations, i.e., extrusion and film blowing, the quality of the products is a strong function of surface-related dynamical phenomena, such as melt fracture [14]. In lamination of composites, the polymer layers are annealed near the glass transition temperature of both components to improve their interfacial adhesion. The time and temperature allowed for this process directly affect the adhesive strength via the interfacial width achieved at the interface [6].

For the case of resists, encapsulants, and dielectrics found in the field of microelectronics, the ability to relate the interfacial properties to the chemical composition would facilitate an advance in design of these components [14].

In summary, tailoring adhesive properties at polymer interfaces is possible through molecular design. Specifically, the controlling mechanism of interdiffusion may change with varying conditions. Due to the immiscibility in most polymer blends, the characteristics of the 'interphase' of the components determine the properties of the material. In a partially miscible multiphase system composed of both homopolymers and copolymers, there will be preferential segregation of copolymers in order to minimize free energy, which leads to macroscopic surface and interface properties dictated by underlying microstructure and chemistry. Surface segregation and interpenetration between phases affects the mechanical properties of these interfaces. Thus, the motivation for this work is that meaningful

relationships need to be established between molecular properties (interdiffusion mechanism(s), interfacial width, interaction parameter, phase behavior, and blend morphology) and macroscopic properties (interfacial fracture energy).

References:

1. de Gennes, P.G., *Mechanical Properties of Polymer Interfaces*, in *Physics of Polymer Surfaces and Interfaces*, I.C. Sanchez, Editor. 1992, Butterworth Heinemann: Stoneham. p. 55-71.
2. Zhuang, H. and J.A. Gardella, *Spectroscopic Characterization of Polymer Surfaces.* MRS Bulletin, 1996. **January**: p. 43-48.
3. Jabbari, E. and N.A. Peppas, *A Model for Interdiffusion at Interfaces of Polymers with Dissimilar Physical Properties.* Polymer, 1995. **36**(3): p. 575-586.
4. Agrawal, G., et al., *Interdiffusion of Polymers Across Interfaces.* J. Polymer Science: Part B: Polymer Physics, 1996. **34**: p. 2919-2940.
5. Jabbari, E. and N.A. Peppas, *Polymer-polymer Interdiffusion and Adhesion.* J. M. S. - Rev. Macromol. Chem. Phys., 1994. **C34**(2): p. 205-241.
6. Jabbari, E. and N.A. Peppas, *Molecular Weight and Polydispersity Effects on Interdiffusion at the Interface Between Polystyrene and Poly(vinyl methyl ether).* J. Materials Science, 1994. **29**: p. 3969-3978.
7. Genzer, J. and R.J. Composto, *Effect of Molecular Weight on the Interfacial Excess, Tension, and Width in a Homopolymer/Binary Polymer Blend System.* Macromolecules, 1998. **31**: p. 870-878.

8. Lee, S.M.E., *International Encyclopedia of Composites*. Vol. 1. 1990, New York: VCH Publ. vii.

9. Yeung, C. and A.-C. Shi, *Formation of Interfaces in Incompatible Polymer Blends: A Dynamical Mean Field Study*. Macromolecules, 1999. **32**: p. 3637-3642.

10. Faldi, A., J. Genzer, and R.J. Composto, *Segregation at the Interface between a Homopolymer and a Binary Polymer Blend*. Physical Review Letters, 1995. **74**(17): p. 3388-3391.

11. Kulasekere, R., et al., *Homopolymer Interfaces Reinforced with Random Copolymers*. Macromolecules, 1996. **29**: p. 5493-5496.

12. Koberstein, J.T., *Surface and Interface Modification of Polymers*. MRS Bulletin, 1996. **January**: p. 19-23.

13. Scheutjens, J.M.H.M., *Mean-Field Lattice Models of Polymers Interfaces*, in *Physics of Polymer Surfaces and Interfaces*, I.C. Sanchez, Editor. 1992, Butterworth Heinemann: Stoneham. p. 117-137.

14. Theodorou, D.N., *Molecular Modeling of Polymer Surfaces and Polymer/Solid Interfaces*, in *Physics of Polymer Surfaces and Interfaces*, I.C. Sanchez, Editor. 1992, Butterworth Heinemann: Stoneham. p. 138-161.

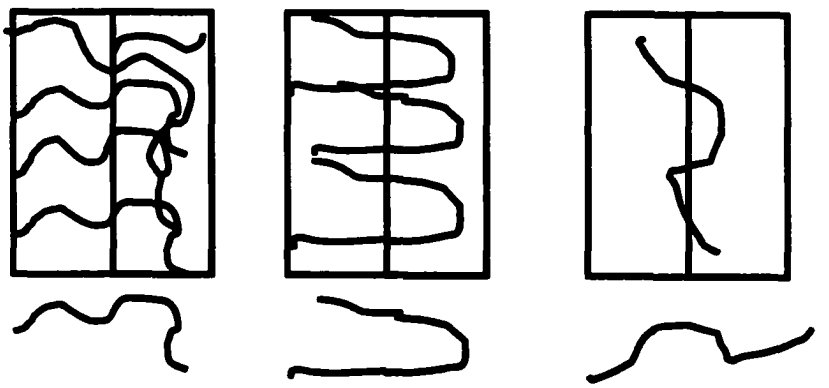

Figure 1.1: Using copolymers to reinforce interfaces between incompatible or partially miscible polymers. a) block copolymer; b) triblock copolymer; c) random copolymer

CHAPTER 2

BACKGROUND AND LITERATURE REVIEW

2.1 Introduction

This chapter provides a review of relevant research on the effect of miscibility on interdiffusion phenomena in polymer systems (Section 2.2), the prevalent theories of polymer-polymer interdiffusion (Section 2.3), a description of the analytical tools employed for such research (Section 2.4), and the relationship between microscopic properties and macroscopic behavior (Section 2.5). A summary concludes this chapter.

2.2 Prevalent theories of polymer-polymer interdiffusion

Diffusion and wetting theories are the most important theories of adhesion at polymer-polymer interfaces [1]. When sufficiently miscible polymers are brought into contact at an interface and subsequently welded above their glass transition temperature, interdiffusion commences and an 'interphase' is formed, as shown in Fig. 2.1.

Partially miscible interfaces have an interaction parameter, χ, close to the spinodal interaction parameter, χ_S, above which phase separation occurs. Most polymers are immiscible due to chain-length independent enthalpy being overcome by decreased entropy of mixing resulting from long chains [2]. Interdiffusion at partially miscible polymer interfaces depends on a number of parameters including, but not limited to: temperature, composition of the interface, molecular weight, polydispersity, chain orientation, and molecular structure of the polymers, including volume fraction of monomer in a copolymer, should a copolymer be one of the interfacing materials. Interfacial width, a measure of the

thickness of the interphase, is on the order of microns for miscible polymer bilayers, but only Angstroms in the immiscible limit [3]. It has been shown that measurement of the interfacial width is a means to directly obtain the interaction parameter, χ, in polymer blends [4]. The dynamics of chains at interfaces includes, with respect to time, short-range Fickian diffusion of monomers, Rouse relaxation of entanglements followed by Rouse relaxation of the whole chain, reptation, and long-range Fickian diffusion [5].

2.2.1 Rouse Theory

Rouse theory can be used to describe the limiting case of short polymer chains at short diffusion times. The main assumptions of Rouse theory are ideal chain elasticity, i.e., polymer chains can be modeled as beads of inertia attached by springs, that a physical chain undergoing Rouse motion cannot cross itself, and locality of response, where a bead only experiences forces exerted by its two nearest neighbors. Each bead is considered a point source of friction and the forces between them purely elastic [6]. The Rouse model of interdiffusion allows chains to move in three dimensions [1].

2.2.2 Reptation Theory

Currently, the most widely accepted theory of interdiffusion is reptation [7]. The reptation theory treats each polymer chain as if it were confined to move within a fixed tube defined by interactions and entanglements with other polymer chains in the melt. It is assumed that the movement of the whole chain proceeds only by movement of the chain ends [8]. The polymer chain moves within this tube due to thermal fluctuations. The time it takes a chain to completely diffuse out of its original tube is defined as the reptation time, t_r [6]. The reptation time is proportional to the cube of the molecular weight of the polymer chain,

M^3 [1]. Many efforts have expressed the interface structure in terms of underlying molecular properties based on reptation. Other theories that contribute to present understanding include the Rouse model and minor chain reptation. Portions of a reptating polymer chain that have lost memory of their initial conformation are minor chains. These minor chains, which are leaving the initial tube, lengthen over time, leading to reptation [5]. Felcher and co-workers have shown that for low molecular weight PS, reptation could not control the transport, because the Rouse width and the reptation length are similar. They also show that for high molecular weight PS there is a decreasing "concentration gap" [9] as the reptation time is approached, indicating the presence of reptation. The formation of a 'concentration gap' at the interface results from the prediction that only chains with their ends near the interface will be able to cross the interface [9]. More recently, Lin et al. used neutron reflectivity to study PMMA/d-PMMA interfaces and observed a reduction in the interdiffusion coefficient (D) near the interface as opposed to a bulk value away from the interface[10]. They show that the bulk D is consistent with reptation while careful observation of D near the interface reveals that it is not consistent with reptation. Since segmental interactions exist between protonated and deuterated monomers [11, 12], it appears that in partially miscible systems, miscibility significantly alters chain dynamics, resulting in a miscibility-controlled interdiffusion mechanism.

2.2.3 Fast mode v. slow mode theories of interdiffusion

The mutual diffusion across the interface between two polymeric species can be described as a product of a kinetic term involving the intrinsic (i.e., tracer) diffusion coefficients of the species, the degrees of polymerization of the species and their

composition, and a thermodynamic term that represents the driving force for mixing. The kinetic term has been modeled using appropriate definitions of the segmental fluxes of the species across the interface, leading to the so-called "fast mode" and "slow mode" theories. The thermodynamic term is given by $2\,\phi\,(1-\phi)\,(\chi_S - \chi)$ [1], where ϕ is the volume fraction of one of the polymers, χ is the interaction parameter, and χ_S is the interaction parameter at the spinodal, given by $\chi_S = \frac{1}{2}\left(\frac{1}{N_A\phi_A} + \frac{1}{N_B\phi_B}\right)$.

The fast and slow mode theories of interdiffusion were independently developed in an effort to elucidate the molecular weight dependence of the interdiffusion coefficient, specifically the mechanism of interdiffusion when the polymers have very different mobility. Brochard-Wyart and co-workers [13] derived the slow-mode theory for interdiffusion using the chemical potential as the driving force for interdiffusion (based on previous work by de Gennes in 1981 [14]) and assuming equal but opposite fluxes of the interdiffusing components. The slow-mode theory predicts the interdiffusion coefficient, D, to be:

$$D = \left(\frac{\Lambda_A\Lambda_B}{\Lambda_A + \Lambda_B}\right)\left(\frac{1}{N_A\phi_A} + \frac{1}{N_B\phi_B} + 2\chi\right) \tag{2.1}$$

where Λ_A and Λ_B are the polymer mobility of species A and B, N_A and N_B are the respective degrees of polymerization, ϕ_A and ϕ_B are the volume fractions, and χ the Flory-Huggins interaction parameter. The slow mode theory predicts that interdiffusion is dominated by the slower diffusing species [15]. The mobility of each species can be directly related to their tracer diffusion coefficients. The assumption of equal but opposite fluxes of the diffusing species is a limitation of this theory, resulting in symmetric interdiffusion for symmetric

boundary conditions [15]. The assumption of composition-independent monomer-monomer friction coefficients is another limitation of this approach [13].

The fast mode theory, developed by Kramer and co-workers [16], showed that as interdiffusion proceeds, the interface in an N-asymmetric system moves toward the lower molecular weight polymer. N-symmetric bilayers have polymers of the same degree of polymerization, N, on both sides of the interface; N-asymmetric bilayers have polymers of different N on either side of the interface. Assuming that unequal fluxes of species A and B are balanced by a net flux of vacancies across the interface, Kramer and co-workers described interdiffusion for the case of a moving interface. The fast mode theory expression for the interdiffusion coefficient, D, is given by:

$$D = \phi_A \phi_B \left(\frac{\phi_B}{\phi_A} \Lambda_A + \frac{\phi_A}{\phi_B} \Lambda_B \right) \left(\frac{1}{\phi_A N_A} + \frac{1}{\phi_B N_B} + 2\chi \right) \tag{2.2}$$

with the terms in the expression given above. The form of this equation leads to an interdiffusion coefficient dominated by the faster moving component.

As the flux of vacancies is a strong factor in the fast mode theory, and slow mode theory ignores the flux of such vacancies (essentially assuming there are few, slow moving vacancies), it has been concluded that the fast and slow mode theories describe interdiffusion above and below the glass transition temperature. Most research, both experimental and computational, supports the fast mode theory [15-20]. It is instructive to note that the form of the thermodynamic component of the interdiffusion coefficient is common to both theories.

2.3 The effect of miscibility on interdiffusion phenomena in polymer systems

Polymer interfaces have been studied extensively by models and experiments that relate structure to strength. The evolution of the interface when two polymers are brought into contact above T_g has been studied by Wool [5], Voyutskii [21], Krausch [22, 23], Kramer [24], Peppas [3, 25], and Stamm [2, 26]. Much work has been done on the partially miscible system of PS/PBS and will be discussed here for its relevance to this work. Bruder and Brenn [18] have investigated interdiffusion at d-PS/PBS interfaces in the two phase region of the phase diagram using FRES and found that the equilibrium composition of the interface represented the binodal concentrations for that system. Strobl used small angle x-ray scattering to measure the interaction parameter, χ, of the PS/PBS system [27] and observed a weak composition dependence.

Stamm and co-workers [2] have used deuterated polystyrene, d-PS, and PBS for interfacial width studies (using neutron reflectivity) and PS/PBS for fracture studies and showed the presence of various regimes in which the interfacial width was correlated to the fracture energy [28]. The quantitative relationship obtained by Stamm is limited since d-PS/PS has a small, but positive χ. In order to vary the miscibility in their system, PBS copolymers with varying degrees of bromination were used. Kambour and co-workers also studied phase behavior in d-PS/PBS films [29, 30]. Rafailovich and co-workers have used both NR and XRR to measure interface formation in the d-PS/PBS system [31] to establish agreement between the methods.

Krausch and co-workers have used symmetric blends (ϕ = 0.05) of PS/PBS to investigate surface directed spinodal decomposition [22]. They compared behavior in blends to that of multilayered samples at near-binodal compositions. Results of their work show

evidence of preferential segregation of the lower surface tension component to the film surface to form a 'wetting layer'[23]. The surface composition of a polymer, copolymer, or blend is determined by interfacial or surface tension[32]. The surface segregation phenomenon alluded to in the Introduction section is a result of lower energy constituents moving to the surface to lower the overall surface free energy [32] and can be used to induce ordering in polymer films [23].

Jabbari and Peppas used ATR-FTIR to elucidate time dependence, molecular weight, and polydispersity effects in a polystyrene/poly(vinyl methyl ether) system. They have shown that the faster diffusing species swells the slower diffusing species for polymer interfaces with dissimilar properties, both above and below the glass transition of the slower diffusing component [25]. Their results agree with a time dependent interdiffusion mechanism, as well as a strong dependence on molecular weight. Further research in this group determined that in the immiscible limit, the extent of interdiffusion is limited by miscibility effects, regardless of the respective mobilities of the polymers [3].

The classical Cahn-Hilliard square-gradient theory of the interface between two partially miscible polymers is based on the equation for free energy of polymer blends described by the Flory Huggins lattice gas model for binary solutions [33] and modified by the Cahn-Hilliard constant to incorporate effects of large-scale concentration fluctuations across the interface [34]. The equation is dominated by entropic effects arising from the connectivity of polymer chains, but becomes inadequate for very immiscible systems, i.e., in the limit of strongly segregating polymer chains. Also, it has been noted that interfacial widths calculated on the basis of square gradient theory are significantly lower than experimentally measured values, indicating that there are additional influences present that

the theory does not account for [35]. The diffusion equation derived from this approach is given by (see Appendix 2 for complete derivation):

$$\frac{\partial\phi}{\partial t}=\frac{\partial}{\partial z}\left(\begin{array}{l}\dfrac{\phi(1-\phi)N_A D_A}{N_B}+(1-\phi)^2 D_B+\phi^2 D_A+\dfrac{\phi(1-\phi)N_B D_B}{N_A}- \\ 2\chi\phi^2(1-\phi)N_A D_A-2\chi\phi(1-\phi)^2 N_B D_B\end{array}\right)\frac{\partial\phi}{\partial z}- \\ \frac{b^2\phi N_A D_A}{18}\left(\frac{\partial^3\phi}{\partial z^3}\right)-\frac{b^2(1-\phi)N_B D_B}{18}\left(\frac{\partial^3\phi}{\partial z^3}\right)+ \\ \frac{b^2 N_A D_A\left(\phi(1-\phi)+(1-2\phi)^2\right)}{18\phi(1-\phi)^2}\left(\frac{\partial\phi}{\partial z}\right)^3+\frac{b^2 N_B D_B\left(\phi(1-\phi)+(1-2\phi)^2\right)}{18\phi^2(1-\phi)}\left(\frac{\partial\phi}{\partial z}\right)^3 \tag{2.3}$$

where ϕ = volume fraction of polymer i, z = spatial position, t = time, N_i = degree of polymerization of species i, D_i = tracer-diffusion coefficient of species i. The self-consistent field method provides a way to track the polymer configurations in the systems described in the previous section [34]. The premise of the self-consistent theory is to model the interactions of polymer chains as analogous to the interactions of electrons, i.e., the influence of surrounding chains on any particular chain in the system is treated as a potential. The diffusion equation in this situation takes on a form equivalent to Schrodinger's equation for free electrons.

Many researchers have used computer simulations to model the complex behavior of polymer chains in the melt. Wang and Shi [36] have modeled interdiffusion in partially miscible polymer systems using a Flory-Huggins approach and reported the effect of miscibility on both the extent of interdiffusion and the interfacial width achieved in the system. Their predictions agree qualitatively with experimental data. Yeung and Shi [37] used a dynamical mean field approach to model the interdiffusion in an incompatible system and obtained results also in qualitative agreement with experiment.

Jabbari and Peppas developed a model to describe interdiffusion at interfaces of polymers with dissimilar physical properties [15]. Their model system comprised one fast moving component (high mobility) and one slow moving component (low mobility). They neglect the effect of vacancies in their system by assuming that they make up only a small fraction of the overall concentration and therefore do not substantially affect the free energy of mixing. A chemical potential gradient exists across an interface for polymers with different chemical structure and molecular weight. As in square-gradient theory, the chemical potential gradient is assumed to be the driving force for interdiffusion and only one-dimensional flux perpendicular to the interface is allowed. Using the Flory-Huggins equation to relate chemical potential to the entropy and enthalpy of mixing of the two polymers, and by estimating values of the Onsager and friction coefficients and the blend zero-shear viscosity, they propose the following [15]:

$$D = \left(\frac{RTN_b^e}{f_b^m} \right) \left(\frac{1-\phi_S}{N_S} + \frac{\phi_S}{N_f} \right) \left(\frac{1-\phi_S}{N_S} + \frac{\phi_S}{N_f} + 2N\chi_{Sf}\phi_S(1-\phi_S) \right) \tag{2.4}$$

where R is the gas constant, T, temperature, N_b^e is the average number of repeat units between entanglements for the blend, f_b^m is the blend molar monomeric friction coefficient, f_S is the volume fraction of the slower moving component, N_S, N_f are the degrees of polymerization of the slower and faster components, respectively. From comparisons of model to data for PS/PVME (poly(vinyl-methyl-ether)) system, they found the friction coefficients to be strongly composition dependent in systems of very dissimilar polymers [15]. They also reported highly asymmetric diffusion profiles as further evidence of swelling of the slower moving component by the faster one. Other researchers have noted that

asymmetric interdiffusion profiles will occur for strong concentration and temperature dependence of the molecular mobility [1, 36, 38].

Using Monte Carlo techniques, Wool and co-workers [6] simulated Rouse dynamics (bead-spring model) in off-lattice mode for random walks of one chain. In the same work, reptation simulations were performed for chains of length N whose chain end distribution function was constant with depth near the interface. Here, a random walk was simulated on a two dimensional lattice. The results of this work, when compared to experimental data, showed that Rouse motion can be used to predict the behavior of molecules at short times, while minor chain reptation is valid at longer times. However, computer simulation of interdiffusion raises several issues including the presence of "blocking layers" [39] in miscible systems, and the non-universality of the slow and fast mode theories [1].

2.4 Analytical tools to study polymer interdiffusion and interfacial width

Many analytical techniques are currently used to measure concentration profiles and interdiffusion coefficients, interfacial widths, and phase morphology in blends and interfaces. These include forward recoil spectroscopy (FRES, also known as elastic recoil detection, ERD); infrared (IR) microdensitometry [17], and attenuated total reflectance-Fourier transform infrared (ATR-FTIR) spectroscopy; neutron and X-ray scattering; secondary ion mass spectroscopy (SIMS); Rutherford backscattering spectroscopy (RBS); and neutron and X-ray reflectivity (NR, XRR). To be able to accurately distinguish diffusion regimes and explore interfacial chain dynamics, it is necessary to use techniques that can measure

concentrations and distances at submolecular size scales [40]. Table 2.1 shows the common analytical tools, their depth resolution, and comments on analysis.

Polymer interdiffusion at interfaces can be detected using ATR-FTIR spectroscopy to measure composition. The composition of the polymer sample is manifested through characteristic absorption bands in the spectra. An infrared beam impinges on the ATR crystal from one of the side faces. The IR beam is totally reflected at the crystal/polymer interface if the incident angle of the beam is greater than the critical angle of the crystal and the refractive index of the crystal is greater than that of PS. The IR beam travels inside the crystal and leaves from the side face. A fraction of the beam penetrates the polymer layer and is absorbed due to diffraction at the crystal/polymer interface. The absorption bands in the spectrum arise from this amount of absorbed beam [25]. Composition v. depth information is gained from the exponential relation between the relative intensity of IR radiation and distance away from the crystal surface (penetration depth). Peppas and co-workers used ATR-FTIR to elucidate time dependence, molecular weight, and polydispersity effects in a PS/ poly(vinyl methyl ether) system [15, 25].

Neutron and x-ray scattering, specifically small angle neutron scattering (SANS), are among the most sensitive techniques available to study interdiffusion; spatial resolution is of the order of 1nm. In neutron techniques, contrast is based on difference in scattering length density of the materials. In x-ray techniques, the contrast is provided by electron density difference in the materials. An advantage the use of neutrons in polymer studies is that the greatest contrast (and arguably the least thermodynamic perturbation) can be achieved by deuteration [40]. Bates and Wignall have shown that an upper critical solution temperature

exists for homopolymers and their deuterated counterparts [11]. Results from Green and Doyle support this and discuss a 'thermodynamic slowing down' of the interdiffusion coefficient at a critical volume fraction of deuterated polymer [12]. Incompatibility in the hydrogenated/deuterated systems is due to the reduction in average bond length when hydrogen is replaced by deuterium [9, 10].

Ion beam techniques such as RBS, SIMS, and FRES have the advantage of allowing direct, unambiguous measurement of interphase composition profiles [38]. The energy of the ion beams in these analytical techniques are typically 1-5MeV [41].

RBS detects elemental nuclei, preferentially heavier nuclei due to scattering cross section. Highly energetic collimated beams of ^{4}He particles provided by an accelerator impinge on the sample and are scattered backwards into a detector-analysis setup (semiconductor nuclear particle detector) that measures the energies of the particles. The particle energy is a signature of the target nuclear mass that it collides with as well as the depth of that nucleus. Because collisions are elastic, they are governed by Coulomb repulsions and are independent of chemical bonding, thus rendering the technique quantitative.

The ratio of the energy of the backscattered beam to that of the incident beam is the kinematic factor and provides a means of identifying the atomic masses of the nuclei in the sample. The energy of the backscattered spectrum also depends on the depth of the target nucleus, and hence the energy scale in the RBS spectrum can be converted to a depth profile. Composto and Kramer have provided a discussion of RBS analysis [42] of polymer bilayers.

RBS is an excellent candidate for diffusion studies near interfaces; depth resolution is on the order of 50Å at the surface.

Kramer and co-workers have successfully used RBS to obtain concentration v. depth profiles in polymer systems. They studied 'marker molecule' diffusion at polymer interfaces [16, 24] and interdiffusion in preferentially stained polymer bilayers. A limit to the method of preferential staining is that it cannot be used for interfaces in which chemically similar polymers are present on either side of the interface.

In SIMS, momentum transfer from the impinging ion beam to the sample surface causes ejection of charged atoms and molecules from the sample [43]. The primary ion range is the average distance a primary ion penetrates into the sample. Target atoms, which have enough kinetic energy to overcome the surface potential within a certain escape depth, smaller than the primary ion range, are ejected from the sample. Some of the ejected species form secondary ions, which are detected by a mass spectrometer. SIMS can be operated in several modes. The static (s-SIMS) mode is used to probe just the first 10nm of surface. The dynamic (d-SIMS) mode gives concentration v. depth information by sputtering into the sample, creating a crater as the molecular fragments are ejected. Time of flight, TOF-SIMS, analysis makes it possible to detect high mass ions [44].

The principle of FRES is similar to that of RBS [41]. A $^{4}He^{++}$beam is incident on a sample position at a 15° angle. The beam is scattered forward to a detector identical to the one used in RBS, which is at a 30° angle to the incident beam. An absorbing foil usually precedes the FRES detector in order to reduce the background caused by the forward scattered ions impinging directly on the detector. The detector reports the energies of

hydrogen and deuterium ions that recoil from the surface of the sample and pass through the absorber foil. FRES can be used to measure interdiffusion coefficients in systems of deuterated and protonated polymers [41]. TOF-FRES has been used to analyze lateral ordering as a result of phase separation in the polystyrene/poly(styrene-*r*-4-bromo-styrene) (PS/PBS) system to be discussed in the next section [22].

NR and XR are typically used to measure interfacial widths in polymer bilayers[4, 8]. These techniques are extremely sensitive to surface and interfacial roughness[35], which cause damping of reflectivity data and thus limit resolution. Also, data analysis can become ambiguous if the multi-layer sample is not well defined, i.e., the scattering length or electron density profile used to fit the data may not be unique [35]. NR receives more attention in polymer applications due to the relative ease of using deuterated samples as compared to the heavy element labeling necessary to achieve sufficient electron density contrast for analysis using XR. In a reflectivity experiment, a well-collimated beam (of neutrons or x-rays) is incident on a sample surface at a glancing angle. The detector records the energy (wavelength) of the beam leaving the sample, and features in the reflectivity correspond to depths in the sample [9].

X-ray photoelectron spectroscopy (XPS) has become a preferred method of surface analysis because quantitative determination of elemental and functional group concentrations at the surface is possible, in addition to qualitative information gained from chemical shifts in the spectra which allow the surface functionality of a polymer to be identified [44]. XPS complements the other techniques mentioned here due to its small penetration depth and resolution.

2.5 Relating microscopic properties to macroscopic behavior

As mentioned previously, there has been some work, notably by Stamm and co-workers, to relate the interfacial width at a polymer interface to the fracture energy measured in a similar system [2, 45, 46]. It was determined that for small interfacial widths (<~10nm), the fracture energy was correspondingly low until a minimum value of interfacial width is achieved, at which point the fracture energy increases steeply with interfacial width. Once an interfacial width is reached such that there is significant interpenetration of chains across the interface, the fracture energy reaches a plateau approaching the bulk fracture toughness and no further increase in fracture energy is observed with increasing values of interfacial width[46]. Other researchers have investigated the use of random copolymers to reinforce interfaces in the interest of determining the optimal composition of the copolymer to achieve maximum fracture strength [47]. It should be noted that the time it takes to reach the equilibrium value of the interfacial width is a direct result of the interdiffusion behavior in a system. Therefore, when designing partially miscible polymer interfaces and their corresponding processing conditions at the molecular level, it is necessary to know both the interdiffusion and phase behavior of the system in order to predict the interfacial width and corresponding fracture energy.

2.6 Summary

There is currently a great deal of interest in controlling interdiffusion dynamics at polymer-polymer interfaces due to the plethora of technological applications of these interfaces. The current understanding of polymer interdiffusion is based on reptation, Rouse

dynamics, and slow mode and fast mode theories. Modeling techniques make use of square-gradient theory, self-consistent field theory, and Monte Carlo simulations. Several analytical tools are available to investigate polymer surfaces, interfaces, and bulk morphology at resolutions of the order of the radius of gyration. However, very little work has been done to directly relate microscopic studies to macroscopic behavior.

2.7 References:

1. Jabbari, E. and N.A. Peppas, *Polymer-polymer Interdiffusion and Adhesion.* J. M. S. - Rev. Macromol. Chem. Phys., 1994. **C34**(2): p. 205-241.
2. Guckenbiehl, B., M. Stamm, and T. Springer, *Interface Properties of blends of incompatible polymers.* Physica B, 1994. **198**: p. 127-130.
3. Jabbari, E. and N.A. Peppas, *Comparison of Interdiffusion at Polystyrene-Poly(vinyl methyl ether) and Polystyrene-Poly(isobutyl vinyl ether) Interfaces.* Polymer International, 1995. **38**: p. 65-69.
4. Schubert, D.W. and M. Stamm, *Influence of Chain Length on the Interface Width of an Incompatible Polymer Blend.* Europhysics Letters, 1996. **35**(6): p. 419-424.
5. Wool, R.P., *Polymer Interfaces Structure and Strength.* 1995, New York: Hanser Publishers.
6. Agrawal, G., et al., *Interdiffusion of Polymers Across Interfaces.* J. Polymer Science: Part B: Polymer Physics, 1996. **34**: p. 2919-2940.
7. de Gennes, P.G., *Physics of Polymer Surfaces and Interfaces*, ed. I.C. Sanchez, Boston: Butterworth-Heinemann.

8. Kunz, K. and M. Stamm, *Initial Stages of Interdiffusion of PMMA across an Interface.* Macromolecules, 1996. **29**(7): p. 2548-2554.

9. Felcher, G.P. and A. Karim, *Interdiffusion at the Interface of Polymeric Bilayers: Evidence for Reptation?* J. Noncrystalline Solids, 1991. **131-133**: p. 703-708.

10. Lin, E.K., et al., *Reduced Polymer Mobility near the Polymer/Solid Interface as Measured by Neutron Reflectivity.* Macromolecules, 1999. **32**(11): p. 3753-3757.

11. Bates, F.S. and G.D. Wignall, *Isotope-Induced Quantum-Phase Transitions in the Liquid State.* Physical Review Letters, 1986. **57**(12): p. 1429-1432.

12. Green, P. and B.L. Doyle, *Isotope Effects on Interdiffusion in Blends of Normal and Deuterated Polymers.* Physical Review Letters, 1986. **57**(19): p. 2407-2409.

13. Brochard, F., J. Jouffroy, and P. Levinson, *Polymer-Polymer Diffusion in Melts.* Macromolecules, 1983. **16**: p. 1638-1641.

14. de Gennes, P.G., 1981.

15. Jabbari, E. and N.A. Peppas, *A Model for Interdiffusion at Interfaces of Polymers with Dissimilar Physical Properties.* Polymer, 1995. **36**(3): p. 575-586.

16. Green, P., et al., *Marker Displacement Measurements of Polymer-Polymer Interdiffusion.* Macromolecules, 1985. **18**: p. 501-507.

17. Jordan, E.A., et al., *Mutual Diffusion in Blends of Long and Short Entangled Polymer Chains.* Macromolecules, 1988. **21**: p. 235-239.

18. Bruder, F. and R. Brenn, *Measuring the Binodal by Interdiffusion in Blends of Deuterated Polystyrene and Poly (styrene-co-4-bromostyrene).* Macromolecules, 1991. **24**: p. 5552-5557.

19. Jabbari, E. and N.A. Peppas, *Use of ATR-FTIR to Study Interdiffusion in Polystyrene and Poly(vinyl methyl ether).* Macromolecules, 1993. **26**(9): p. 2175-2186.

20. Sauer, B.B. and D.J. Walsh, Macromolecules, 1991. **24**: p. 5948-.

21. Voyutskii, S.S., *Autohesion and Adhesion of High Polymers*, in *Polymer Reviews*, H.F. Mark and E.H. Immergut, Editors. 1963, Wiley-Interscience: New York.

22. Krausch, G., et al., *Order-Induced Period Doubling during Surface-Directed Spinodal Decomposition.* Europhysics Letters, 1994. **28**(5): p. 323-328.

23. Krausch, G., et al., *Self-assembly of a Homopolymer Mixture via Phase Separation.* Applied Physics Letters, 1994. **64**(20): p. 2655-2657.

24. Kramer, E.J., P. Green, and C.J. Palmstrom, *Interdiffusion and Marker Movements in Concentrated Polymer-polymer Diffusion Couples.* Polymer, 1984. **25**(4): p. 473-480.

25. Jabbari, E. and N.A. Peppas, *Molecular Weight and Polydispersity Effects on Interdiffusion at the Interface Between Polystyrene and Poly(vinyl methyl ether).* J. Materials Science, 1994. **29**: p. 3969-3978.

26. Guckenbiehl, B., M. Stamm, and T. Springer, *Interface Formation and Thin Film Properties of an Incompatible Polymer System.* Mat. Res. Soc. Symp. Proc., 1993. **280**: p. 275-280.

27. Koch, T. and G.R. Strobl, *Concentration Dependence of the Flory-Huggins Interaction Parameter of a Polymer Blend as Determined by SAXS Experiments.* J. Polymer Science: Part B: Polymer Physics, 1990. **28**: p. 343-353.

28. Huttenbach, S., et al., *The Interface between Two Strongly Incompatible Polymers: Interfacial Broadening and Roughening near Tg.* Langmuir, 1991. **7**: p. 2438-2442.

29. Kambour, R.P. and J.T. Bendler, *Miscibilities in Monodisperse Mixtures of Polystyrene, Poly(p-bromostyrene) and Their Copolymers.* Macromolecules, 1986. **19**: p. 2679-2682.

30. Strobl, G.R., et al., *Thermally Reversible Phase Separation in Polystyrene/Poly(styrene-co-4-bromostyrene) Blends.* Macromolecules, 1986. **19**: p. 2683-2689.

31. Zhao, W., et al., *Neutron and X-ray Reflectivity Measurements of Polystyrene/ Polybromostyrene (PS/PBrS) Interfaces.* Physica B, 1991. **173**: p. 43-46.

32. Koberstein, J.T., *Surface and Interface Modification of Polymers.* MRS Bulletin, 1996. **January**: p. 19-23.

33. Zeng, X.C., et al., *On Square-gradient Theories of Polymer Blend Interfaces.* J. Chem. Phys., 1992. **96(6)**: p. 4816-7.

34. Jones, R.A.L. and R.W. Richards, *Polymers at Surfaces and Interfaces.* 1999, Cambridge: Cambridge University Press.

35. Stamm, M. and D.W. Schubert, *Interfaces between Incompatible Polymers.* Annu. Rev. Mater. Sci., 1995. **25**: p. 325-356.

36. Wang, S.-Q. and Q. Shi, *Interdiffusion in Binary Polymer Mixtures.* Macromolecules, 1993. **26**: p. 1091-1096.

37. Yeung, C. and A.-C. Shi, *Formation of Interfaces in Incompatible Polymer Blends: A Dynamical Mean Field Study.* Macromolecules, 1999. **32**: p. 3637-3642.

38. Tomba, P., J. Carella, and E. Pardo, *Development of a Simple Experimental Method to Measure Interphase Composition Profiles Generated by Diffusion in Polymers.* J. Polymer Science: Part B: Polymer Physics, 1997. **35**: p. 2435-2445.

39. Olaj, O.F., T. Petrik, and G. Ziffeger, *Monte Carlo Simulations of Symmetric Blends II: Chain properties in interface regions.* J. Chem. Phys., 1998. **108**: p. 8226-8234.

40. Russell, T.P., *Characterizing Polymer Surfaces and Interfaces.* MRS Bulletin, 1996. **January**: p. 49-53.

41. Kramer, E.J., *Ion-Beam Analysis of Polymer Surfaces and Interfaces.* MRS Bulletin, 1996. **January**: p. 37-41.

42. Composto, R.J. and E.J. Kramer, *Mutual Diffusion studies of polystyrene and poly(xylenyl ether) using Rutherford Backscattering Spectrometry.* J. Materials Science, 1991. **26**: p. 2815-2822.

43. Whitlow, S.J. and R.P. Wool, *Investigation of Diffusion in Polystyrene Using Secondary Ion Mass Spectroscopy.* Macromolecules, 1989. **22**: p. 2648-2652.

44. Zhuang, H. and J.A. Gardella, *Spectroscopic Characterization of Polymer Surfaces.* MRS Bulletin, 1996. **January**: p. 43-48.

45. Schnell, R., M. Stamm, and C. Creton, *Direct Correlation between Interfacial Width and Adhesion in Glassy Polymers.* Macromolecules, 1998. **31**: p. 2284-2292.

46. Schnell, R., M. Stamm, and C. Creton, *Mechanical Properties of Homopolymer Interfaces: Transition from Simple Pullout to Crazing with Increasing Interfacial Width.* Macromolecules, 1999. **32**(10): p. 3420-3425.

47. Kulasekere, R., et al., *Homopolymer Interfaces Reinforced with Random Copolymers.* Macromolecules, 1996. **29**: p. 5493-5496.

48. Rafailovich, M.H., et al., *Interface Formation in a Partially Miscible Polymer Blend.* Europhysics Letters, 1988. **5**(7): p. 657-662.

49. Composto, R.J., E.J. Kramer, and D.M. White, *Mutual Diffusion in the Miscible Polymer Blend Polystyrene/Poly(xylenyl ether).* Macromolecules, 1988. **21**: p. 2580-2588.

50. Mills, P.J., et al., Applied Physics Letters, 1984. **45**: p. 957-.

51. Composto, R.J., E.J. Kramer, and D.M. White, *Reptation in Polymer Blends.* Polymer, 1990. **31**: p. 2320-2327.

52. Green, P.F., D.B. Adolf, and L.R. Gilliom, Macromolecules, 1991. **24**: p. 3377-.

53. Zheng, X., et al., *Diffusion in Linear Deuterated Polystyrene Chains in Cross-Linked Polystyrene Networks.* Macromolecules, 1993. **26**: p. 6431-6435.

54. Reiter, G., et al., *Time Regimes in Polymer Interdiffusion Determined by Marker Movement.* Macromolecules, 1991. **24**: p. 1179-1184.

55. Agrawal, G., et al., *Short-Time Interdiffusion at Polymer Interfaces.* Macromolecules, 1994. **27**: p. 4407-4409.

56. Karim, A., G.P. Felcher, and T.P. Russell, Polymer Prepr., 1990. **31**(2): p. 69-.

Table 2.1: Analytical tools used to analyze polymer-polymer systems.

Technique	Resolution (nm)	Comments	References
RBS	5-20	Requires heavy element to detect	[24, 41, 48]
FRES	>10	Requires deuteration of sample	[35,41,49-52]
SIMS	10	Destructive (d-SIMS)	[6,35,43,44,53]
ATR-FTIR	10,000	Poor resolution	[15,25,44]
NR, XRR	0.2-1	Sensitive to interfacial and surface roughness effects	[2,4,6,9,28,31,3547,54-56]
SAXS	0.5 -1	Requires electron density contrast	[1,35]

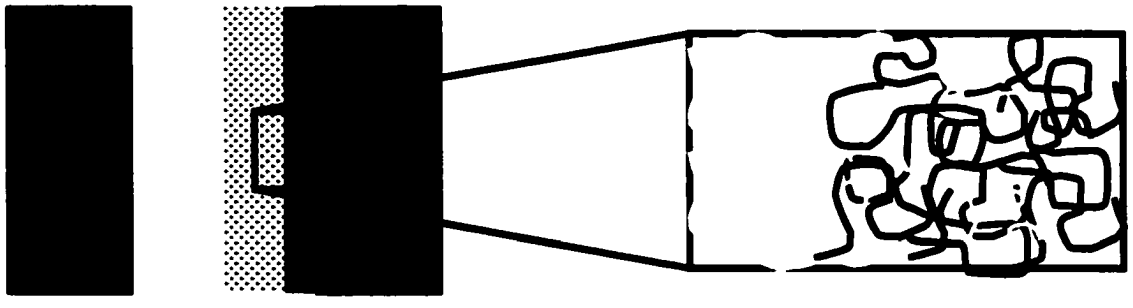

Figure 2.1: Schematic of interdiffusion. Interdiffusion is the result of interpenetration of the polymer chains across the interface.

CHAPTER 3

RESEARCH OBJECTIVES

In consideration of the significant use of sophisticated polymeric materials in a wide variety of applications from biomaterials to microelectronics, a more complete understanding of the relationship between microscopic attributes (chain architecture, copolymer composition, molecular weight, etc.) and the corresponding behavior at the macroscopic level (fracture energy, surface properties) has become essential. Current research in the area of partially miscible polymer interfaces has investigated some of these relationships, but a complete study from the microscopic to macroscopic level on an identical system is still necessary. With knowledge of how microscopic properties change the macroscopic behavior, it will be possible to design materials by tailoring at the molecular level. Especially important is the area of partially miscible interfaces, specifically those involving a homopolymer (A) and a copolymer (AB), due to the increased presence of such copolymers as a means of reinforcement at interfaces and as surfactants. The overall goal of this research is to understand the complex interplay between miscibility and interdiffusion phenomena at polymer interfaces in order to tailor adhesion, surface properties, and interphase morphology in order to relate these to the fracture energy of the same system. The specific research objectives of this work are to:

(1) quantify interdiffusion and surface encapsulation in partially miscible polymer bilayers of polystyrene (PS) and the statistically random copolymer poly(styrene-*r*-4-bromo-styrene) (PBS) experimentally using Rutherford backscattering spectroscopy (RBS). Interdiffusion studies were performed on the following systems:

(a) miscible, partially miscible, and immiscible monodisperse N-symmetric bilayers

(b) miscible, partially miscible, and immiscible monodisperse N-asymmetric bilayers

(c) miscible, partially miscible, and immiscible polydisperse N-symmetric bilayers

(d) miscible, partially miscible, and immiscible polydisperse and monodisperse N-symmetric bilayers having disparate film thickness

(2) quantify interfacial width in PS/PBS bilayers using x-ray reflectivity (XR) in order to relate the interfacial width to the observed interdiffusion behavior and to take advantage of the greater resolution of this technique to gain insight into interfacial conditions in partially miscible and immiscible bilayers.

(3) theoretically predict interdiffusion profiles using a diffusion equation based on the square-gradient modification to the Flory-Huggins expression for free energy and the fast-mode expression for mobility.

Figure 3.1 schematically shows the overall objectives of this research including complementary fracture studies for the same system. To accomplish the first objective, a partially miscible bilayer system of polystyrene (PS) and a statistically random copolymer of poly(styrene-co-4-bromostyrene), $(C_8H_{(8-x)}Br_x)_N$, where x is the mole fraction of bromine in the copolymer and N is the degree of polymerization is studied using Rutherford backscattering spectroscopy (RBS). Miscibility in these systems is controlled by volume fraction of bromine (f) in the PBS copolymer, degree of polymerization (N), and temperature (T). To examine the effects of miscibility on the interdiffusion in these bilayers, these parameters are varied such that the system spans a range of miscibility. From analysis of the RBS spectra of miscible bilayers, it is possible to extract a mutual diffusion coefficient, D_M. For partially miscible systems, the equilibrium layer compositions are representative of binodal concentrations and are compared to phase diagrams predicted using a Flory-Huggins

interaction parameter measure using small angle x-ray scattering (SAXS). Knowledge of the effects of f, N, and T on D will provide understanding of interdiffusion dynamics and correlations with other studies for the same conditions.

For the second objective, x-ray reflectivity (XR) is used to determine interfacial width in PS/PBS bilayers. From fitting reflectivity data to an electron density profile, it is possible to calculate an interfacial width based on composition v. depth information. The XR studies are done for the same experimental conditions (f, N, T, t) as the RBS studies to allow direct correlation. Measurement of interfacial width for these systems provides a key piece of information for relating interdiffusion mechanisms to fracture energy.

The final objective is to model the parametric effects on the interdiffusion mechanism. The square-gradient mean field theory will be used to model the experimental data, making it possible to calculate the respective mutual diffusion coefficients and interfacial widths.

Attainment of the research objectives stated here will be a significant contribution to understanding miscibility effects on the microscopic behavior at polymer interfaces. Developing a relationship between the interdiffusion dynamics, phase morphology, and macroscopic properties will enable researchers to molecularly design interfaces and materials tailored to specific applications.

Dissertation Organization

The dissertation is organized as follows: Objectives (1a) and (3) are discussed in Chapter 4; (1b) and 3 in Chapter 5; (1c) and (1d) in Chapter 6, and (2) in Chapter 7. Chapters 8 and 9 are the conclusions and future directions for this project, respectively.

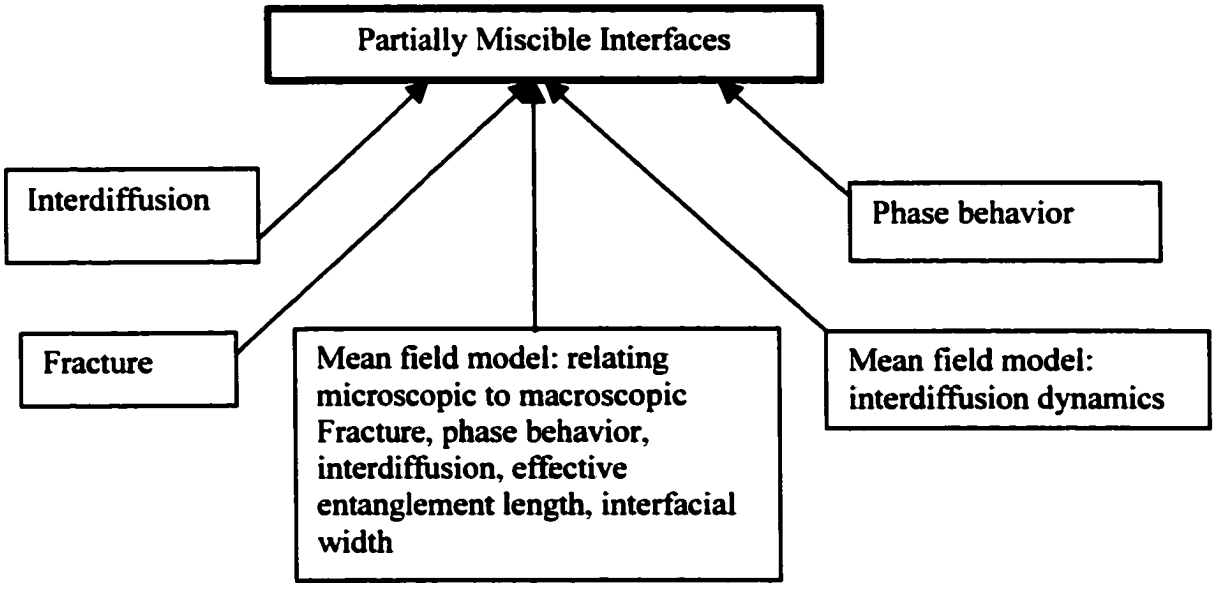

Figure 3.1: Schematic presentation of the overall research objectives described here, including complementary fracture studies for the same system.

CHAPTER 4

INTERDIFFUSION IN PARTIALLY MISCIBLE N-SYMMETRIC INTERFACES

4.1 Abstract

Interdiffusion in partially miscible polymer bilayers of polystyrene (PS) and the statistically random copolymer poly(styrene-co-4-bromostyrene) (PBS), $(C_8H_{(8-x)}Br_x)_N$, where x is the mole fraction of brominated repeat units in the copolymer and N the degree of polymerization, was studied using Rutherford backscattering spectroscopy (RBS). PBS volume fraction v. depth profiles were obtained from the evolution of the bromine peak in the RBS spectra. Mutual diffusion coefficients were determined by comparison of the RBS data to a mean-field interdiffusion model with the square-gradient modification using a concentration dependent mobility expression. The mutual diffusion coefficient is shown to decrease with increasing degree of polymerization and extent of bromination of the PBS copolymer and increase with temperature. As the phase boundary is approached, interdiffusion occurs until layer compositions indicative of binodal conditions are reached. These observations are in agreement with phase diagrams obtained using Flory-Huggins theory and a PS/PBS Flory-Huggins interaction parameter measured using small angle x-ray scattering (SAXS). The implications of this miscibility dependence of the mutual diffusion coefficient, based on both composition of the copolymer and degree of polymerization, are discussed.

4.2 Introduction

Composite polymeric materials tailored to possess properties of strength, elasticity, and adhesion are considerably affected by their interfacial characteristics. A detailed understanding of interfacial molecular phenomena and the parameters controlling the driving force for interdiffusion in partially miscible polymer systems can have significant impact on the design of such materials. Applications include injection molding, compatibilizer/blend technology, co-extrusion, adhesives, electronic materials, and high performance nano-composites [1]. Overall, our work aims to identify molecular properties that influence interface performance and obtain meaningful relationships between molecular properties (interdiffusion, interfacial width, interaction parameter, phase behavior, and blend morphology) and macroscopic properties (interfacial fracture energy).

The evolution of the interface when two polymers are brought into contact above T_g has been studied extensively through experiments and models [1-13]. Many polymer/polymer interfaces (and blends) are partially miscible, i.e., they have a Flory-Huggins interaction parameter, χ, near the spinodal interaction parameter, χ_s. This work explores the effect of miscibility on interdiffusion in partially miscible bilayer systems of polystyrene (PS) and the statistically random copolymer poly(styrene-*r*-4-bromostyrene) (PBS), $(C_8H_{(8-x)}Br_x)_N$, where x is the mole fraction of brominated repeat units in the copolymer and N is the degree of polymerization. There has been much research using the partially miscible system of PS/PBS (or similar systems) and is discussed here for its relevance to this work. The PS/PBS system has been shown to exhibit an upper critical solution temperature (UCST) [14]. Bruder and Brenn have investigated interdiffusion at

deuterated polystyrene (d-PS)/PBS interfaces in the two-phase region of the phase diagram using elastic recoil detection (ERD) and found that the equilibrium composition of the interface represented the binodal concentrations for that system [4]; from this work the Flory-Huggins interaction parameter was calculated and compared to the value obtained from SAXS measurements on similar systems. In addition, interdiffusion coefficients were calculated from concentration profiles for similar systems [4,15]. Stamm and co-workers [12,16,17] have used d-PS/PBS for interfacial width studies (using neutron reflectivity) and PS/PBS for fracture studies and shown the presence of various regimes in which the interfacial width is correlated to the fracture energy. The quantitative relationship obtained in that work is instructive, but limited because d-PS/PS has a small but positive χ due to the isotope effect [18]. To vary miscibility in the system, PBS copolymers with different extents of bromination were used. Green and Kramer have used the d-PS/PS system to perform a comprehensive study of the self-diffusion coefficient of PS and shown the effects of temperature and molecular weight in these systems [8,19,20]. SAXS has been used to measure the interaction parameter, χ, of the PS/PBS system and a weak dependence on blend composition has been observed [21]. Rafailovich and co-workers [11] have used both neutron and x-ray reflectivity to measure interface formation in the d-PS/PBS system to establish agreement between the methods. Other researchers have used this partially miscible system to study phase behavior and spinodal decomposition [22-24]. In addition, Green and Doyle [19,25] and Klein and co-workers [26,27] have used d-PS/PS systems and reported on the effects of thermodynamic slowing down, i.e., the slowing of diffusion as the system approaches the phase boundary due to thermodynamic limitations (immiscibility).

Jabbari and Peppas [28] have developed a model to describe interdiffusion at interfaces of polymers with dissimilar physical properties. The model system comprises one fast moving component (high mobility) and one slow moving component (low mobility). The approach assumes that vacancies make up only a small fraction of the overall concentration and therefore do not substantially affect the free energy of mixing. A chemical potential gradient exists across an interface for polymers with different chemical structure and molecular weight; as in square-gradient theory, the chemical potential gradient is assumed to be the driving force for interdiffusion and only one-dimensional flux perpendicular to the interface is allowed [29]. Using the Flory-Huggins equation to relate chemical potential to the entropy and enthalpy of mixing of the two polymers and estimating values of the Onsager and friction coefficients and the blend zero-shear viscosity, they propose the following:

$$D_M = \left(\frac{RTN_b^e}{f_b^m} \right) \left(\frac{1-\phi_s}{N_s} + \frac{\phi_s}{N_f} \right) \left(\frac{1-\phi_s}{N_s} + \frac{\phi_s}{N_f} - 2N\chi_{sf}\phi_s(1-\phi_s) \right) \qquad (4.1)$$

where R is the gas constant; T, temperature; N_b^e is the average number of repeat units between entanglements for the blend; f_b^m is the blend molar monomeric friction coefficient; ϕ_S is the volume fraction of the slower moving component; N_S and N_f are the degrees of polymerization of the slow and fast components, respectively. From comparisons of model to data for PS/PVME (poly(vinyl-methyl-ether)) system, they found the friction coefficient to be strongly composition dependent. They also report highly asymmetric diffusion profiles as further evidence of swelling of the slower moving component by the faster one, both above

and below the glass transition of the slower diffusing component [30]. Further research in this group determined that, in the immiscible limit, miscibility effects, regardless of the respective mobility of each polymer, limit the extent of interdiffusion [9]. Other researchers have noted that asymmetric interdiffusion profiles will occur for strong concentration and temperature dependence of the molecular mobility [5]. The approach suggested by Jabbari is valuable in situations where one would like to compare interdiffusion and fracture data by relating the number of entanglements across the interface, interfacial width, and the monomeric friction coefficient. For a chemically similar system such as ours (PS/PBS at low extents of bromination in the copolymer), it is reasonable to assume that the values of the average number of repeat units between entanglements and the blend molar friction coefficient are approximately the same as the values for pure PS [16,17,28,31].

With knowledge of what has been done by others, we report here the mutual diffusion coefficient for the PS/PBS system at various f, the volume fraction of brominated repeat units in the copolymer, and N, and demonstrate the correlation with phase behavior in this system. As mentioned before, the effect of miscibility on the interdiffusion in the partially miscible bilayer system PS/PBS is examined using Rutherford backscattering spectroscopy (RBS). The overall goal is to provide a basis to discern the mechanism of interdiffusion at partially miscible polymer interfaces and the nature of the thermodynamic (miscibility) and kinetic (mobility) dependence of the mutual diffusion coefficient. Combinations of f and N designed to span a range of miscibility have been chosen; for given N, system miscibility is controlled by f. Additionally, systems having the same f were studied at different N. Phase diagrams for various extents of bromination and molecular weight have already been obtained and χ

parameters have been measured using SAXS [32]. The PS/PBS systems, defined in terms of f and N, undergo phase transitions within the temperature range considered in this study [32]. In order to directly relate interdiffusion and phase behavior, identical polymers were used in the respective studies.

4.3 Experimental Techniques

Monodisperse PS and PBS were obtained from Polymer Source, Inc (Dorval, Quebec). PBS was synthesized by the procedure described by Kambour and co-workers [22].

4.3.1 Synthesis of PBS

In a typical reaction, 10g of PS and a glass-coated magnetic stirrer in a clean Erlenmeyer flask is placed in vacuum for an hour to dry. 100ml of nitrobenzene is then added to the flask, which is covered with aluminum foil to prevent light-catalyzed free radical reactions that would produce backbone bromination and cross-linking of the polymer chains. The reaction flask is stirred for 45min in the dark under nitrogen, allowing the PS to completely dissolve. The desired amount of bromine is then added to the reaction flask (20% excess). Under nitrogen atmosphere, the reaction is carried out in the dark with stirring for 4-22h. The reaction mixture is then poured in a thin stream into 2l of methanol. The precipitate is recovered from methanol by filtration, dissolved in THF, and filtered to remove insolubles. The solution is again washed with 2l of methanol to finally yield 9.4g of brominated PS (PBS), which is dried in vacuum for 24h. ^{13}C-NMR, elemental analysis, DSC, TGA, GPC, and UV-Vis spectroscopy are used to characterize the polymer to ensure

substitution of bromine in the para-position of the benzene ring and an unchanged degree of polymerization. By controlling the amount of bromine added and the reaction time, PBS with varying extents of bromination was synthesized (see Table 4.1).

4.3.2 Preparation of RBS bilayers

The bilayers are composed of a bottom layer of PS and a top layer of PBS. For the PS layer, a solution of PS in toluene was prepared and cast onto a pretreated silicon wafer using a spin coater (Headway Research, Garland, TX). The wafers were pretreated for 24h in a solution of chromic/sulfuric acid to remove any organics and residual polishing silicones, and then cleaned by the RCA method [33]. The films were then dried at room temperature in a controlled atmosphere for 24h followed by in vacuum at 25°C for 6h. Film thickness and surface roughness were measured by profilometry to yield relatively smooth ($\pm$ 3nm) PS films of thickness 1 - 2μm. For the PBS layer, a solution of PBS in toluene was prepared and cast onto glass slides using a spin coater, then dried in the same manner as the PS layers to yield thickness 0.3μm to 1.5μm. Film thickness was measured (on silicon) using an automated film thickness apparatus (Tencor, Mountain View, CA). The glass slides used for the PBS films were pretreated in a solution of chromic/sulfuric acid for 24h, then for 10min. in each of the following: acetone, de-ionized water, 2-propanol, and toluene. The PBS films were floated off the slides onto de-ionized water. The corresponding PS film on the silicon wafer was used to pick up the floating PBS film to create the desired bilayer. The bilayer was then dried in a controlled atmosphere at room temperature for 24h and in vacuum at 60°C for

24h. Samples were annealed at $\leq 10^{-3}$ Torr for appropriate times at various temperatures (150 $< T <$ 250°C), above the glass transition temperature of both species, to allow interdiffusion.

4.3.3 RBS Analysis Technique

Rutherford backscattering spectroscopy (RBS) provides quantitative composition and depth information [34] with resolution at the interface (for our configuration) on the order of 500Å. A schematic of the experimental setup is shown in Figure 4.1. The method to obtain concentration v. depth profiles from RBS spectra has previously been reported [5]. Kramer and co-workers have successfully used RBS to study 'marker molecule' diffusion at polymer interfaces[35] and to obtain concentration v. depth profiles in polymer systems where one of the species was preferentially stained with a heavy element [5]. However, interfaces in which chemically similar polymers are present on either side of the interface (as in this study) cannot be preferentially stained. For our studies, the bromine in the copolymer serves as a tag to follow the change in the composition of each layer with time.

The software used to analyze the RBS data was QUARK (QUantitative Analysis of Rutherford Kinematics) [36]. The input parameters include the type of ion used (He^{++}), beam energy, configuration (IBM or Cornell), detector angle, target angle, and solid angle. The adjustable parameters are charge on the sample, detector resolution, and dispersion (channel to energy conversion). Once these parameters are known the spectra are converted to energy v. depth profiles. The depth resolution of the technique used (RBS with slightly defocused beam) is estimated (using the detector resolution, dispersion, and stopping range of ions in matter [37]) to be 50Å at the surface and approximately 500Å at the interface (assuming an

average interface at 8000Å PBS + 100Å gold overlayer). This resolution is reported but not taken into account directly; rather, the mutual diffusion coefficient is assumed to be relatively constant with time and therefore represented by the resulting composition of the layers at a given time.

Figure 4.2a shows a typical RBS spectrum for an unannealed PS/PBS bilayer (N = 7144, f = 0.04) reported as normalized yield v. channel with a simulated fit. The simulations are constructed to estimate layer thickness and atomic compositions [38,39]. In this spectrum, the bromine peak corresponding to the PBS layer is clearly discernible. The corresponding concentration v. depth profile for the bromine peak is shown in Figure 4.2b. For the example considered in Figures 4.2a and 4.2b, the PBS layer is 3100Å thick. It is instructive to note that the example shown in Figures 4.2a and 4.2b corresponds to the lowest extent of bromination in our study for which mutual diffusion coefficients are reported. Since it is possible to detect bromine levels at f = 0.04, the bromine peak in the spectra for the greater extents of bromination are also detectable. Figures 4c and 4d show the raw data with simulation for a much higher extent of bromination (N = 1370, f = 0.55) and thicker film. The corresponding bromine peak is shown in the inset.

It has been reported that PBS is sensitive to radiation damage [4,5,15,40]. RBS spectra of PBS have been observed to change appreciably and a depletion of bromine that increased towards the surface of the sample was detected; this depletion was attributed to loss of mobile HBr. A reported means of reducing this effect was to cool the sample [5,15,41]. In our work minimization of sample damage during analysis was achieved through gold-coating the sample to prevent charging and analyzing over a large annular region, as shown in

Figure 4.3. Analyzing over this relatively large surface (ca. 200mm^2) also allows for an averaging of heterogeneous effects whereas an intensely focused beam would impinge on the center of the sample with a total analysis surface of ca. 2mm^2. To ensure that the above procedures minimized damage, spectra of the same sample were sequentially collected for multiple analysis times. Figure 4.4 shows that there was no change observed in the spectra for times up to four times the typical analysis time. Another issue that was addressed is the appearance of contaminants in the sample spectra. Using an angle-resolved experiment [34,42], depicted in Figure 4.5, it was determined that the contaminants reside on the surface of the gold layer, and therefore do not interfere with interdiffusion at the PS/PBS interface. In many of the spectra a slightly reduced bromine concentration was observed near the surface, while peak integration indicated mass conservation; this may be explained by the preferential diffusion of PS to the surface, which has been observed by other researchers [11,24,32,43].

4.4 Results and Discussion

As mentioned in the Introduction, the PS/PBS system exhibits UCST behavior [14]. We have performed phase behavior studies on thin film blends of PS/PBS using scanning probe microscopy and SAXS [32] and measured the interaction parameter $\chi_{S\text{-}BrS}$ between brominated and non-brominated styrene segments as

$$\chi_{S-BrS} = -0.0833 + \frac{73.75}{T} \tag{4.2}$$

where T is temperature reported in K. This expression assumes that $\chi_{S\text{-}BrS}$ is independent of composition, in agreement with previous studies [21]. The Flory-Huggins interaction

parameter, χ, of a homopolymer, A, and a statistically random copolymer, A-B, is expressed as [4,15]

$$\chi = f^2 \chi_{AB} \tag{4.3}$$

Here f is the volume fraction of B repeat units in the random copolymer. Knowing the ratio of the molar volume of a styrene unit to that of a brominated styrene unit (0.862), f can be related to the extent of bromination, x, as

$$f = \frac{x}{x + 0.862(1 - x)} \tag{4.4}$$

The mutual diffusion across the interface between two polymeric species can be described as a product of a kinetic term involving the intrinsic (i.e., tracer) diffusion coefficients, degrees of polymerization, and compositions of the species, and a thermodynamic term that represents the driving force for mixing [44]. The thermodynamic term is given by $2\phi(1-\phi)(\chi_s - \chi)$ [9], where, for our system, ϕ is the volume fraction of PBS copolymer and χ_S is the interaction parameter at the spinodal, given by $\chi_S = \frac{1}{2}\left(\frac{1}{N_{PS}(1-\phi)} + \frac{1}{N_{PBS}\phi}\right)$. Thus, for values of $f > f_S$, the system becomes phase separated, with f_S given by

$$f_S = \sqrt{\frac{1}{2\left(-.0833 + \frac{73.75}{T}\right)}\left(\frac{1}{N_{PS}(1-\phi)} + \frac{1}{N_{PBS}\phi}\right)} \tag{4.5}$$

For miscible systems, the mutual diffusion coefficient can be expressed as

$$D_M = 2D_0\phi(1-\phi)(\chi_s - \chi) \tag{4.6}$$

where D_0 is the kinetic term, a function of D_{PS} and D_{PBS}, the tracer-diffusion coefficients of PS and PBS (and hence temperature and degree of polymerization) and their relative compositions. It is important to note that the tracer-diffusion coefficient of the PBS copolymer is a function of the composition of the copolymer (f), but this dependence is expected to be weak for small f. In the limit as $N_{PS} = N_{PBS}$ and $D_{PS} \approx D_{PBS}$, (good assumption for small f) the expressions for D_M is given by the product of a constant kinetic term, D_0 ($\approx D_{PS} \approx D_{PBS}$), and the thermodynamic term, which remains unchanged.

Using this composition dependent D_M, profiles in the miscible PS/PBS systems can be fit to a mean-field interdiffusion model given by

$$\frac{\partial \phi}{\partial t} = \frac{\partial}{\partial z}\left(D_M(\phi) \frac{\partial \phi}{\partial z} \right) \tag{4.7}$$

Here z is the spatial position (depth), and t, time. This equation was solved numerically using an implicit finite difference method and compared to the RBS data using D_0 as the fitting parameter.

The equation 4.7 is sufficient to model interdiffusion in miscible bilayer systems, however, for partially miscible systems, it is necessary to use the square-gradient modification to the Flory Huggins expression for free energy, which, is given by

$$f_{FH} = \frac{\phi}{N_B}\ln\phi + \frac{1-\phi}{N_A}\ln(1-\phi) + \chi\phi(1-\phi) + \frac{b^2}{36\phi(1-\phi)}\left(\frac{\partial \phi}{\partial x}\right)^2 \tag{4.8}$$

and includes the effect of miscibility through the term $\chi\phi(1-\phi)$. The square-gradient term, which accounts for the effect of concentration fluctuations across the interface and the formation of interfaces between coexisting phases, is sufficient to describe the interdiffusion

behavior as the phase boundary is approached and $N^*\chi$ values exceed 2. The overall diffusion equation derived from combining the Flory-Huggins free energy with the square-gradient term is given in Appendix 2. We do not neglect any of the higher order derivative terms, noting that each make a contribution that, while small, play a role in dictating the behavior at the interface when $N^*\chi$ values approach ~2.5. The diffusion equation including the square-gradient modification was also solved using an implicit finite difference method; those programs are shown in Appendix 3.

Interdiffusion in the PS/PBS bilayers

The characteristics of the PS/PBS system are shown in Table 4.2. At each of the annealing temperatures, the bilayers were annealed for various times from 15 to 180 minutes. As shown in Figure 4.2, RBS spectra were converted to PBS volume fraction v. depth, (ϕ v. z), profiles. Figure 4.6 shows ϕ v. normalized depth with a theoretical fit for PS/PBS for N = 424, f = 0.08 annealed for 15 minutes at 200°C. Normalized depth is z divided by the total thickness of the bilayer. Using Eq. 4.5, it can be verified that f = 0.08 is in the one-phase region for all temperatures considered in this study. Because the PS/PBS system is completely miscible, we see extensive interdiffusion after only 15 minutes. The D_0 value determined from this fit is 4.5 x 10^{-12} cm^2/s; this value is lower than the value for D_{PS} (at the same N and T) reported in the literature, 25.4 x 10^{-12} cm^2/s [45]. However, this value is reasonable when compared to values obtained by Bruder and Brenn, which are reported to be a factor of 20 different than the value expected for similar systems [15]; the reason for this discrepancy is due to the use of an inadequate model using an error function expression to

predict the interdiffusion profiles. As mentioned earlier, increasing f decreases miscibility, which can be quantified by the term $N\chi$. The value of χ_S at $\phi = 0.5$ with $N_{PS} = N_{PBS} = N$ is given by $\chi_S = 2/N$, therefore, we use the criterion $N\chi < 2$ to define completely miscible systems. The value of $N\chi$ is shown in Table 4.2 for each system. For N = 424, f = 0.22 at the annealing temperature of 200°C, the system is still one phase, but approaching the phase boundary ($N\chi$ approaching 2) and would therefore be expected to have a decreased mutual diffusion coefficient. This dependence is reflected in the form of the thermodynamic term in Eq. 4.8; noting that the kinetic term D_0 should not change appreciably for small f, assuming D_{PBS} is a relatively weak function of copolymer composition for small f. Figure 4.7 shows this effect for the case of f = 0.22; comparing this profile to Figure 4.6, it is shown that for the same conditions of N and T, the interdiffusion in the system decreases due to decreased miscibility. It is important to note that, in Figure 4.6, the initial PS and PBS layers have equal thickness and the equilibrium PBS volume fraction in the bilayer is 0.5. For the case in Figure 4.7, the initial PBS layer is 40% of the total thickness of the bilayer, giving an equilibrium composition of 0.4. As discussed above, the D_0 value remains nearly unchanged ($D_0 = 4.0 \times 10^{-12}$ cm^2/s), while D_M decreases due to the higher value of f (see Table 4.2).

At a still higher value of f = 0.28, the system reaches the phase boundary and interdiffuses only while layer compositions remain in the one phase region; this interesting aspect is shown clearly in the RBS data. In Figure 4.8, interdiffusion is observed at 150, 175, and 200°C until the binodal compositions are reached; Figure 4.8d is a fit of the data from Figure 4.8c using the square-gradient modified diffusion equation with $D_0 = 4.0 \times 10^{-12}$ cm^2/s. The phase diagram for PS/PBS (N=424, f = 0.28) has been independently predicted

using the χ parameter measured from SAXS and Flory Huggins theory [32] and is shown with the binodal compositions, calculated from the RBS data, in Figure 4.9. The binodal compositions determined from the RBS data are the average composition of the respective layers. There is very good agreement between the two independent measurements. This system is close to spinodal, thus, the term $(\chi - \chi_s)$ is small. It is known that the interfacial width, *w*, between two polymers is inversely proportional to the square root of $(\chi - \chi_s)$ [46], thus leading to measurable interfacial widths during the annealing times considered in this study. As mentioned above, concentration v. depth profiles in these systems can be predicted by using the mean-field model, which includes the square-gradient modification. Using this approach, it was found that the tracer-diffusion coefficient did not change appreciably, even as f was increased to 0.28. For the same system, increasing f to 0.46, the spinodal temperature well exceeds 200°C and Figure 4.10 shows the result when the interdiffusion in the system cannot be detected within the resolution of RBS, denoted "ND".

To quantify the effect of mobility in the system, N was varied from N = 424 to N = 7670. The profile for N =1370, f = 0.09 at 225°C is qualitatively similar to those for the N=424 case and is shown in Figure 4.11. It should be noted that the peak which appears at z = 0.75 corresponds to a contaminant from the gold-coating procedure which has been determined to reside on the surface. Once again we observe experimental profiles slightly steeper than those predicted. The value of D_0 from this fit is 3.5×10^{-12} cm^2/s, in agreement with the value of D_{PS} from literature of 6.3×10^{-12} cm^2/s [45]. Investigating the effect of miscibility in a system with decreased mobility, Figure 4.12 shows the interdiffusion profiles for N=1370, f = 0.25, for annealing temperatures of 175 and 200°C. As in Figure 4.8, this

system reaches the phase boundary, thus giving rise to very steep interdiffusion profiles. At 175°C, interdiffusion cannot be detected within the resolution of RBS and is denoted "ND". At 200°C, however, sufficient interdiffusion has taken place and the binodal compositions can be measured. The binodal compositions calculated from RBS are shown on the predicted phase diagram in Figure 4.13; as before, the agreement is very good. Although this system does diffuse to binodal conditions, $N\chi >> 2$ (see Table 4.2), the square-gradient modified diffusion equation is inadequate to describe interdiffusion in such systems.

When the degree of polymerization is further increased to N = 4087, all extents of bromination studied show no interdiffusion. As N is further increased to 7670, no interdiffusion is observed when f exceeds 0.22, even at a temperature of 250°C. Figure 4.14 shows the result when there is visible interdiffusion (f = 0.04) at 200°C and 225°C, however, there is substantial scatter due to the very low extent of bromination. The D_0 value calculated from these fits are 8.0×10^{-14} cm^2/s at 200°C and 4.0×10^{-13} cm^2/s at 225°C, consistent with literature values for D_{PS} of 7.8×10^{-14} cm^2/s and 2.0×10^{-13} cm^2/s at the respective temperatures [45]. Since the monomeric friction factor does not change appreciably for such small values of f, it is expected that D_{PBS} is very similar to the value of D_{PS} for the same N and T, therefore we expect very little difference between D_{PS} and D_{PBS} due to the very low extent of bromination, f = 0.04.

In summary, the D_0 values determined from fitting the RBS data ranged from 10^{-14} to 10^{-12} cm^2/s. For immiscible systems, the RBS spectra for all the annealing temperatures and times remained unchanged, indicating that there is no interdiffusion and that mass is conserved. The values of D_0 obtained from the fits were used to calculate the mutual

diffusion coefficient, D_M, using the expression given by Eq. 4.6. The values of D_M are evaluated at $\phi = 0.5$. Table 4.2 summarizes the effect of both miscibility and mobility, as quantified by the term $N\chi$, on D_M for all values of T, f, and N studied; for given N, the system becomes more immiscible as the bromine content in the copolymer increases, and D_M decreases. When the phase boundary is crossed, interdiffusion is severely limited by the immiscibility in the system. This process has been referred to as "uphill diffusion" and leads to spinodal decomposition. We have observed spinodal decomposition in thin film blends of PS/PBS for extents of bromination exceeding f_s using scanning probe microscopy as described elsewhere [32].

The results of the N-symmetric PS/PBS systems show the significant effect of the thermodynamic argument on the overall mutual diffusion coefficient and the necessity of using the square-gradient modification to the diffusion equation for partially miscible systems. Our studies also show that decreased miscibility leads to a decreased mutual diffusion coefficient and that this thermodynamic effect dominates the kinetic effect argument (evidenced by a relatively unchanged D_0 for increasing f). This result has been observed by other researchers and termed thermodynamic slowing down [19,25-27].

It has been shown that the fracture energy of an interface is directly proportional to the interfacial width [17]. Thus, by appropriately choosing χ (for example, by blending [47, 48]), strategies can be developed to strengthen incompatible interfaces. Hence, understanding miscibility-mediated interdiffusion phenomena might offer an alternative approach to reinforcement of polymer interfaces.

4.5 Conclusions

Mutual diffusion coefficients for the partially miscible PS/PBS system were calculated by comparison of interdiffusion data from RBS spectra to a mean-field interdiffusion model. The results indicate that the mutual diffusion coefficient increases with temperature and decreases with increasing degree of polymerization and extent of bromination in the PBS copolymer. We also observed limited interdiffusion in systems where binodal conditions were approached; layer compositions from the RBS data agreed with values expected from the binodal curve of the phase diagrams predicted using Flory-Huggins theory and an interaction parameter measured using SAXS. Quantitative comparisons of the data with the interdiffusion equation derived from the Flory-Huggins expression for free energy in partially miscible polymer systems yielded good agreement. For partially miscible cases it was shown that by incorporating the square-gradient modification in the diffusion equation it is possible to fit the concentration v. depth profiles. The implications of miscibility effects on interdiffusion and the relationship to strengthening partially miscible polymer interfaces are discussed.

4.6 References

1. Wool, R.P., *Polymer Interfaces Structure and Strength*. 1995, New York: Hanser Publishers.

2. Agrawal, G., et al., *Interdiffusion of Polymers Across Interfaces*. J. Polymer Science: Part B: Polymer Physics, 1996. **34**: p. 2919-2940.

3. Brochard, F. and P.G. de Gennes, *Polymer-Polymer Interdiffusion.* Europhysics Letters, 1986. **1**(5): p. 221-224.

4. Bruder, F., et al., *Interdiffusion in the Partially Miscible Polymer Blend of Deuterated Polystyrene and Poly(styrene-co-bromostyrene).* Macromolecules, 1989. **22**: p. 4434-4437.

5. Composto, R.J. and E.J. Kramer, *Mutual Diffusion studies of polystyrene and poly(xylenyl ether) using Rutherford Backscattering Spectrometry.* J. Materials Science, 1991. **26**: p. 2815-2822.

6. de Gennes, P.G., *Polymers at Interfaces: A Simplified View.* Advances in Colloid and Interface Science, 1987. **27**: p. 189-209.

7. Composto, R.J., E.J. Kramer, and D.M. White, *Mutual Diffusion in the Miscible Polymer Blend Polystyrene/Poly(xylenyl ether).* Macromolecules, 1988. **21**: p. 2580-2588.

8. Green, P., et al., *Marker Displacement Measurements of Polymer-Polymer Interdiffusion.* Macromolecules, 1985. **18**: p. 501-507.

9. Jabbari, E. and N.A. Peppas, *Polymer-polymer Interdiffusion and Adhesion.* J. M. S. - Rev. Macromol. Chem. Phys., 1994. **C34**(2): p. 205-241.

10. Jordan, E.A., et al., *Mutual Diffusion in Blends of Long and Short Entangled Polymer Chains.* Macromolecules, 1988. **21**: p. 235-239.

11. Rafailovich, M.H., et al., *Interface Formation in a Partially Miscible Polymer Blend.* Europhysics Letters, 1988. **5**(7): p. 657-662.

12. Stamm, M. and D.W. Schubert, *Interfaces between Incompatible Polymers.* Annu. Rev. Mater. Sci., 1995. **25**: p. 325-356.

13. Whitlow, S.J. and R.P. Wool, *Investigation of Diffusion in Polystyrene Using Secondary Ion Mass Spectroscopy.* Macromolecules, 1989. **22**: p. 2648-2652.

14. Kambour, R.P., J.T. Bendler, and R.C. Bopp, *Phase Behavior of Polystyrene, Poly(2,6-dimethyl-1,4-phenyl oxide) and Their Brominated Derivatives.* Macromolecules, 1983. **16**: p. 753-757.

15. Bruder, F. and R. Brenn, *Measuring the Binodal by Interdiffusion in Blends of Deuterated Polystyrene and Poly (styrene-co-4-bromostyrene).* Macromolecules, 1991. **24**: p. 5552-5557.

16. Schnell, R., M. Stamm, and C. Creton, *Direct Correlation between Interfacial Width and Adhesion in Glassy Polymers.* Macromolecules, 1998. **31**: p. 2284-2292.

17. Schnell, R., M. Stamm, and C. Creton, *Mechanical Properties of Homopolymer Interfaces: Transition from Simple Pullout to Crazing with Increasing Interfacial Width.* Macromolecules, 1999. **32**(10): p. 3420-3425.

18. Bates, F.S. and G.D. Wignall, *Isotope-Induced Quantum-Phase Transitions in the Liquid State.* Physical Review Letters, 1986. **57**(12): p. 1429-1432.

19. Green, P. and B.L. Doyle, *Isotope Effects on Interdiffusion in Blends of Normal and Deuterated Polymers.* Physical Review Letters, 1986. **57**(19): p. 2407-2409.

20. Green, P.F., D.B. Adolf, and L.R. Gilliom, Macromolecules, 1991. **24**: p. 3377-.

21. Koch, T. and G.R. Strobl, *Concentration Dependence of the Flory-Huggins Interaction Parameter of a Polymer Blend as Determined by SAXS Experiments.* J. Polymer Science: Part B: Polymer Physics, 1990. **28**: p. 343-353.

22. Kambour, R.P. and J.T. Bendler, *Miscibilities in Monodisperse Mixtures of Polystyrene, Poly(p-bromostyrene) and Their Copolymers.* Macromolecules, 1986. **19**: p. 2679-2682.

23. Guckenbiehl, B., M. Stamm, and T. Springer, *Interface Formation and Thin Film Properties of an Incompatible Polymer System.* Mat. Res. Soc. Symp. Proc., 1993. **280**: p. 275-280.

24. Bruder, F. and R. Brenn, *Spinodal Decomposition in Thin Films of a Polymer Blend.* Physical Review Letters, 1992. **69(4)**: p. 624-627.

25. Green, P.F. and B.L. Doyle, Macromolecules, 1987. **20**: p. 2471-4.

26. Losch, A., D. Woermann, and J. Klein, Macromolecules, 1994. **27**: p. 5713-5715.

27. Steiner, U., et al., Mat. Res. Soc. Symp. Proc., 1990. **177**(Macromol. Liq.): p. 367-72.

28. Jabbari, E. and N.A. Peppas, *A Model for Interdiffusion at Interfaces of Polymers with Dissimilar Physical Properties.* Polymer, 1995. **36**(3): p. 575-586.

29. Sanchez, I.C., ed. *Physics of Polymer Surfaces and Interfaces.* 1992, Butterworth Heinemann: Stoneham, MA.

30. Jabbari, E. and N.A. Peppas, *Molecular Weight and Polydispersity Effects on Interdiffusion at the Interface Between Polystyrene and Poly(vinyl methyl ether).* J. Materials Science, 1994. **29**: p. 3969-3978.

31. Jabbari, E. and N.A. Peppas, *Comparison of Interdiffusion at Polystyrene-Poly(vinyl methyl ether) and Polystyrene-Poly(isobutyl vinyl ether) Interfaces.* Polymer International, 1995. **38**: p. 65-69.

32. Gorga, R.E., et al., *Quantifying Phase Behavior in Partially Miscible Polystyrene/ Poly (styrene-co-4-bromostyrene) Blends.* Journal of Polymer Science: Part B, Polymer Physics, 2002. **40**: p. 255-271.

33. Kern, W. and D.A. Puotinen, *Cleaning Solution Based on Hydrogen Peroxide for use in Silicon Semiconductor Technology.* RCA Review, 1970. **31**: p. 187-206.

34. Kramer, E.J., *Ion-Beam Analysis of Polymer Surfaces and Interfaces.* MRS Bulletin, 1996. **January**: p. 37-41.

35. Kramer, E.J., P. Green, and C.J. Palmstrom, *Interdiffusion and marker movements in concentrated polymer-polymer diffusion couples.* Polymer, 1984. **25**(4): p. 473-480.

36. Lennard, W.N. and C.P. McNorgan, *http://www.quarksimulation.com.*

37. Ziegler, J.F., *The Stopping Ranges of Ions in Matter, Vol. 5: Handbook of Stopping Cross Sections for Energetic Ions in all Elements.* Vol. http://www.srim.org. 1980, Oxford, England: Pergamon Press.

38. Doolittle, L.R., Nucl. Instr. Meth., 1985. **9**: p. 344-351.

39. Doolittle, L.R., Nucl. Instr. Meth., 1986. **15**: p. 227-231.

40. Huttenbach, S., et al., *The Interface between Two Strongly Incompatible Polymers: Interfacial Broadening and Roughening near Tg.* Langmuir, 1991. **7**: p. 2438-2442.

41. Jones, R.A.L. and R.W. Richards, *Polymers at Surfaces and Interfaces.* 1999, Cambridge: Cambridge University Press.

42. Feldman, L.C. and J.W. Mayer, *Fundamentals of surface and thin film analysis*. 1986, New York: North Holland.

43. Slep, D., et al., *Phase Separation of Polystyrene and Bromo-Polystyrene Mixtures in Equilibrium Structures inThin Films*. Langmuir, 1998. **14**: p. 4860-4864.

44. Binder, K., *Collective diffusion, nucleation, and spinodal decomposition in polymer mixtures*. J. Chem. Phys., 1983. **79**(12): p. 6387-6409.

45. Tirrell, M., Rubber Chemistry and Technology, 1984. **57**: p. 523-556.

46. Broseta, D., et al., *Molecular Weight an Polydispersity Effects at Polymer-Polymer Interfaces*. Macromolecules, 1990. **23**: p. 132-139.

47. Brochard, F., J. Jouffroy, and P. Levinson, *Polymer-Polymer Diffusion in Melts*. Macromolecules, 1983. **16**: p. 1638-1641.

48. Helfand, E., *Theory of the Homopolymer, Binary-Polymer-Mixture Interface*. Macromolecules, 1992. **25**: p. 1676-1685.

Table 4.1. Degree of polymerization, extent of bromination, and polydispersity of PS/PBS system.

$(C_8H_{(8-x)}Br_x)_N$			
N	x	f	M_w/M
424	0	0	1.03
	0.07	0.08	
	0.20	0.22	
	0.25	0.28	
	0.42	0.46	
	0.63	0.66	
1370	0	0	1.03
	0.08	0.09	
	0.22	0.25	
	0.39	0.43	
	0.51	0.55	
4087	0	0	1.04
	0.25	0.28	
	0.43	0.47	
	0.59	0.63	
7670	0	0	1.05
7144	0.04	0.04	1.1
	0.20	0.22	
	0.48	0.52	

Table 4.2. Mutual diffusion coefficient, D_M, for N-symmetric PS/PBS systems: D_M and $N\chi$ reported at 200°C; D_M evaluated at $\phi = 0.5$.

N	f	T range (°C)	$N\chi$	D_M (cm^2/s)
424	0	150-200	0	4.5×10^{-12}
	0.08		0.20	3.9×10^{-12}
	0.22		1.49	1.1×10^{-12}
	0.28		2.41	Binodal*
	0.46		6.51	ND
	0.66		13.40	ND
1370	0	175-225	0	8.0×10^{-13}
	0.09		0.81	4.5×10^{-13}
	0.25		6.21	Binodal
	0.43		18.38	ND
	0.55		30.08	ND
4087	0	200-250	0	2.7×10^{-13}
	0.28		23.25	ND
	0.47		65.52	ND
	0.63		117.72	ND
7670	0		0	7.8×10^{-14}
7144	0.04	200-250	0.86	7.4×10^{-14}
	0.22		25.98	ND
	0.52		145.16	ND

*For the binodal situations, the D_0 used to fit the data corresponded to the D_0 determined for that N and T.

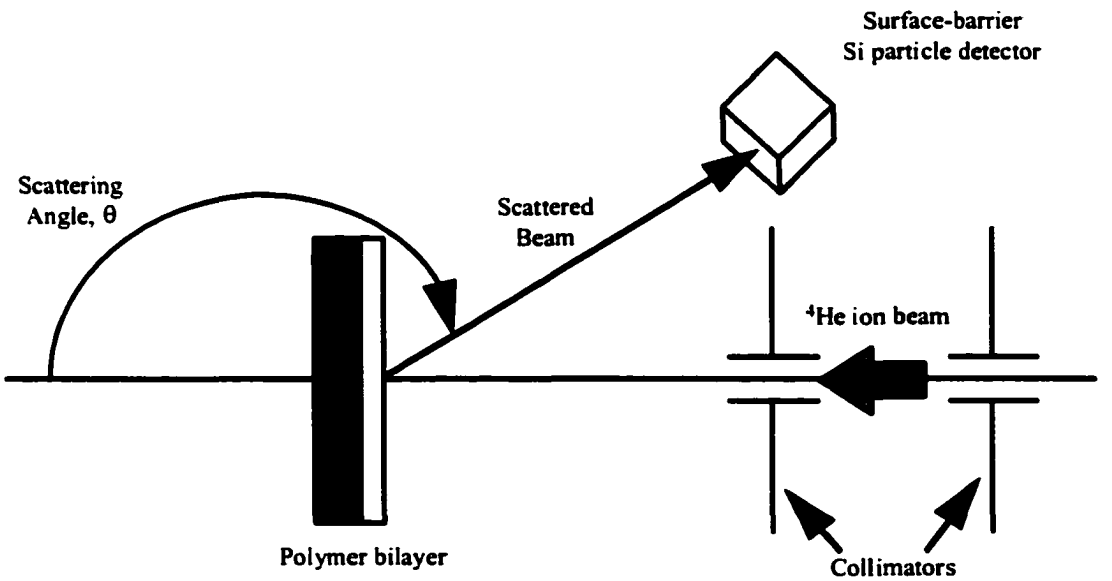

Figure 4.1: Schematic of RBS. ^{4}He ions impinge on the polymer bilayer sample and are backscattered by nuclei within the sample. Energy of the backscattered ion is a function of the mass and depth of the nucleus that it backscatters from (see Appendix 1).

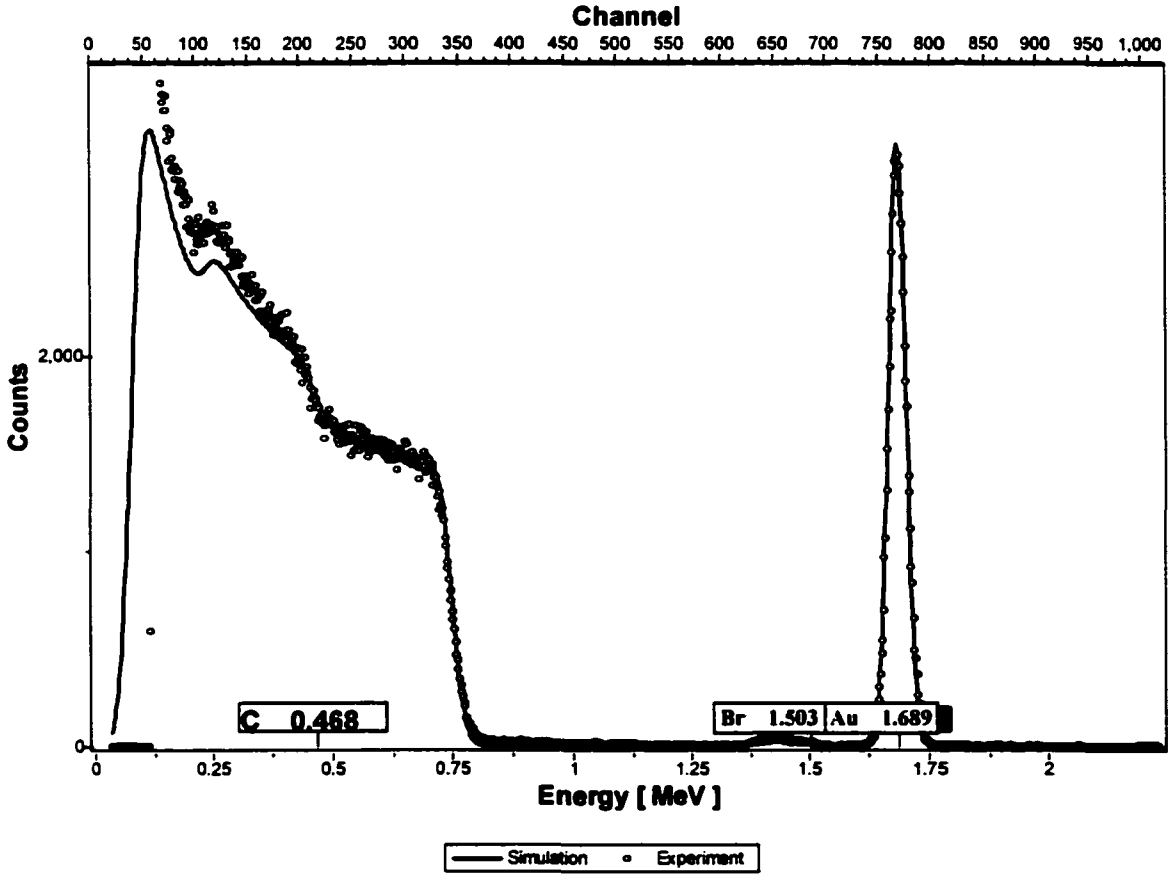

Figure 4.2: Example of conversion from RBS yield v. channel/energy spectrum to PBS volume fraction v. depth profile. (a) Typical RBS spectrum is plotted in yield v. energy (N_{PBS} = 7144, f = 0.04, no anneal). This can be converted to PBS volume fraction v. depth by normalizing overall yield and converting energy to depth using the stopping range of ions in matter [34,36-39]. The peak corresponds to bromine and is representative of the PBS layer.

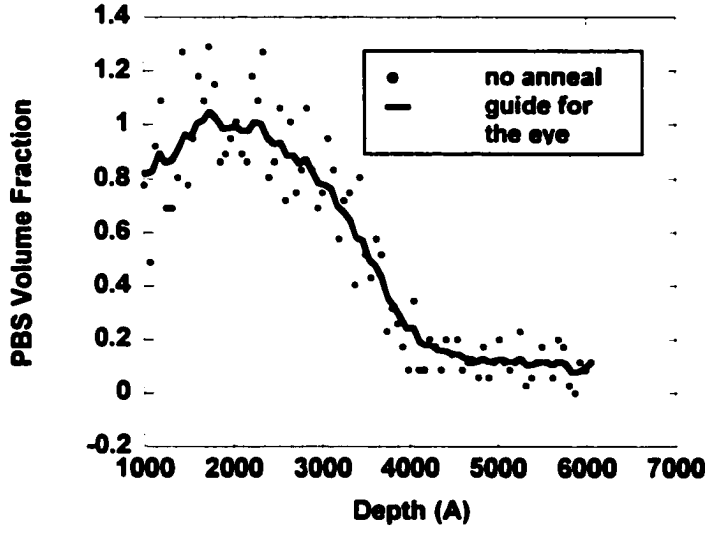

Figure 4.2b: PBS volume fraction, ϕ, v. depth, z (Å), for an unannealed PS/PBS bilayer for $N_{PBS} = 7144$, $f = 0.04$. The thickness of this PBS layer is ~ 3100Å.

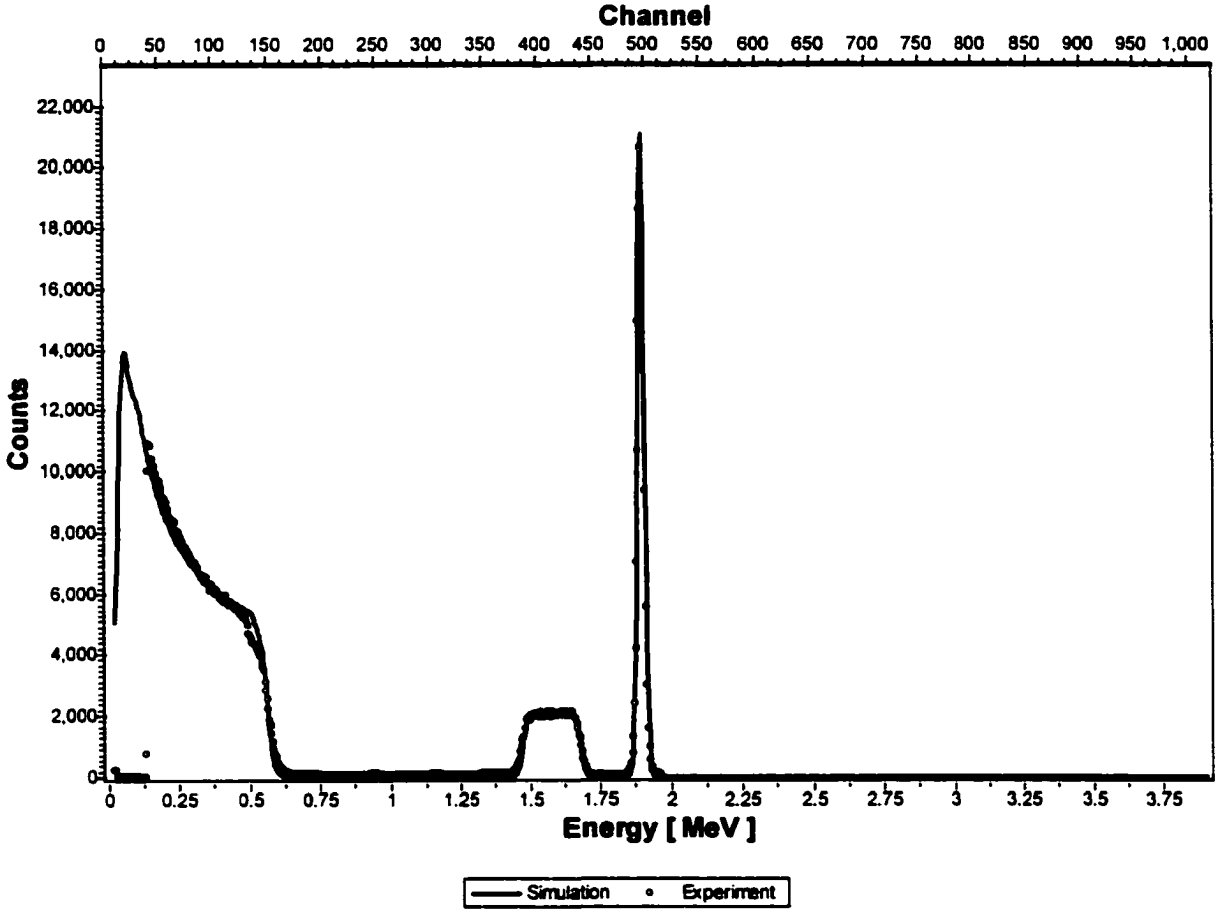

Figure 4.2c: Typical RBS spectrum is plotted in yield v. energy (N_{PBS} = 1370, f = 0.55, no anneal).

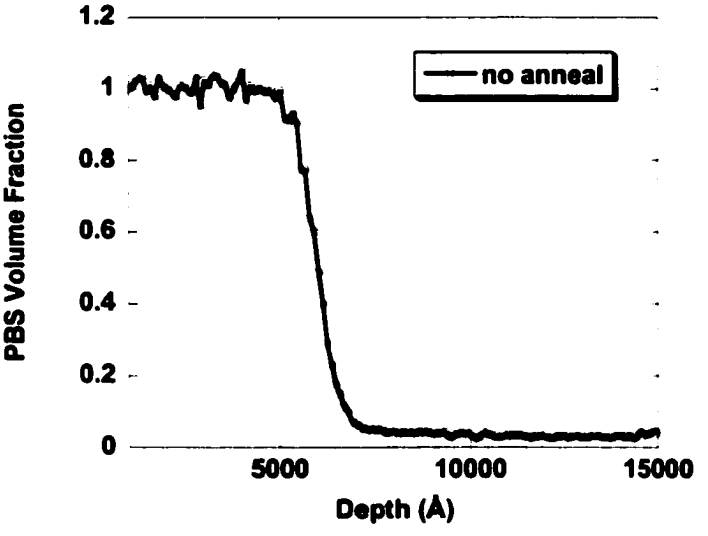

Figure 4.2d: PBS volume fraction, ϕ, v. depth, z (Å), for an unannealed PS/PBS bilayer for $N_{PBS} = 1370$, $f = 0.55$. The thickness of this PBS layer is ~ 5500Å.

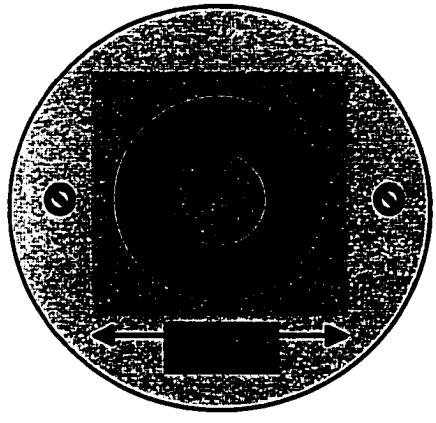

Figure 4.3: Schematic showing large annular area of sample exposed to beam to minimize damage.

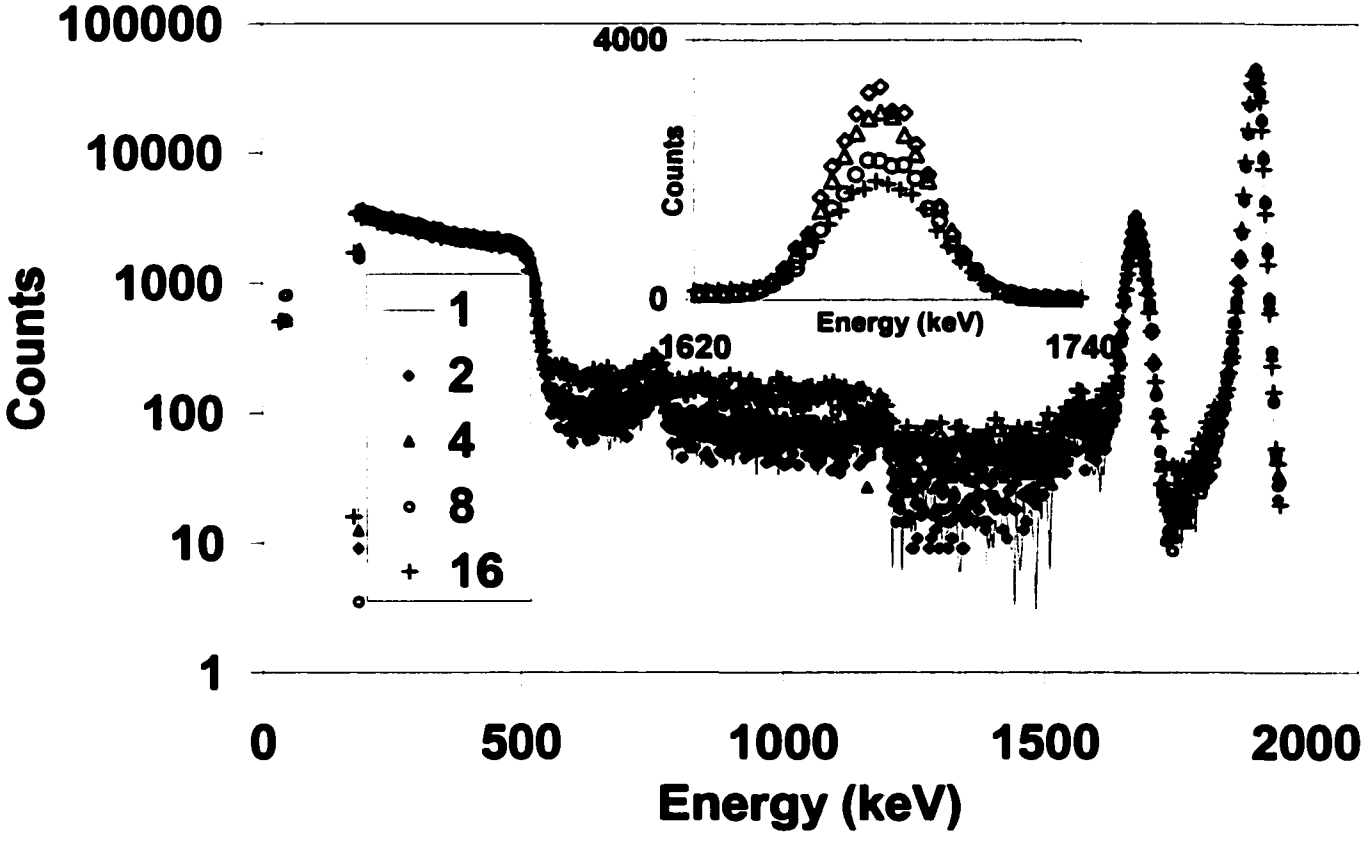

Figure 4.4: Radiation damage study performed on an unannealed $N_{PS} = N_{PBS} = 1370$, $f = 0.55$ bilayer to determine the analysis time for which mass loss becomes significant. As shown in the figure, the sample can incur 4 times the usual dose before liberating HBr.

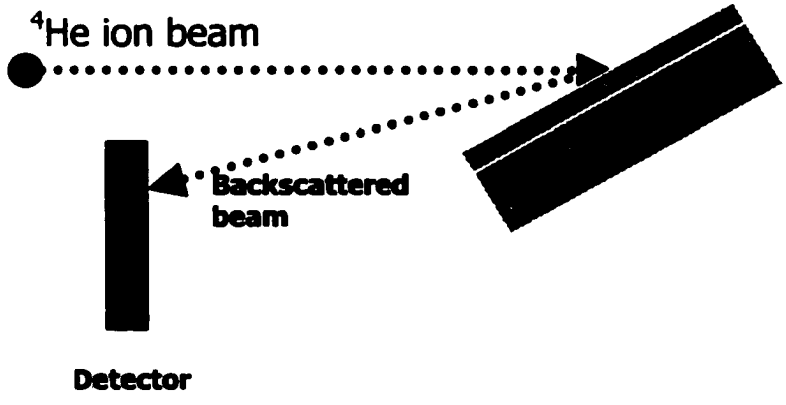

Figure 4.5: RBS angle resolved experiment used to determine location of contaminants. Rotating the sample holder 60° effectively doubles the thickness of the sample layers.

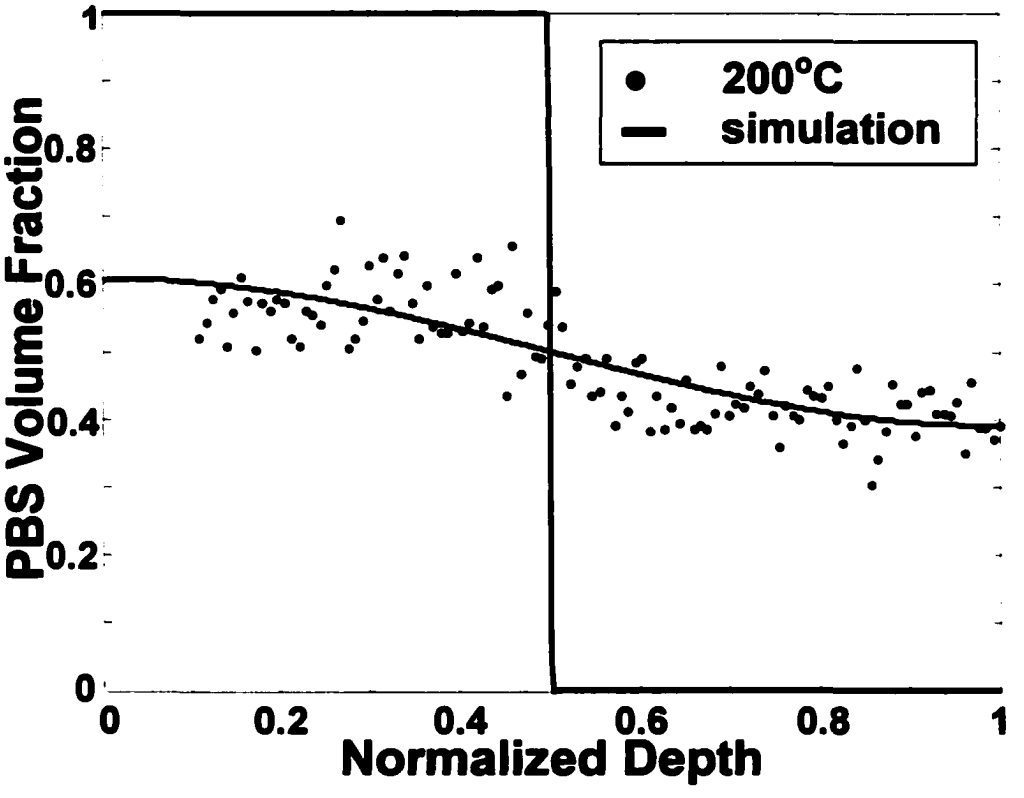

Figure 4.6: PBS volume fraction, ϕ v. normalized depth for PS/PBS bilayer (N = 424, f = 0.08) annealed at 200°C with theoretical fit, • 15m, — simulation.

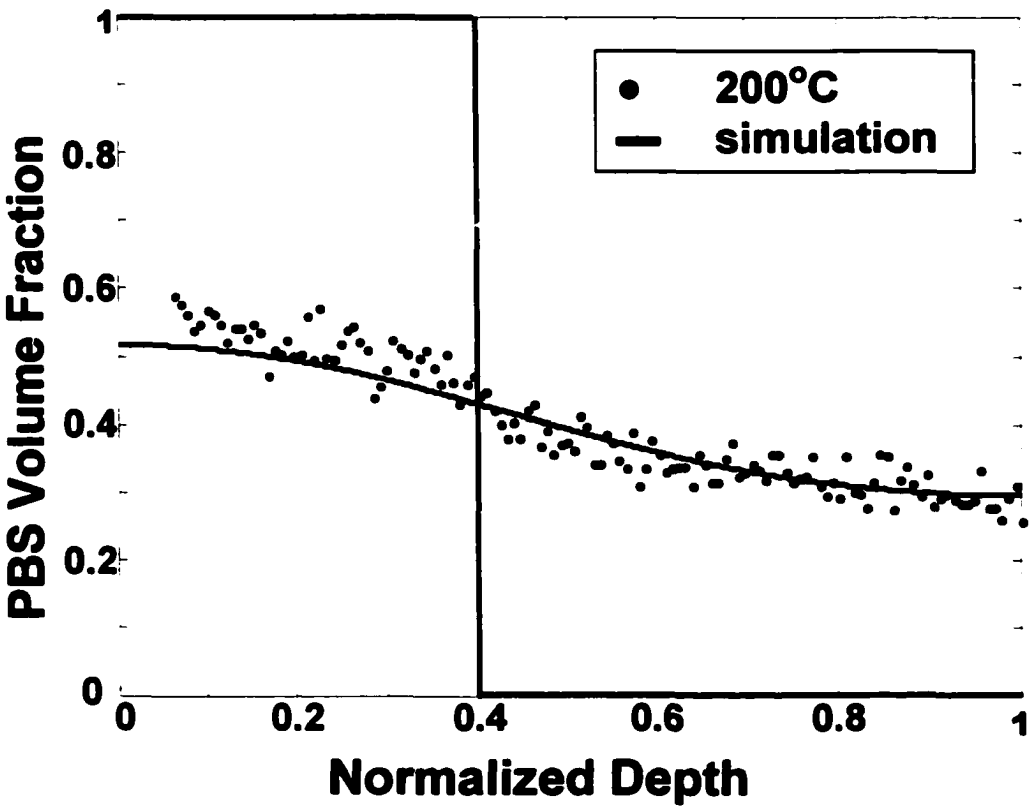

Figure 4.7: PBS volume fraction, ϕ, v. normalized depth (N = 424, f = 0.22) annealed at 200°C, • 15m, — simulation.

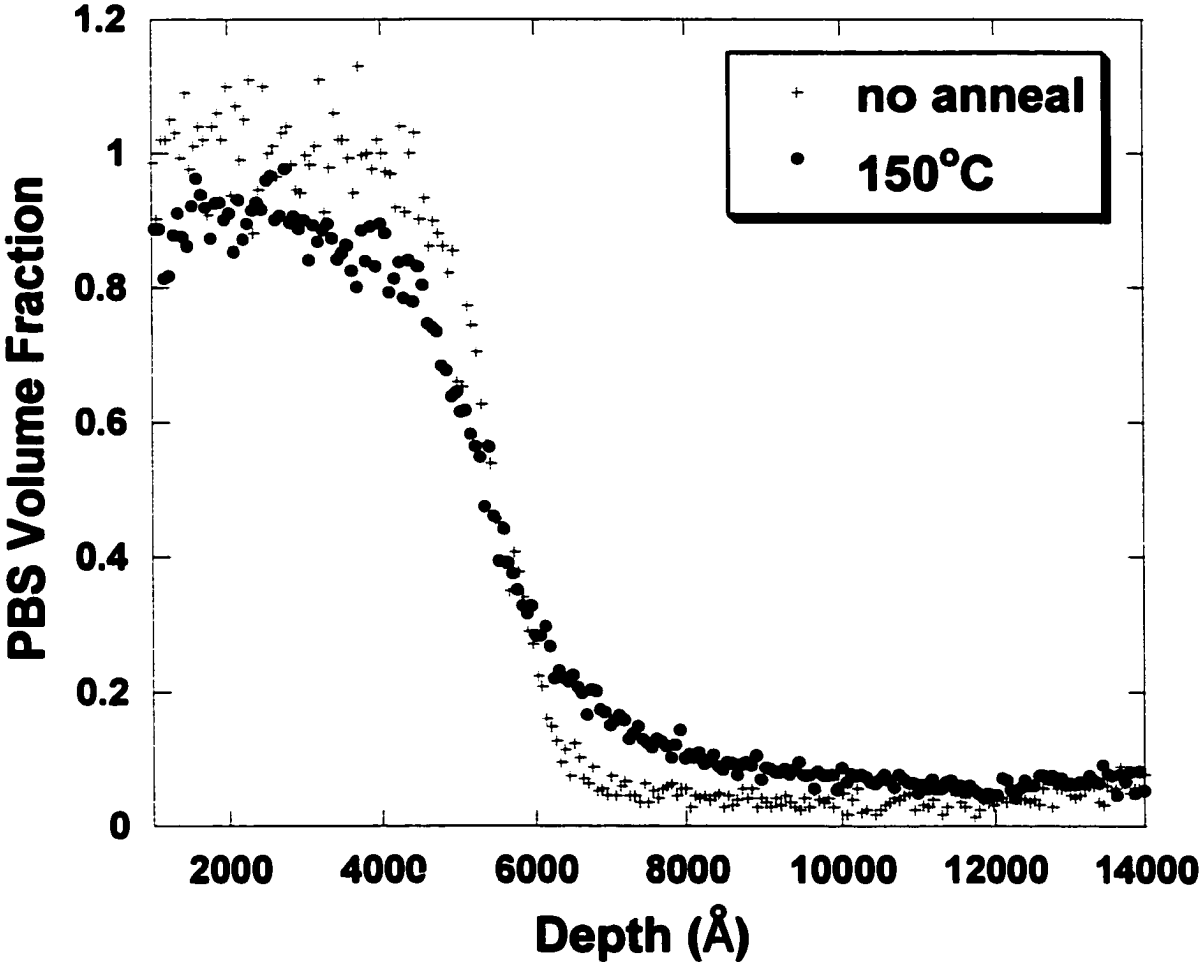

Figure 4.8a: PBS volume fraction v. depth profiles (N = 424, f = 0.28), ϕ v. z, annealed at 150°C, + no anneal, • 3 hour.

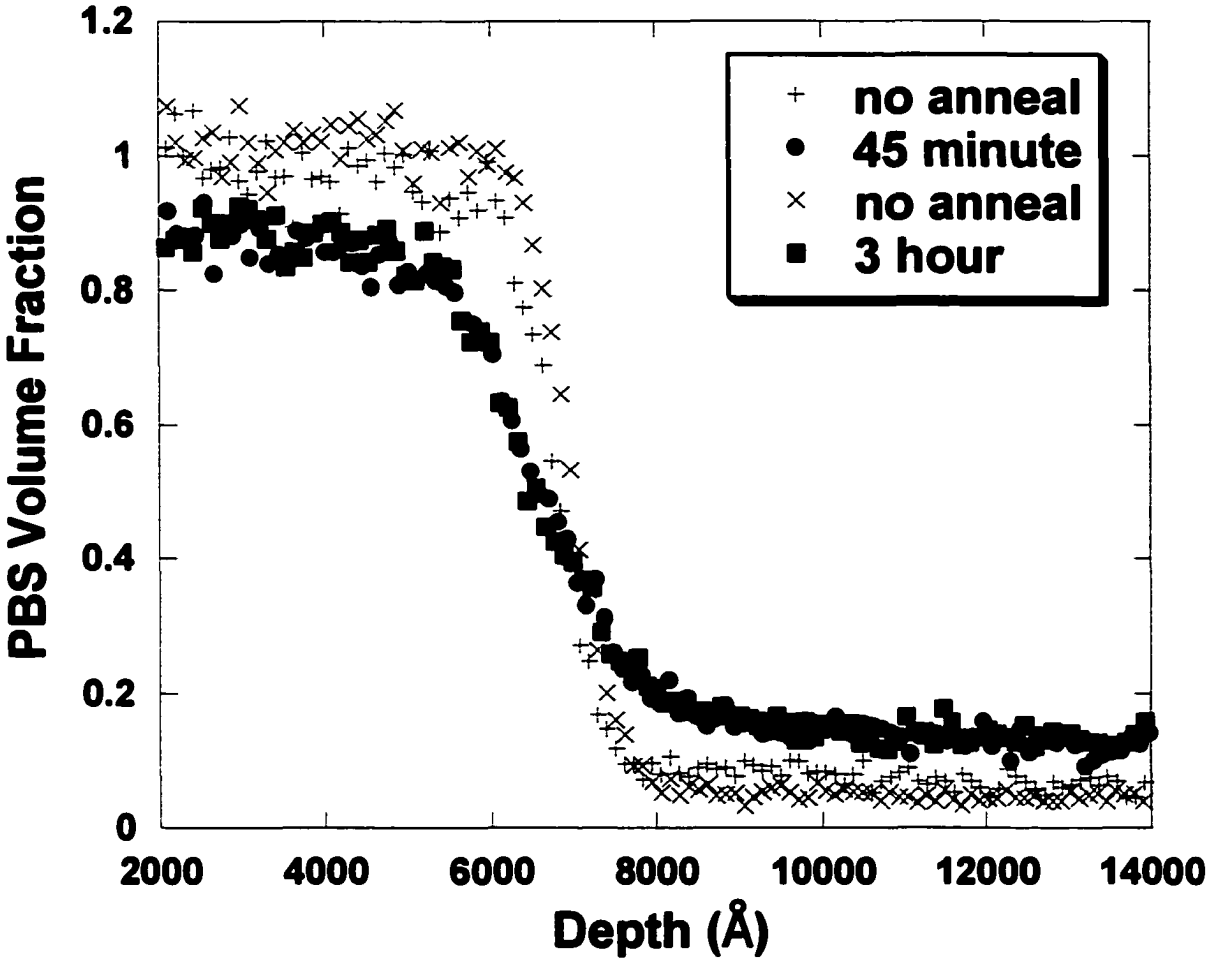

Figure 4.8b: PBS volume fraction v. depth profiles (N = 424, f = 0.28), ϕ v. z, annealed at 175°C, +, x no anneal, • 45 min., ■ 3 hour.

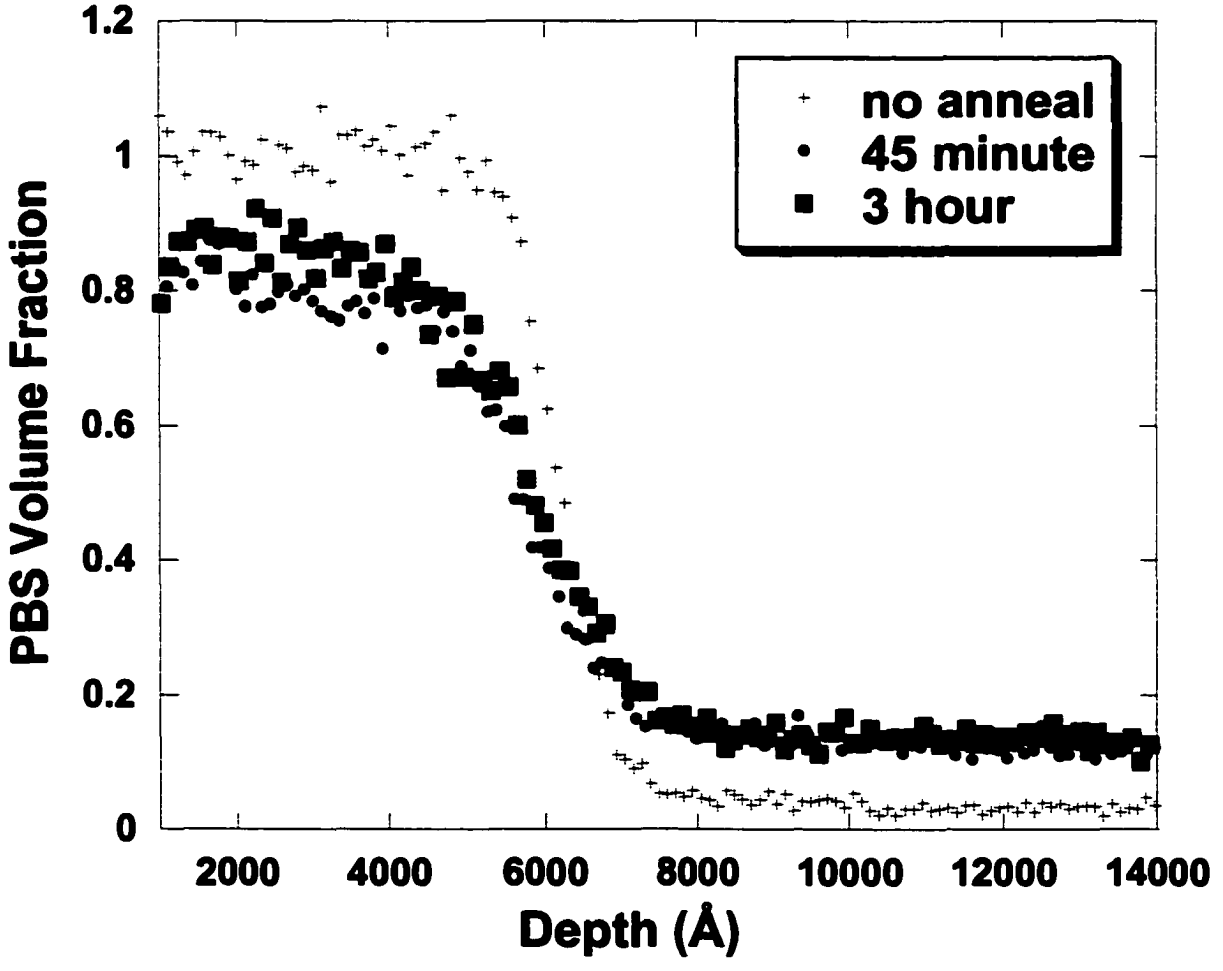

Figure 4.8c: PBS volume fraction v. depth profiles (N = 424, f = 0.28), ϕ v. z, annealed at 200°C, + no anneal, • 45 min., ■ 3 hour.

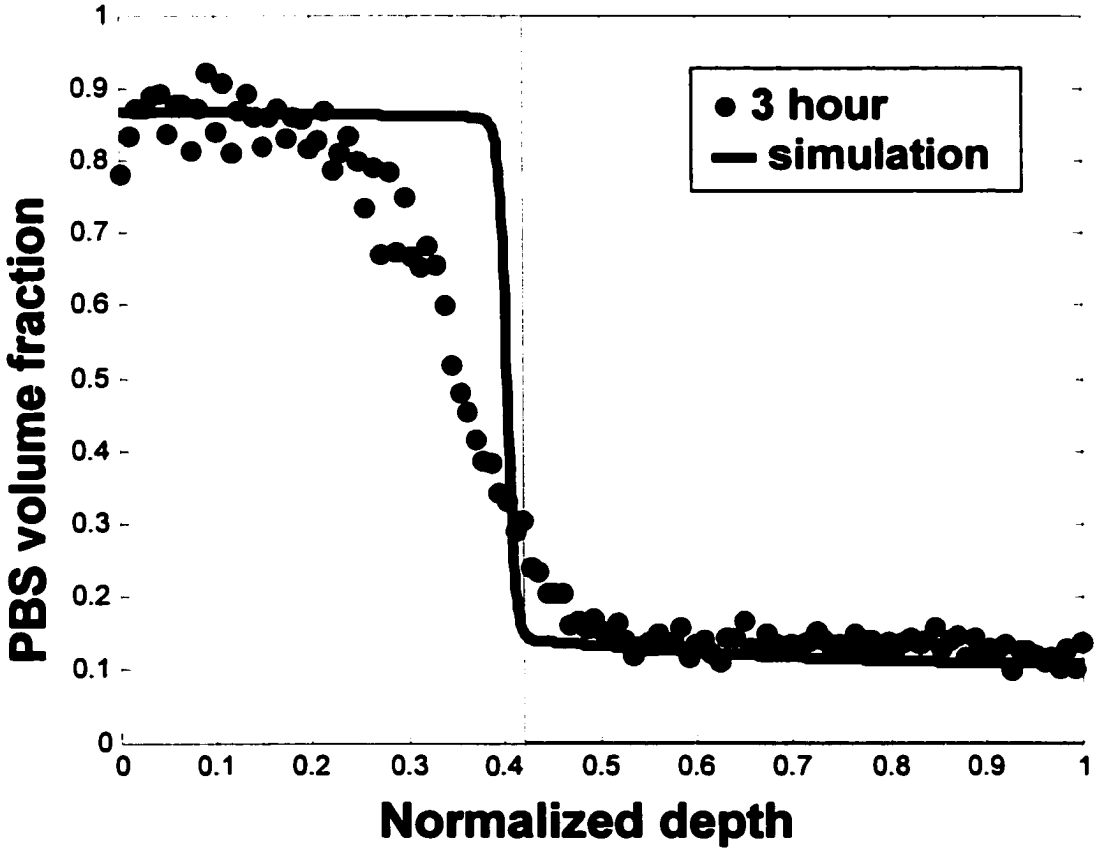

Figure 4.8d: PBS volume fraction, ϕ, v. normalized depth (N = 424, f = 0.28) annealed at 200°C, • 3 hour, — simulation using square-gradient modification.

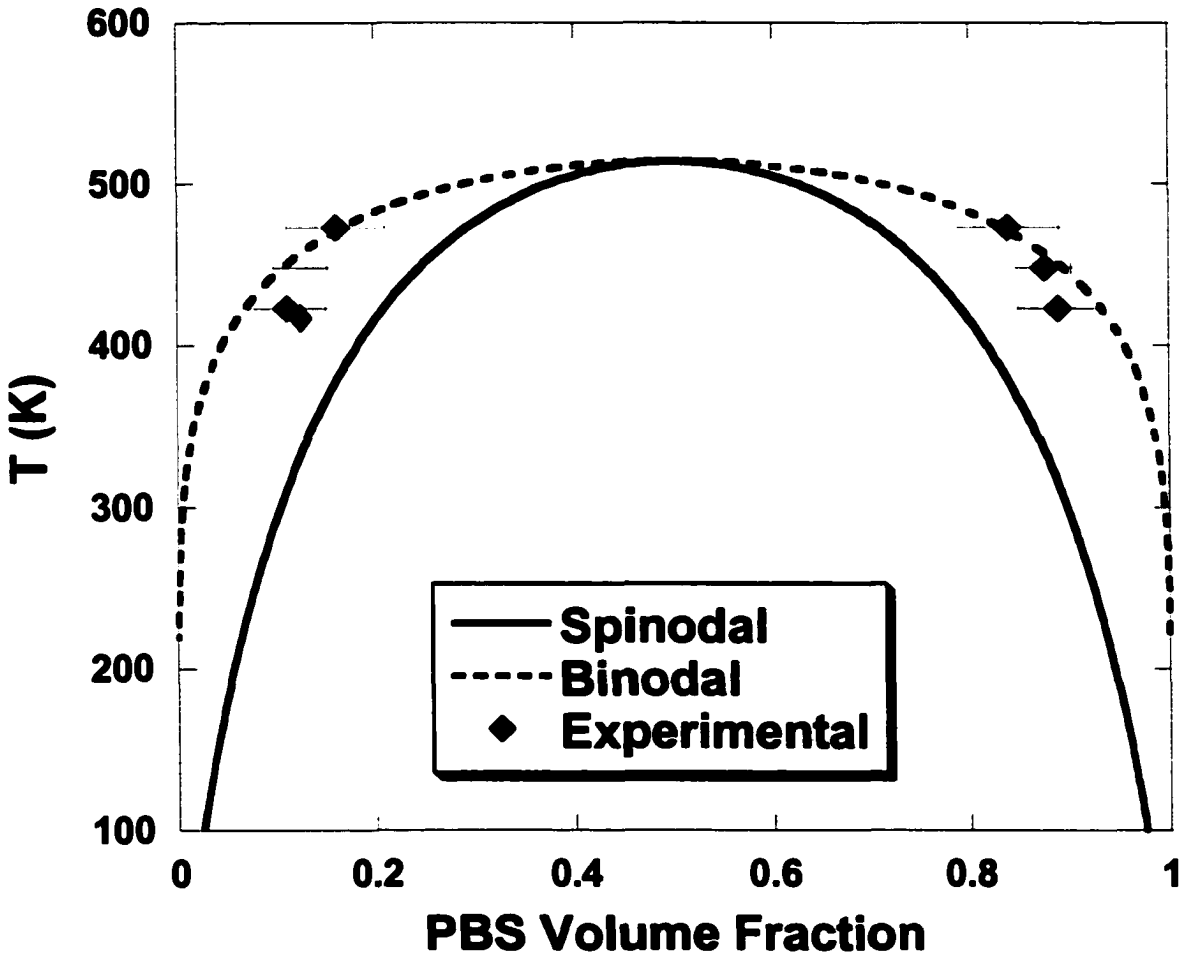

Figure 4.9: Phase diagram for PS/PBS system (N = 424, f = 0.28) predicted from Flory-Huggins theory using χ from SAXS[32]. The ♦ points represent binodal layer compositions obtained from RBS (Figures 4.8a, b, and c).

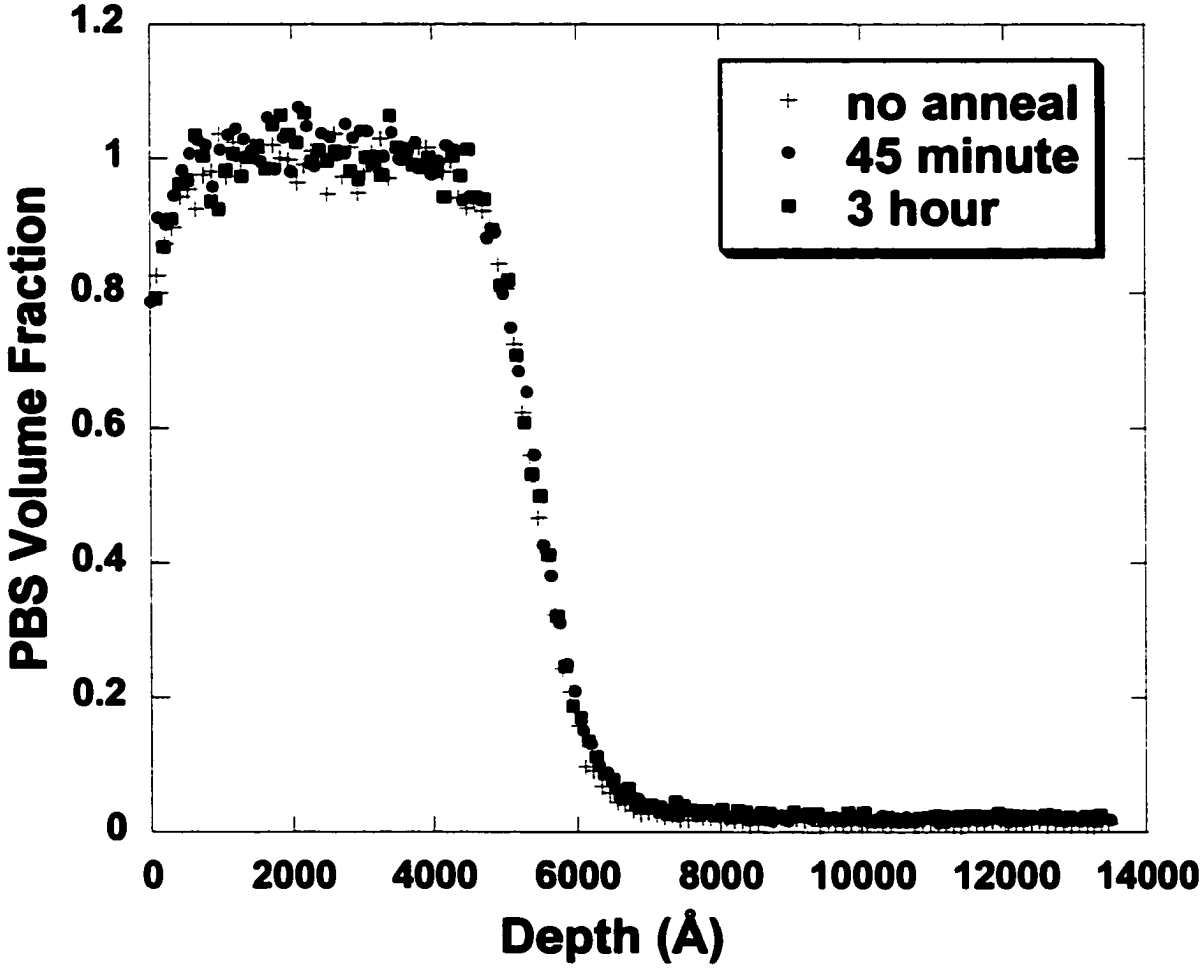

Figure 4.10: PBS volume fraction, ϕ, v. depth, z, (N = 424, f = 0.46), annealed at 200°C, + no anneal, • 45 m, ■ 3 hour.

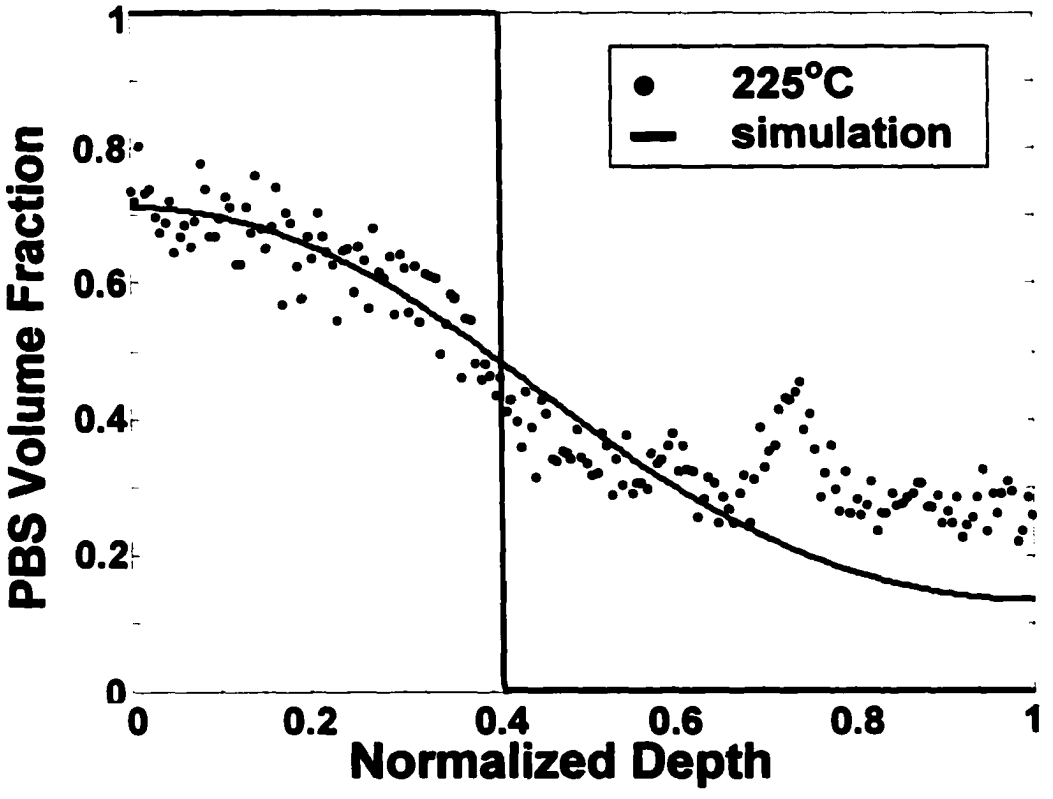

Figure 4.11: PBS volume fraction, ϕ, v. normalized depth (N = 1370, f = 0.09) annealed at 225°C, • 20 min., — simulation. The peak at 0.75 corresponds to a contaminant from the gold-coating procedure that resides on the surface and does not interfere with interdiffusion at the interface.

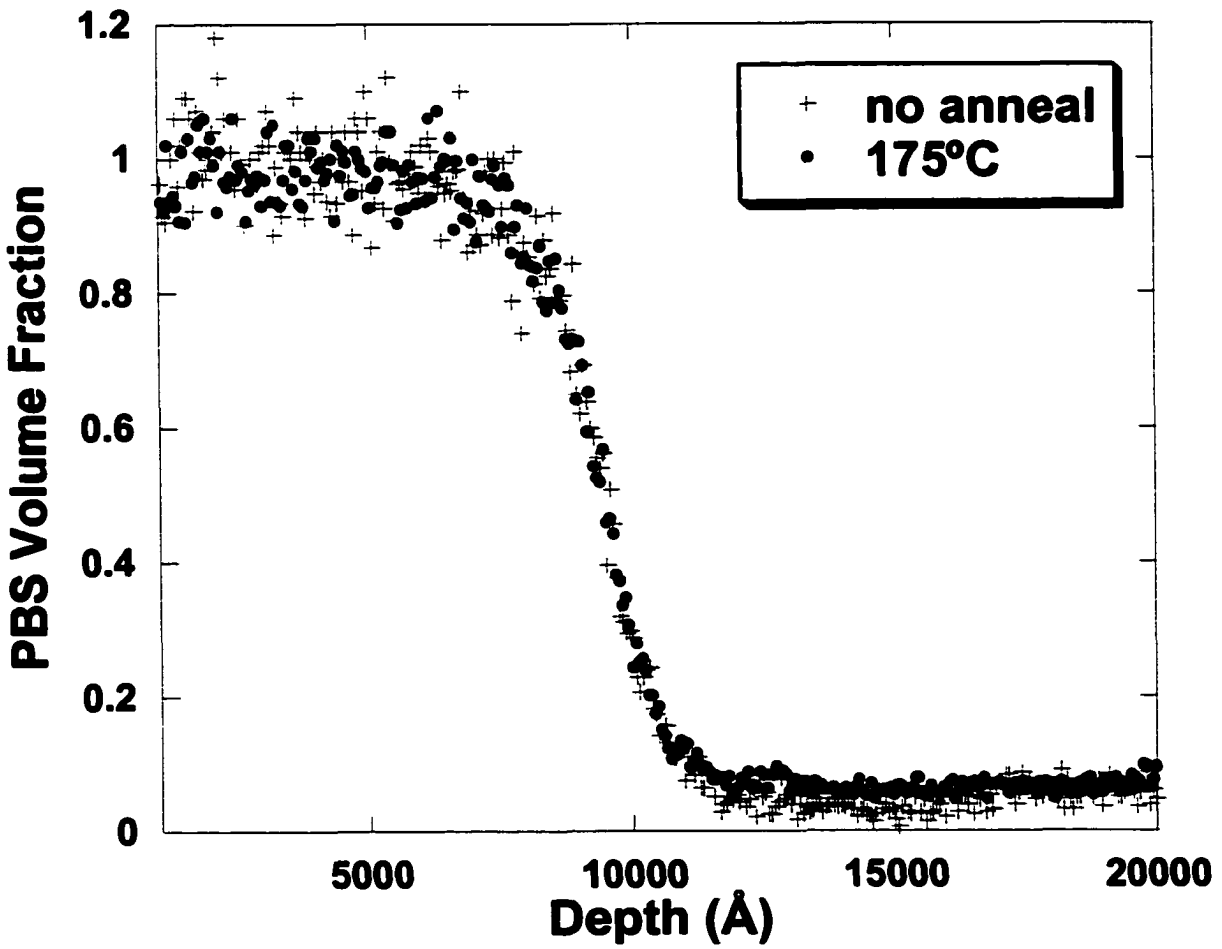

Figure 4.12a: PBS volume fraction v. depth profiles (N = 1370, f = 0.25). ϕ v. z, annealed at 175°C, + no anneal, • 3 hour.

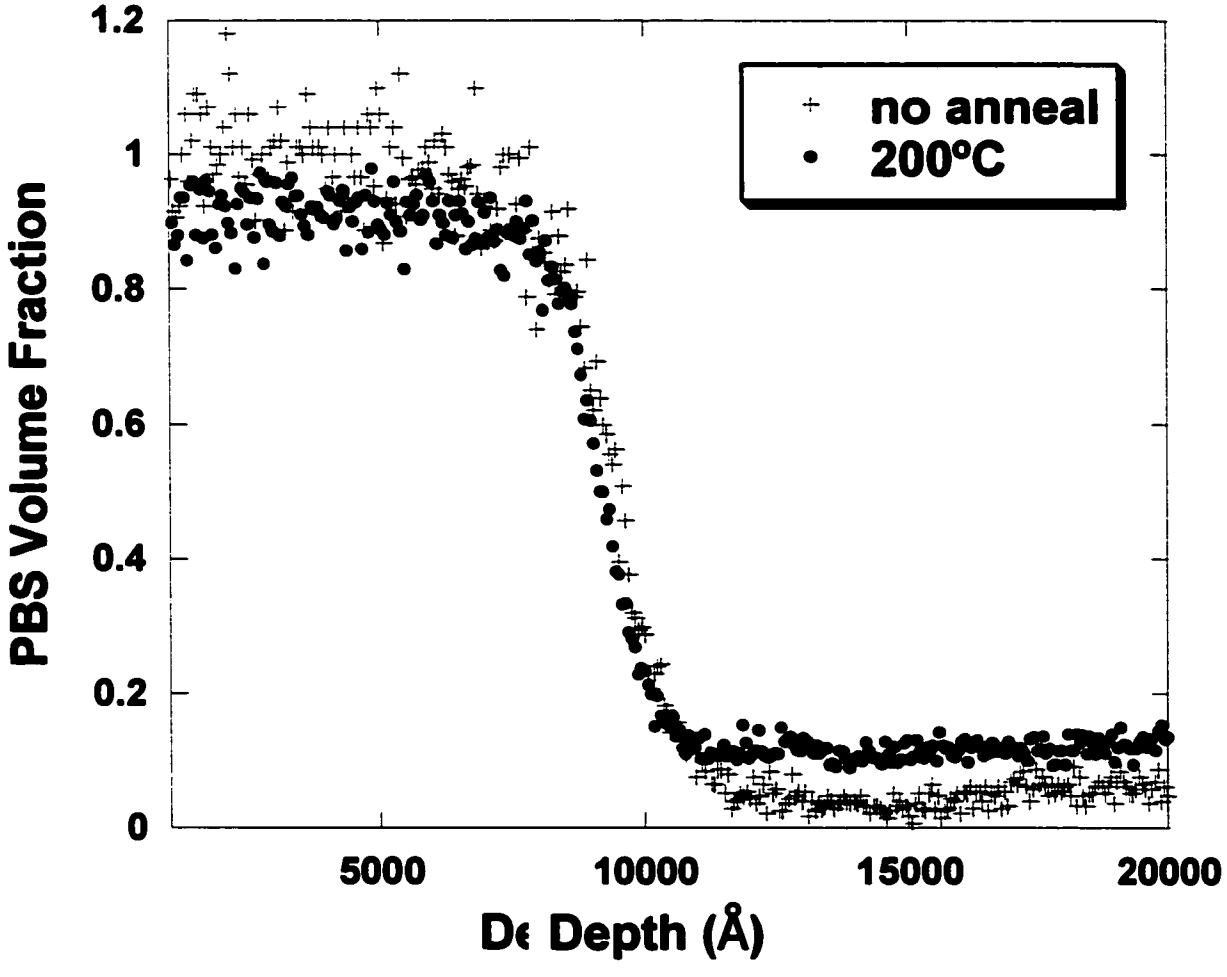

Figure 4.12b: PBS volume fraction v. depth profiles (N = 1370, f = 0.25). ϕ v. z, annealed at 200°C, + no anneal, • 45 min.

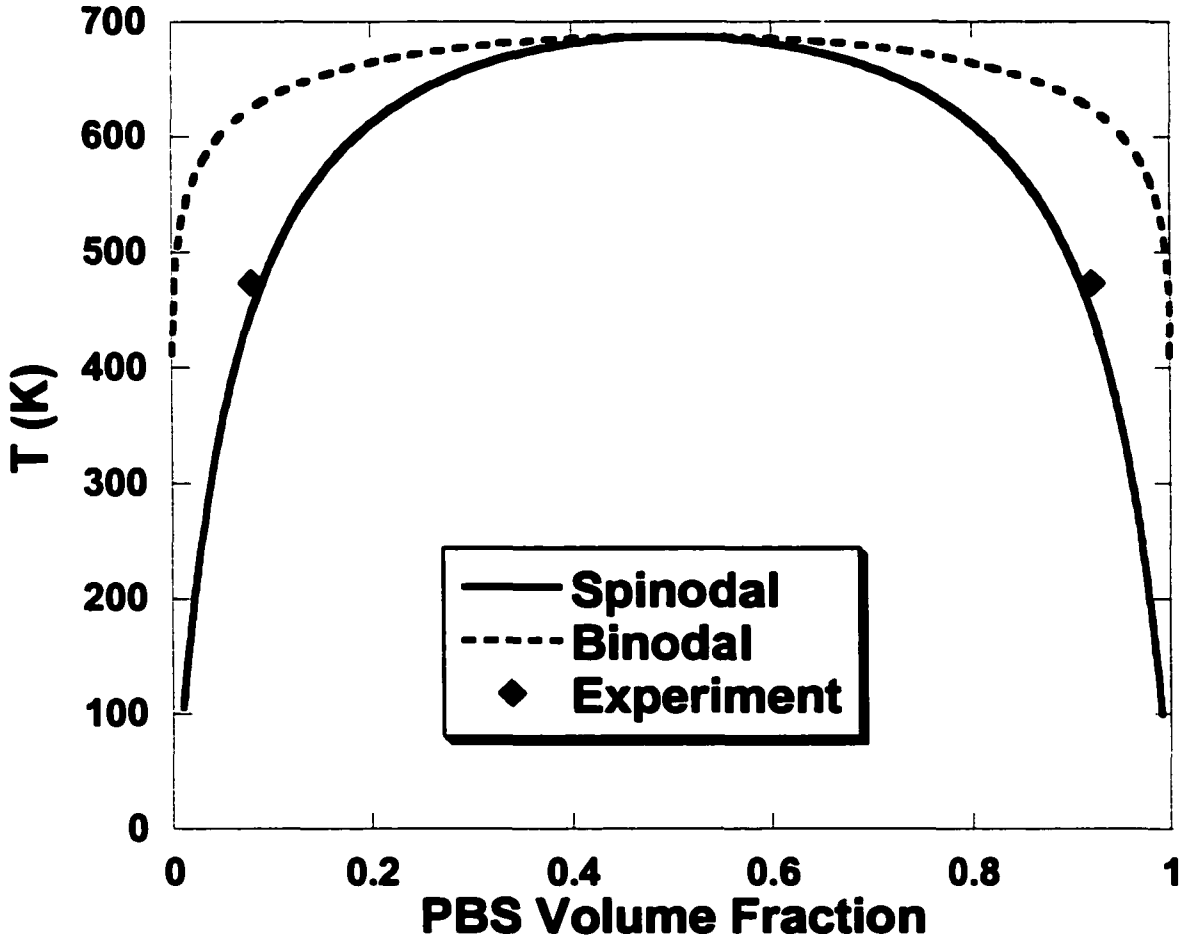

Figure 4.13: Phase diagram for PS/PBS system (N = 1370, f = 0.25) predicted from Flory-Huggins theory using χ from SAXS[32]. The ♦ points represent binodal layer compositions obtained from RBS (Figures 4.12a and b).

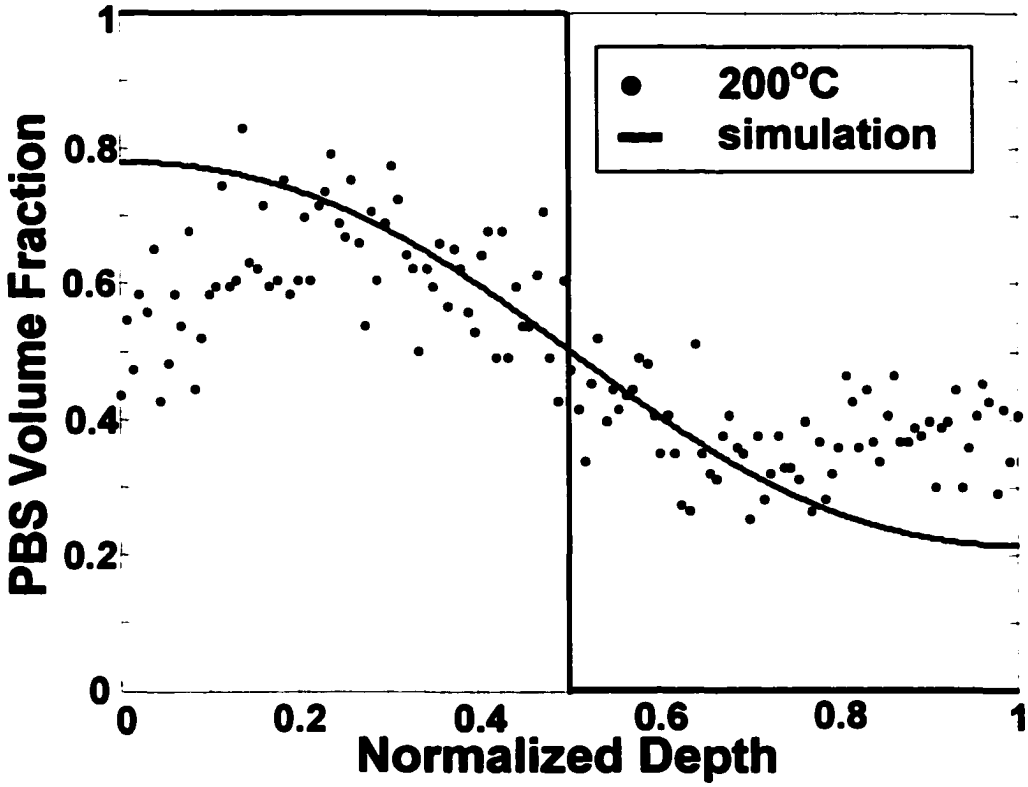

Figure 4.14a: PBS volume fraction ϕ, v. normalized depth profiles (N = 7670, f = 0.04). ϕ v. z, annealed at 200°C, • 3 hour, — simulation.

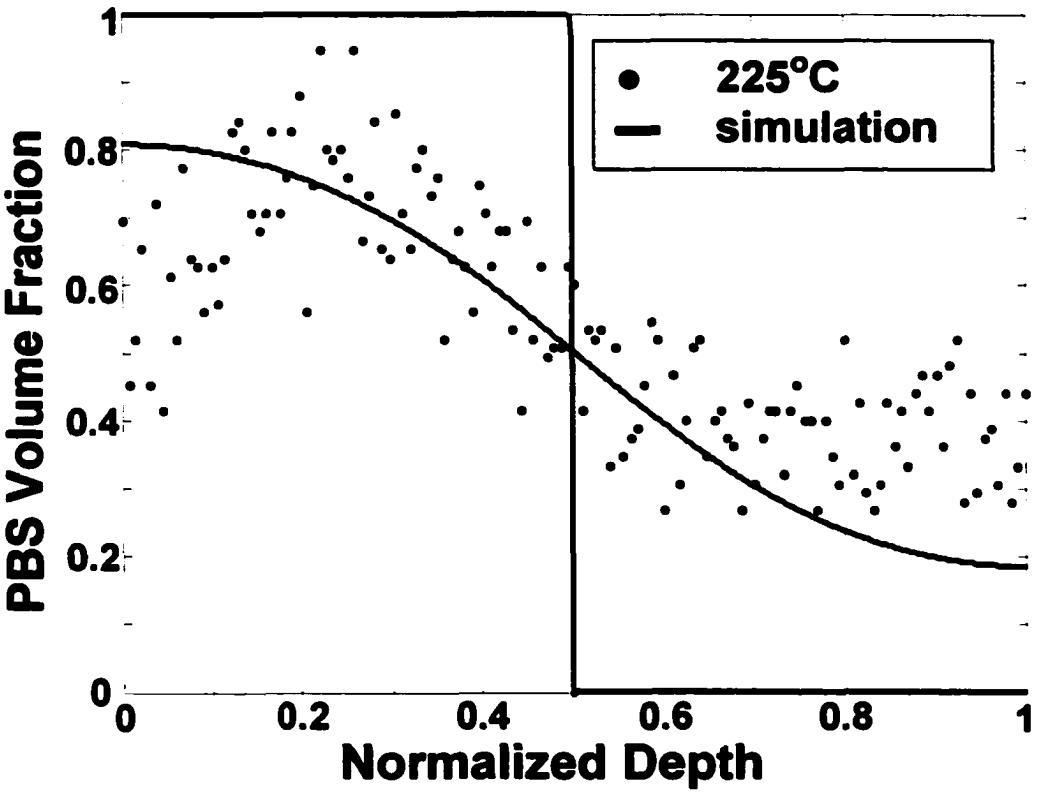

Figure 4.14b: PBS volume fraction ϕ, v. normalized depth profiles (N = 7670, f = 0.04). ϕ v. z, annealed at 225°C, • 45m, — simulation.

CHAPTER 5

INTERDIFFUSION IN PARTIALLY MISCIBLE N-ASYMMETRIC INTERFACES

5.1 Abstract

Interdiffusion in partially miscible polymer bilayers of polystyrene (PS) and the statistically random copolymer poly(styrene-*r*-4-bromostyrene) (PBS), $(C_8H_{(8-x)}Br_x)_N$, where x is the mole fraction of brominated repeat units in the copolymer and N the degree of polymerization, was studied using Rutherford backscattering spectroscopy (RBS). PS/PBS bilayers with $0.04 < x < 0.63$ and the ratio N_{PS}/N_{PBS} varied from $0.06 < N_{PS}/N_{PBS} < 18.1$ were examined. PBS volume fraction v. depth profiles were obtained from the evolution of the bromine peak in the RBS spectra. Tracer-diffusion coefficients were determined by comparison of the RBS data to a mean-field interdiffusion model based on fast mode theory. The mutual diffusion coefficient is shown to decrease with increasing degree of polymerization and extent of bromination of the PBS copolymer and increase with temperature. As spinodal conditions are approached, interdiffusion occurs until layer compositions indicative of the phase boundary are reached. These observations are in agreement with phase diagrams obtained using Flory-Huggins theory and a PS/PBS Flory-Huggins interaction parameter measured using small angle x-ray scattering (SAXS). For $N_{PS}/N_{PBS} \neq 1$, the interdiffusion is dictated by the faster diffusing component, in concurrence with fast mode theory, but limited by miscibility effects.

5.2 Introduction

Many polymer/polymer interfaces (and blends) are partially miscible, i.e., they have a Flory-Huggins interaction parameter, χ, near the spinodal interaction parameter, χ_S. Previously we discussed interdiffusion in partially miscible N-symmetric bilayers of monodisperse PS/PBS and showed excellent agreement with predicted phase diagrams.

This work explores the effect of miscibility on interdiffusion in partially miscible bilayer systems of polystyrene (PS) and the statistically random copolymer poly(styrene-*r*-4-bromostyrene) (PBS), $(C_8H_{(8-x)}Br_x)_N$, where x is the mole fraction of brominated repeat units in the copolymer and N is the degree of polymerization, using Rutherford backscattering spectroscopy (RBS). The mutual diffusion coefficient for the PS/PBS system at various f, the volume fraction of brominated repeat units in the copolymer, and N, is reported and the correlation with phase behavior in this system is discussed. Combinations of f and N designed to span a range of miscibility have been chosen; for given N_{PS} and N_{PBS}, system miscibility is controlled by f. Additionally, systems having the same f were studied for different values of the ratio N_{PS}/N_{PBS}. Phase diagrams for various extents of bromination and molecular weight have already been obtained and χ parameters have been measured using SAXS [1]. The PS/PBS systems, defined in terms of f, N_{PS}, and N_{PBS}, undergo phase transitions within the temperature range considered in this study [1]. In order to directly relate interdiffusion and phase behavior, identical polymers were used in the respective studies.

In order to describe interdiffusion in systems where there are chemically dissimilar species and/or a difference in molecular weight across the interface, theories have been

developed which take into account the molecular weight dependence of mobility as well as the interactions between the constituents across the interface. The fast and slow mode theories of interdiffusion were independently developed in an effort to elucidate the molecular weight dependence of the mutual diffusion coefficient, specifically the mechanism of interdiffusion when the polymers have very different mobility. Brochard-Wyart and co-workers [2] derived the slow mode theory for interdiffusion using the chemical potential as the driving force for interdiffusion (based on previous work by de Gennes in 1981 [3]) and assuming equal but opposite fluxes of the interdiffusing components and composition-independent monomer-monomer friction coefficients. The slow mode theory predicts that interdiffusion is dominated by the slower diffusing species [4]. The fast mode theory developed by Kramer and co-workers [5] predicts that, as interdiffusion proceeds, the interface in a system with polymers of different molecular weight moves toward the lower molecular weight polymer. Assuming that unequal fluxes of species A and B are balanced by a net flux of vacancies across the interface, fast mode theory describes interdiffusion dominated by the faster diffusing polymer. Most research, both experimental and computational, supports the validity of fast mode theory [6-11]. Akcasu has pointed out that there may be a "cooperative component" to the kinetic term of the mutual diffusion coefficient, and that this cooperation will represent the movement of the chains relative to each other due to interactions [6-8]. The theory proposed by Akcasu takes into account variable compressibility across the interface, thereby bridging the gap between the fast and slow mode theories.

5.3 Experimental Techniques

Monodisperse PS and PBS were obtained from Polymer Source, Inc (Dorval, Quebec). PBS was synthesized by the procedure described by Kambour and co-workers [12]. Table 5.1 lists relevant properties of the polymers used in this study. Characterization of the polymers and bilayer preparation has been described elsewhere. We define N-symmetric bilayers as having $N_{PS}/N_{PBS} = 1$; N-asymmetric bilayers have $N_{PS}/N_{PBS} \neq 1$. The method of RBS analysis has been given elsewhere (see Chapter 4).

5.4 Results and Discussion

The PS/PBS system is known to exhibit UCST behavior [13]. As previously reported, we have measured the interaction parameter $\chi_{S\text{-}BrS}$ between brominated and non-brominated styrene segments as

$$\chi_{S-BrS} = -0.0833 + \frac{73.75}{T} \tag{5.1}$$

where T is temperature reported in K. This expression assumes that $\chi_{S\text{-}BrS}$ is independent of composition, in agreement with previous studies [14]. The Flory-Huggins interaction parameter, χ, of a homopolymer, A, and a statistically random copolymer, A-B, is expressed as [15]

$$\chi = f^2 \chi_{AB} \tag{5.2}$$

Here f is the volume fraction of B repeat units in the random copolymer. Knowing the ratio of the molar volume of a styrene unit to that of a brominated styrene unit (0.862), f can be related to the extent of bromination, x, as

$$f = \frac{x}{x + 0.862(1-x)} \tag{5.3}$$

Fast mode v. slow mode theories of interdiffusion

The mutual diffusion across the interface between two polymeric species can be described as a product of a kinetic term involving the intrinsic (i.e., tracer) diffusion coefficients, degrees of polymerization, and compositions of the species, and a thermodynamic term that represents the driving force for mixing [16]. The thermodynamic term is given by $2\phi(1-\phi)(\chi_s - \chi)$ [17], where, for our system, ϕ is the volume fraction of PBS copolymer and χ_S is the interaction parameter at the spinodal, given by $\chi_S = \frac{1}{2}\left(\frac{1}{N_{PS}(1-\phi)} + \frac{1}{N_{PBS}\phi}\right)$. The mutual diffusion coefficient can be expressed as

$$D_M = 2D_0\phi(1-\phi)(\chi_s - \chi) \tag{5.4}$$

where D_0 is the kinetic term, a function of D_{PS} and D_{PBS}, the tracer-diffusion coefficients of PS and PBS (and hence temperature and degree of polymerization) and their relative compositions. It is important to note that the tracer-diffusion coefficient of the PBS copolymer is a function of the composition of the copolymer (f), but this dependence is expected to be weak for small f. For D_0 modeled according to the slow mode theory, the mutual diffusion coefficient, D_M, is given by:

$$D_{MS} = \left(\frac{N_{PS}D_{PS}N_{PBS}D_{PBS}}{N_{PS}D_{PS}(1-\phi) + N_{PBS}D_{PBS}\phi}\right)\left(\frac{\phi}{N_{PS}} + \frac{1-\phi}{N_{PBS}} - 2\phi(1-\phi)\chi\right) \tag{5.5}$$

where N_{PS} and N_{PBS} are the respective degrees of polymerization. The fast mode theory expression for the mutual diffusion coefficient, D_M, is given by:

$$D_{MF} = (\phi N_{PS} D_{PS} + (1-\phi) N_{PBS} D_{PBS}) \left(\frac{\phi}{N_{PS}} + \frac{(1-\phi)}{N_{PBS}} - 2\phi(1-\phi)\chi \right) \quad (5.6)$$

As mentioned before, the form of this equation leads to a mutual diffusion coefficient dominated by the faster moving component. It is instructive to note that the form of the thermodynamic component of the mutual diffusion coefficient is common to both theories. The mutual diffusion coefficients in the N-asymmetric miscible systems were fit using the fast-mode expression for mobility and a diffusion equation derived from the Flory-Huggins expression for free energy. Using this composition dependent D_M, profiles in the partially miscible PS/PBS system can be fit to a mean-field interdiffusion model given by

$$\frac{\partial \phi}{\partial t} = \frac{\partial}{\partial z} \left(D_M(\phi) \frac{\partial \phi}{\partial z} \right) \quad (5.7)$$

Here z is the spatial position (depth), and t, time. This equation was solved numerically using an implicit finite difference method and compared to the RBS data using both D_{PS} and D_{PBS} as fitting parameters. Unless otherwise stated, all profiles were fit using the fast mode definition for the mutual diffusion coefficient (Eq. 5.4).

Interdiffusion in N-asymmetric PS/PBS systems

All combinations of N, f, and T for the N-asymmetric samples studied are shown in Table 5.2. For N-asymmetric bilayers, we define a quantity $N^* = 2N_{PS}N_{PBS}/(N_{PS} + N_{PBS})$ that reduces to N when $N_{PS} = N_{PBS}$ and use the product $N^*\chi$ to quantify miscibility. The N-asymmetric data shows trends with degree of polymerization and extent of bromination that are consistent with those observed for the N-symmetric system. Many binodal situations were encountered for the combinations of N_{PS}, N_{PBS}, f, and T chosen.

Using N-asymmetric bilayers, it is straightforward to show the validity of fast mode versus slow mode theory. For example, in Figure 5.1, the system of N_{PS} = 4087, N_{PBS} = 1370, f = 0.09 at 200°C, is fit with both theories in turn, using the definition for D_M given in Eqs. 5.5 and 5.6. The slow mode theory (Figure 5.1b) gives a qualitatively different shape for the profile from that of fast mode theory (Figure 5.1a). The values of D_{PS} and D_{PBS}, from the fast mode fit, are 2.74 x 10^{-13} cm^2/s and 8.0 x 10^{-13} cm^2/s, which are reasonable when compared to the values of D_{PS} = 2.74 x 10^{-13} cm^2/s and 2.4 x 10^{-12} cm^2/s for the same N and T, respectively, from literature [18].

The first N-asymmetric system of study combined various values of N_{PS} (1370, 4087, 7670) with N_{PBS} = 424 and f = 0.08. All combinations of N_{PBS} = 424 with the various N_{PS} at this f are miscible for the temperature range of study, and most resulted in flat interdiffusion profiles (indicating complete interdiffusion) after only 30 minutes with the exception of the case where N_{PS} = 1370, T = 175°C. This profile with the fast mode fit is shown in Figure 5.2a. The values of D_{PS} and D_{PBS} obtained from this fit are 2.5 x 10^{-13} cm^2/s and 2.0 x 10^{-12} cm^2/s; consistent with the values obtained for the N-symmetric case and in agreement with expected values [18]. Figure 5.2b shows the situation when the degrees of polymerization of PS and PBS are reversed, i.e., N_{PS} = 424, N_{PBS} = 1370 with f = 0.09. The profiles show approximately the same extent of interdiffusion for the same annealing conditions (see Figure 5.2a). The values of D_{PS} and D_{PBS} from this fit are 2.0 x 10^{-12} cm^2/s and 2.5 x 10^{-13} cm^2/s, in agreement with the previous case.

The next system studied was N_{PBS} = 424, with increased extent of bromination (f = 0.22). In this case, all combinations with N_{PS} (as shown in Table 5.2) fall very near the phase

boundary. Figure 5.3 shows the result for N_{PS} = 1370 at three annealing temperatures; the composition of PBS in the PS layer at equilibrium is shown to increase with T, in agreement with UCST behavior. As the layers move toward compositions indicative of the phase boundary, it is also apparent that the interface is moving toward the faster diffusing component (as shown by the arrows) in conformity with fast mode theory. Another interesting aspect is that the composition of PBS in the PBS layer remains almost constant through a 50°C change in temperature; this is attributed to the marked asymmetry of the phase diagram (see Figure 5.4), which clearly shows that the slope $dT/d\phi$ is much higher in the PBS-rich region.

Figures 5.5 and 5.6 show cases where the PS and PBS layers are such that the degrees of polymerization are reversed, i.e., for a given value of f (f = 0.22), Figure 5.5a shows the interdiffusion profile when N_{PBS}/N_{PS} = 0.055; the corresponding phase diagram is shown in Figure 5.5b. Figure 5.6 shows the converse, N_{PS}/N_{PBS} = 0.059, with the interdiffusion profile shown in Figure 5.6a and phase diagram in Figure 5.6b. Once again, the interface moves toward the faster diffusing species and the equilibrium compositions of the respective layers lie very near the phase boundary (the **x** marks are a guide for the eye).

Figure 5.7 shows the miscible N-asymmetric system of N_{PS} = 4087, N_{PBS} = 7144, f = 0.04 at 225°C; the scatter in the data is due to the very low value of f for this system. The value of D_{PBS} obtained from fitting this data to fast mode theory is $D_{PBS} = 3.6 \times 10^{-13}$ cm^2/s. This value is in excellent agreement with the value obtained for the N-symmetric case of N = 7670, f = 0.04 previously reported (see Chapter 4). This result supports the validity of using the fast mode theory approach to model both N-symmetric and N-asymmetric data.

The results of the N-asymmetric studies are summarized in Table 5.2 and show the effect of both the thermodynamic (miscibility) and kinetic (mobility) arguments on the overall mutual diffusion coefficient. An important consequence of the results of both the N-symmetric (see Chapter 4) and N-asymmetric studies is that when χ is small and approaching χ_s, the interfacial width shows sufficient broadening to be measured. Specifically, it should be noted that from the N-symmetric studies, an understanding of the thermodynamic effects was gained without being convoluted with variable mobility in the system. With that knowledge, the studies of N-asymmetric bilayers reported here show the relationship between miscibility, mobility, and overall interdiffusion behavior. Another interesting point is that regardless of the starting position of the interface in partially miscible systems, the equilibrium compositions will always correspond to binodal concentrations.

5.5 Conclusions

Mutual diffusion coefficients for partially miscible N-asymmetric PS/PBS systems were calculated by comparison of interdiffusion data from RBS spectra to a mean-field interdiffusion model using the fast mode expression for mobility and the Flory-Huggins expression for free energy. The results indicate that the mutual diffusion coefficient increases with temperature and decreases with increasing degree of polymerization and extent of bromination in the PBS copolymer. We also observed limited interdiffusion in systems where binodal conditions were approached; layer compositions from the RBS data agreed with values expected from the binodal curve of the phase diagrams predicted using Flory-Huggins theory and an interaction parameter measured using SAXS [1].

5.6 References

1. Gorga, R.E., et al., *Quantifying Phase Behavior in Partially Miscible Polystyrene/ Poly (styrene-co-4-bromostyrene) Blends.* Journal of Polymer Science: Part B, Polymer Physics, 2002. **40**: p. 255-271.
2. Brochard, F., J. Jouffroy, and P. Levinson, *Polymer-Polymer Diffusion in Melts.* Macromolecules, 1983. **16**: p. 1638-1641.
3. de Gennes, P.G., C. R. S. Acad. Sci., Ser. 2, 1981, p. 1505-7.
4. Jabbari, E. and N.A. Peppas, *Comparison of Interdiffusion at Polystyrene-Poly(vinyl methyl ether) and Polystyrene-Poly(isobutyl vinyl ether) Interfaces.* Polymer International, 1995. **38**: p. 65-69.
5. Kramer, E.J., P. Green, and C.J. Palmstrom, *Interdiffusion and Marker Movements in Concentrated Polymer-polymer Diffusion Couples.* Polymer, 1984. **25**(4): p. 473-480.
6. Akcasu, A.Z., *On the "FAST" and "SLOW" Mode Theories of Interdiffusion: the Current Theoretical Situation.* Polym Mater Sci Eng, 1994. **71**: p. 771.
7. Akcasu, A.Z., *The Fast and Slow Mode Theories of Interdiffusion in Polymer Mixtures. Resolution of a Controversy.* Macrmolecular Theory Simul., 1997. **6(4)**: p. 679-702.
8. Akcasu, A.Z., G. Naegele, and R. Klein, *Remarks on the "Fast" and "Slow" Mode Theories of Interdiffusion.* Macromolecules, 1995. **28**(19): p. 6680-6683.
9. Jabbari, E. and N.A. Peppas, *Use of ATR-FTIR to Study Interdiffusion in Polystyrene and Poly(vinyl methyl ether).* Macromolecules, 1993. **26**(9): p. 2175-2186.

10. Jabbari, E. and N.A. Peppas, *A Model for Interdiffusion at Interfaces of Polymers with Dissimilar Physical Properties.* Polymer, 1995. **36**(3): p. 575-586.

11. Meier, H. and G.R. Strobl, *Small-Angle X-ray Scattering Study of Spinodal Decomposition in Polystyrene/ Poly (styrene-co-bromostyrene) Blends.* Macromolecules, 1987. **20**: p. 649-654.

12. Kambour, R.P. and J.T. Bendler, *Miscibilities in Monodisperse Mixtures of Polystyrene, Poly(p-bromostyrene) and Their Copolymers.* Macromolecules, 1986. **19**: p. 2679-2682.

13. Kambour, R.P., J.T. Bendler, and R.C. Bopp, *Phase Behavior of Polystyrene, Poly(2,6-dimethyl-1,4-phenyl oxide) and Their Brominated Derivatives.* Macromolecules, 1983. **16**: p. 753-757.

14. Koch, T. and G.R. Strobl, *Concentration Dependence of the Flory-Huggins Interaction Parameter of a Polymer Blend as Determined by SAXS Experiments.* J. Polymer Science: Part B: Polymer Physics, 1990. **28**: p. 343-353.

15. Bruder, F. and R. Brenn, *Measuring the Binodal by Interdiffusion in Blends of Deuterated Polystyrene and Poly (styrene-co-4-bromostyrene).* Macromolecules, 1991. **24**: p. 5552-5557.

16. Binder, K., *Collective Diffusion, Nucleation, and Spinodal Decomposition in Polymer Mixtures.* J. Chem. Phys., 1983. **79**(12): p. 6387-6409.

17. Jabbari, E. and N.A. Peppas, *Polymer-polymer Interdiffusion and Adhesion.* J. M. S. - Rev. Macromol. Chem. Phys., 1994. **C34**(2): p. 205-241.

18. Tirrell, M., Rubber Chemistry and Technology, 1984. **57**: p. 523-556.

Table 5.1. Degree of polymerization, extent of bromination, and polydispersity of PS/PBS system.

$(C_8H_{(8-x)}Br_x)_N$			
N	x	f	M_w/M
424	0	0	1.03
	0.07	0.08	
	0.20	0.22	
	0.25	0.28	
	0.42	0.46	
	0.63	0.66	
1370	0	0	1.03
	0.08	0.09	
	0.22	0.25	
	0.39	0.43	
	0.51	0.55	
4087	0	0	1.04
	0.25	0.28	
	0.43	0.47	
	0.59	0.63	
7670	0	0	1.05
7144	0.04	0.04	1.1
	0.20	0.22	
	0.48	0.52	

Table 5.2. Mutual diffusion coefficient, D_M, for N-asymmetric PS/PBS systems: D_M and $N^*\chi$ reported at 200°C; D_M evaluated at $\phi = 0.5$.

N_{PS}	N_{PBS}	f	T range (°C)	$N^*\chi$	D_M (cm^2/s)
1370	424	0.08	175-225	0.30	1.9×10^{-12}
4087			200-225	0.36	1.5×10^{-12}
7670			200-225	0.37	1.2×10^{-12}
1370	424	0.22	175-225	2.27	Binodal
4087			200-225	2.70	Binodal
7670			200-225	2.82	Binodal
424	1370	0.09	175-225	0.38	1.8×10^{-12}
4087			200-250	1.21	2.0×10^{-13}
7670			200-250	1.37	1.1×10^{-13}
424	1370	0.25	175-225	2.94	Binodal
4087			200-250	9.31	ND
7670			200-250	10.54	ND
424	7144	0.04	200-225	0.09	1.4×10^{-12}
1370			200-250	0.27	3.0×10^{-13}
4087			200-250	0.60	1.1×10^{-13}
424	7144	0.22	200-225	2.81	Binodal
1370			200-250	8.08	ND
4087			200-250	18.26	ND

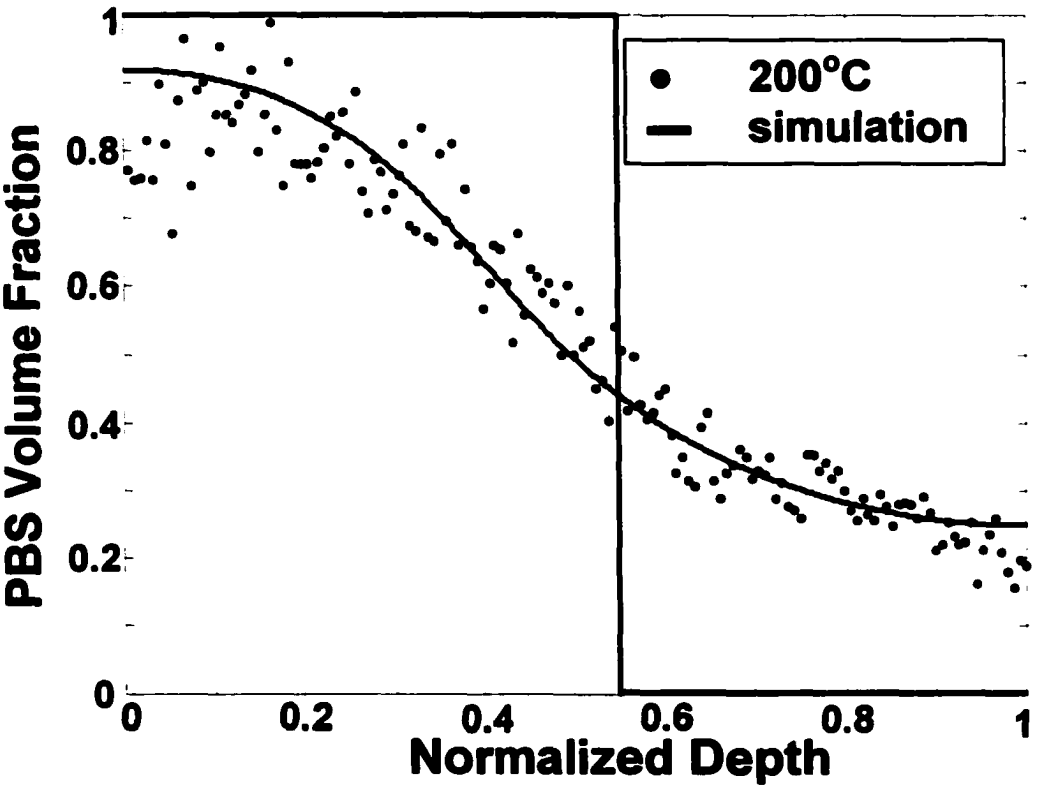

Figure 5.1a: Comparison of fast mode theory to slow mode theory. PBS volume fraction, ϕ, v. normalized depth profiles (N_{PS} = 4087, N_{PBS} = 1370, f = 0.09) annealed at 200°C. Fast mode fit, • 30 min, — simulation.

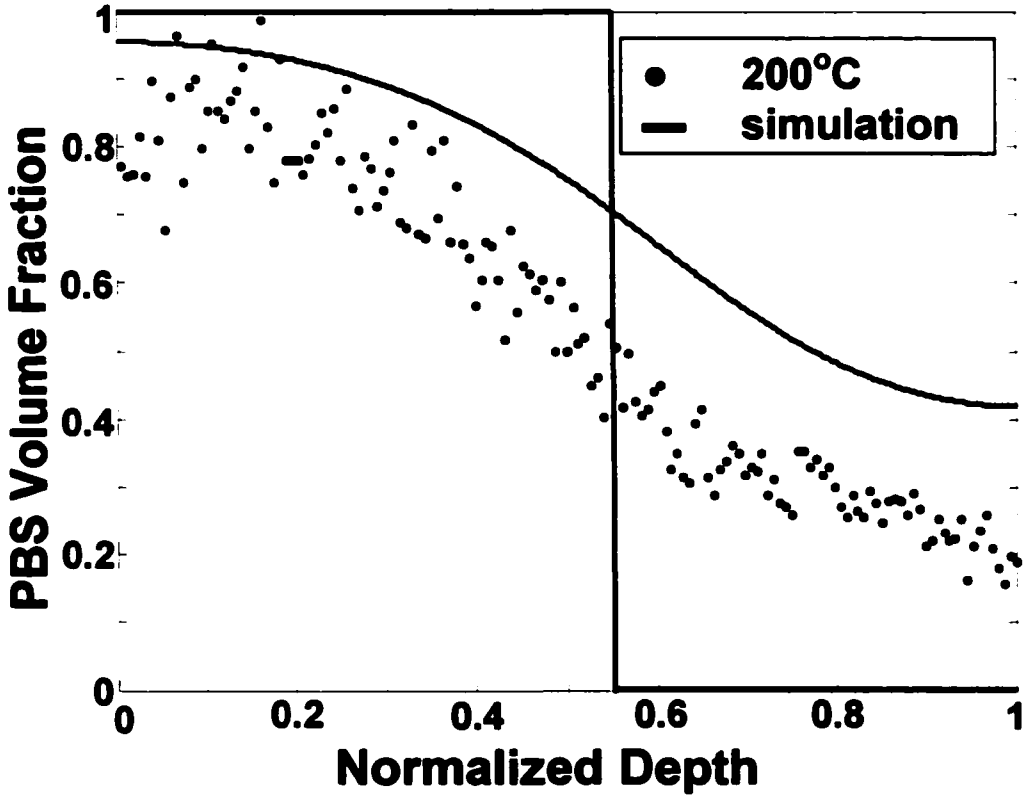

Figure 5.1b: Comparison of fast mode theory to slow mode theory. PBS volume fraction, ϕ, v. normalized depth profiles (N_{PS} = 4087, N_{PBS} = 1370, f = 0.09) annealed at 200°C. Slow mode fit, • 30 min, — simulation.

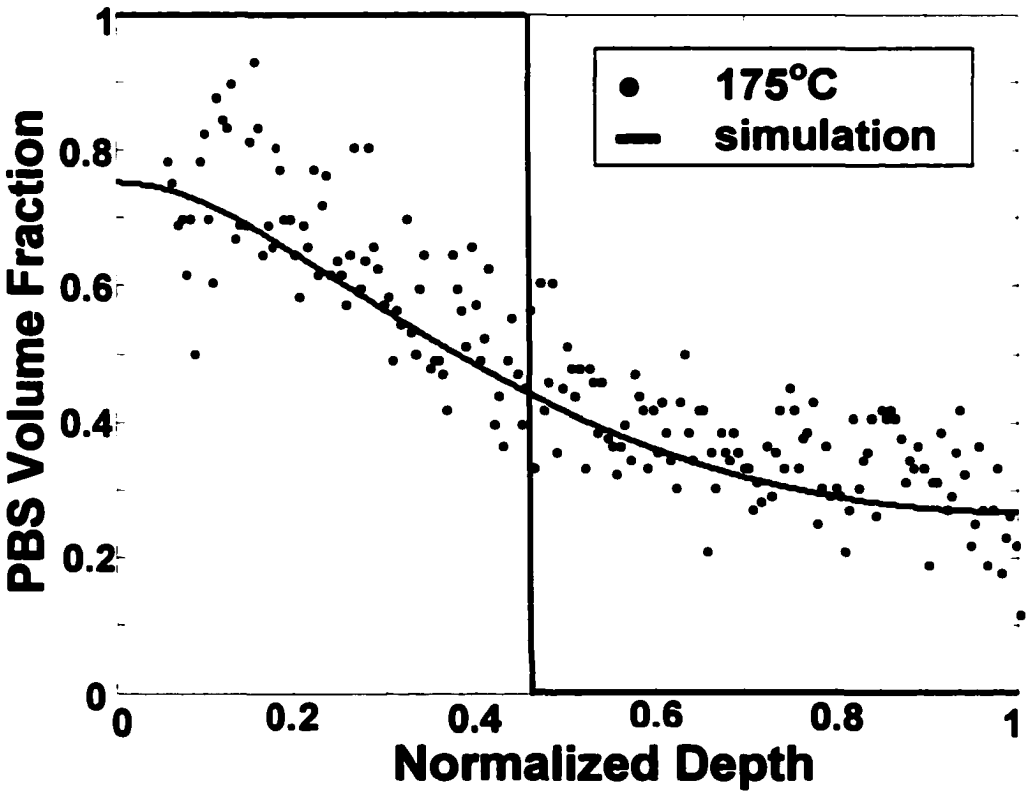

Figure 5.2a: PBS volume fraction, ϕ, v. normalized depth profiles for N-asymmetric PS/PBS systems. $N_{PS} = 1370$, $N_{PBS} = 424$, $f = 0.08$, annealed at 175°C, • 30 min, — simulation.

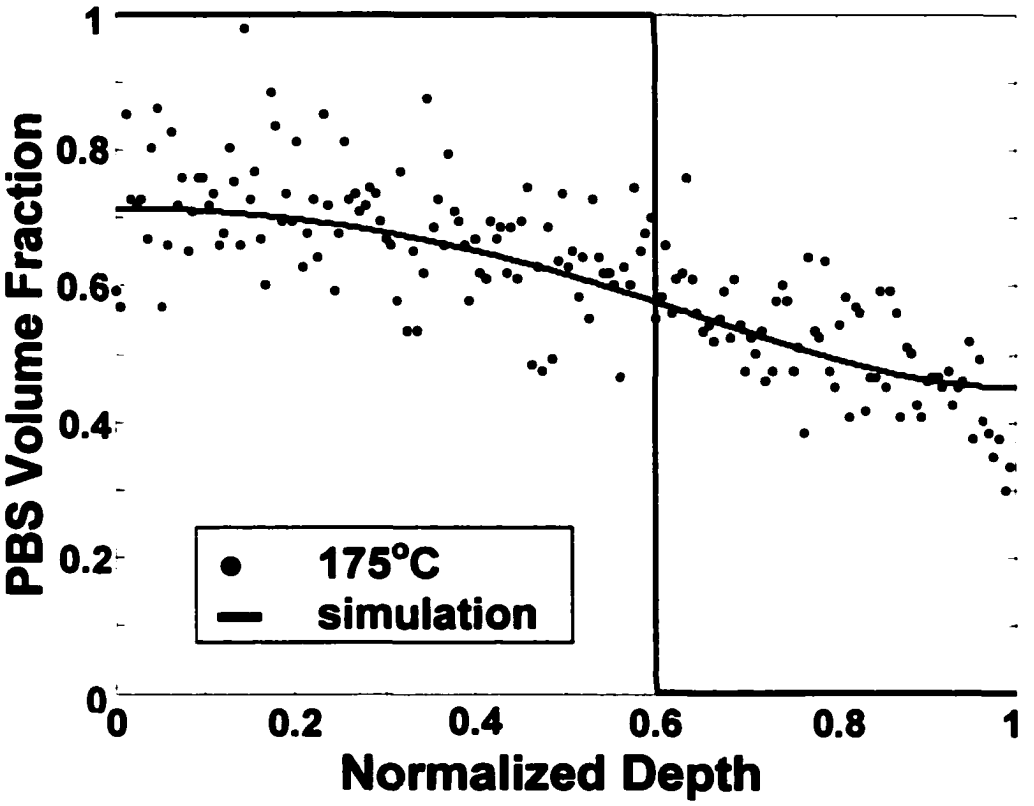

Figure 5.2b: PBS volume fraction, ϕ, v. normalized depth profiles for N-asymmetric PS/PBS systems. $N_{PS} = 424$, $N_{PBS} = 1370$, $f = 0.09$, annealed at 175°C, • 30 min, — simulation.

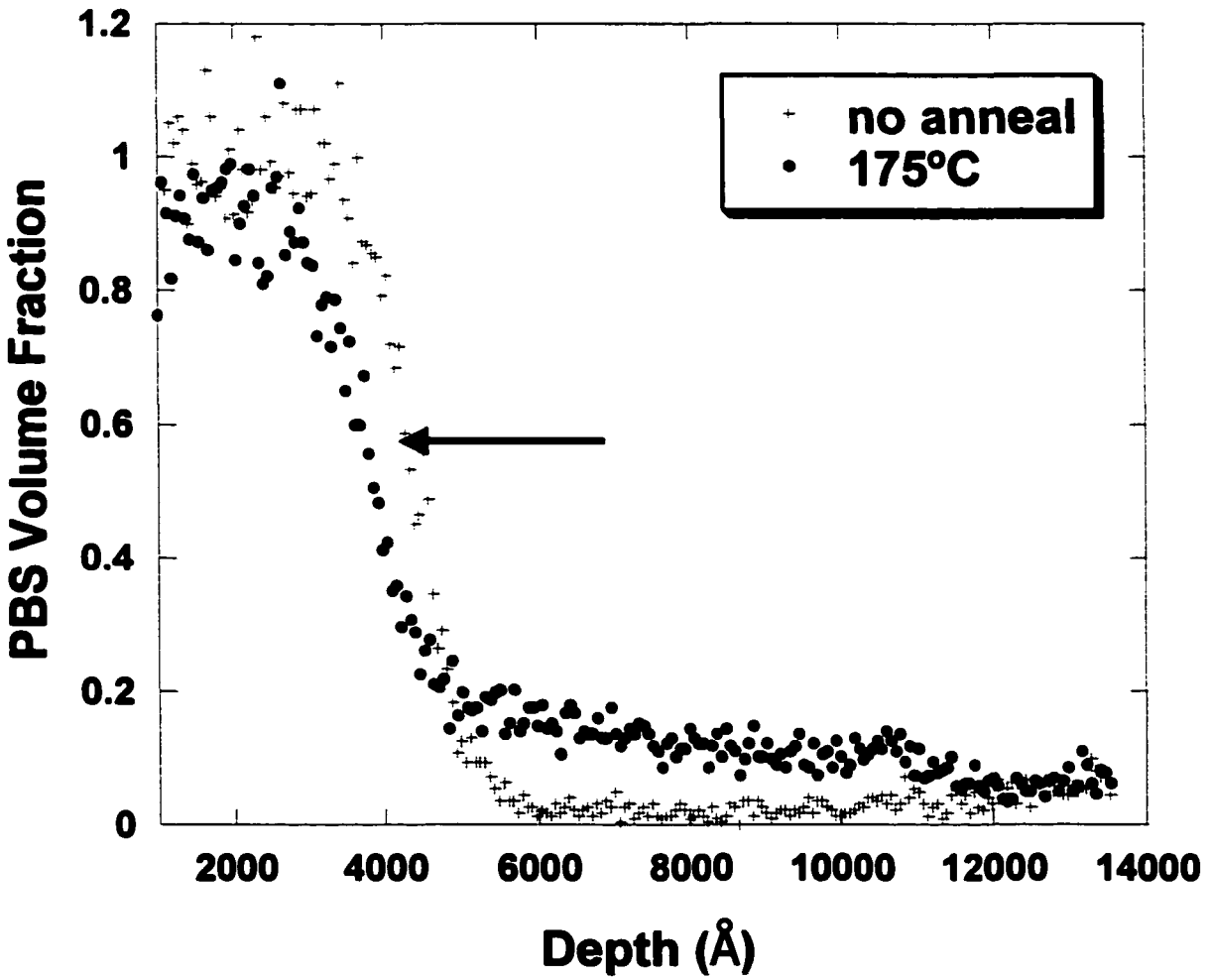

Figure 5.3a: PBS volume fraction, ϕ, v. normalized depth profiles for N-asymmetric PS/PBS bilayers near the binodal (N_{PS} = 1370, N_{PBS} = 424, f = 0.22). ϕ v. z, annealed at 175°C, + no anneal, • 30 min.

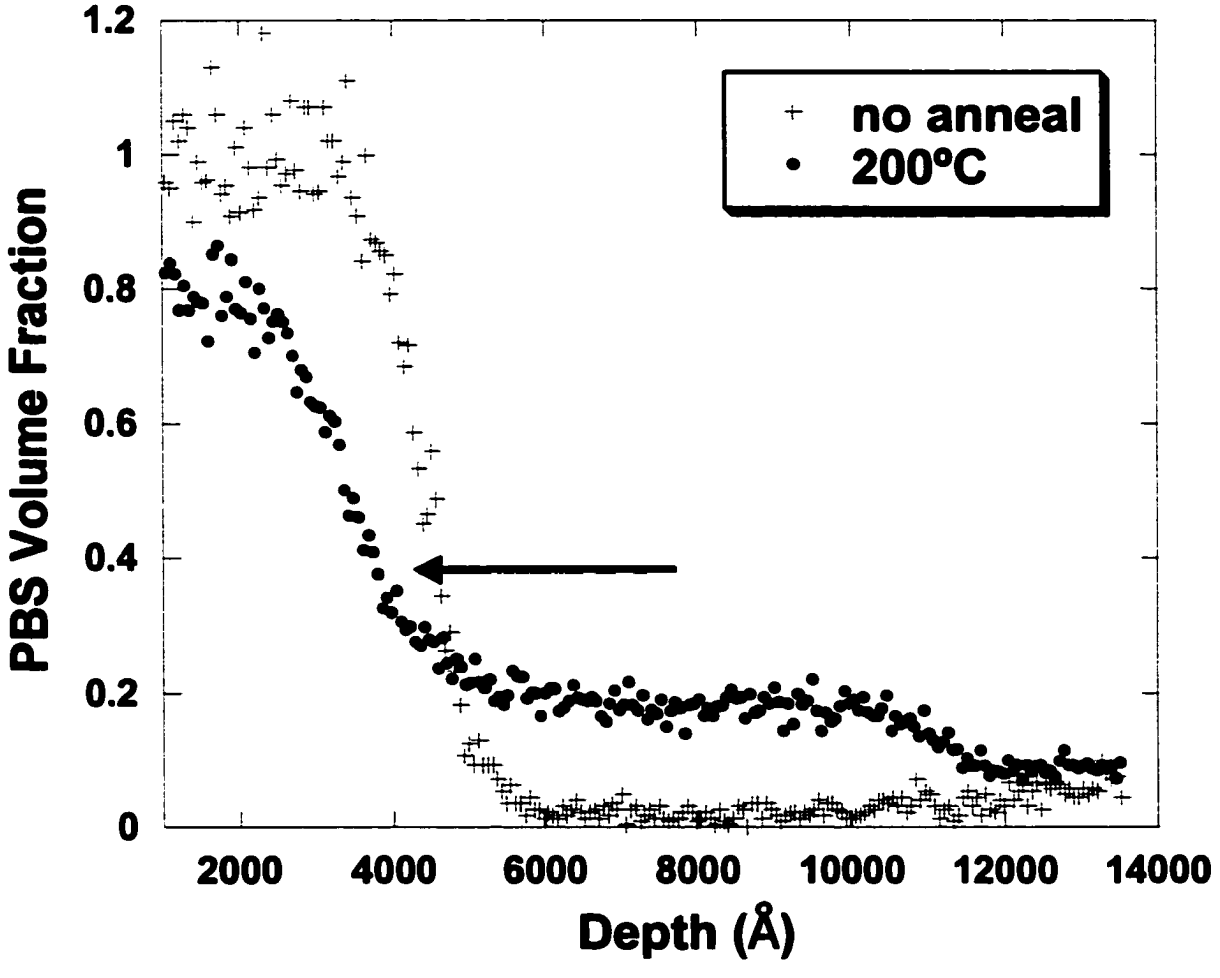

Figure 5.3b: PBS volume fraction, ϕ, v. normalized depth profiles for N-asymmetric PS/PBS bilayers near the binodal ($N_{PS} = 1370$, $N_{PBS} = 424$, $f = 0.22$). ϕ v. z, annealed at 200°C, + no anneal, • 30 min.

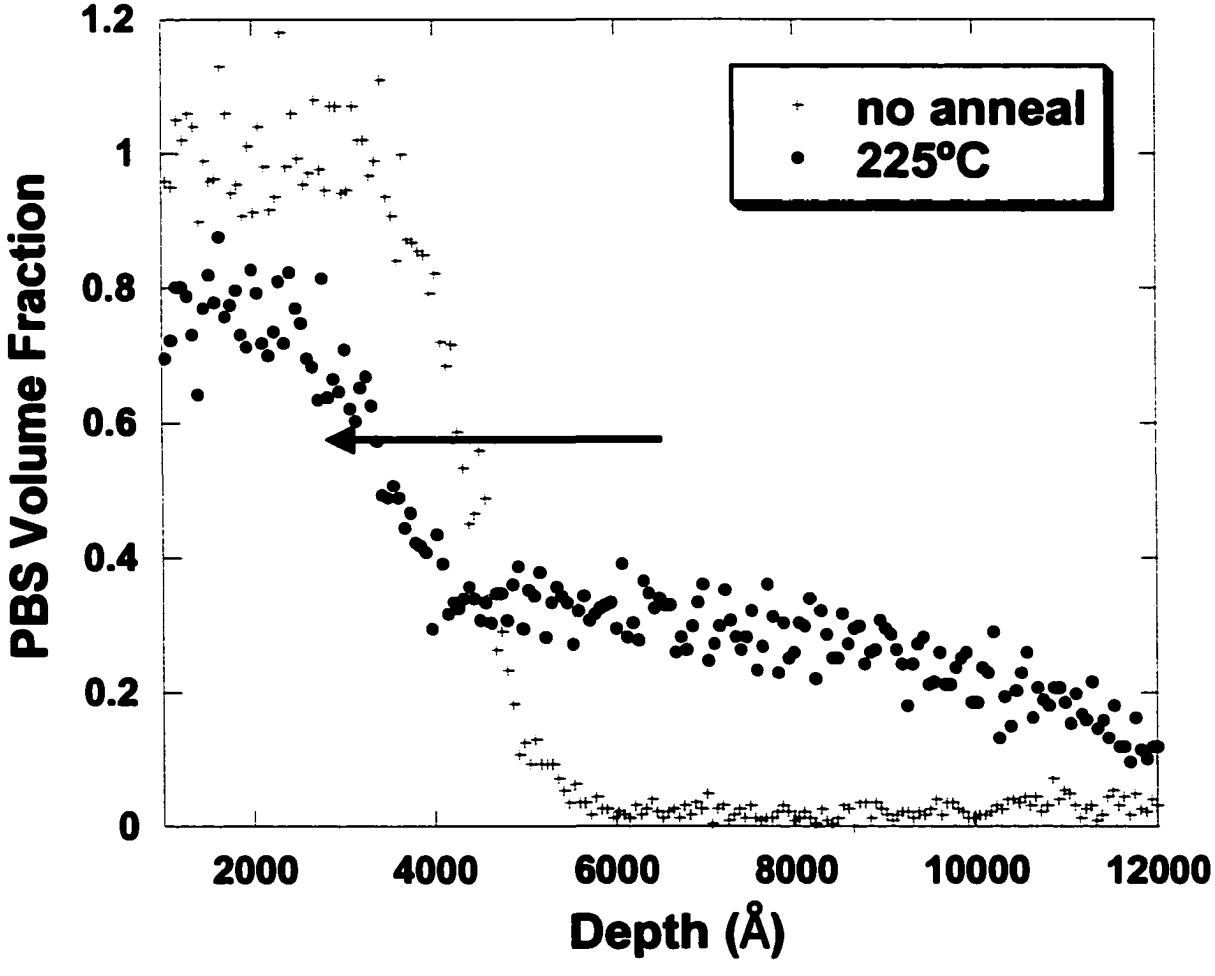

Figure 5.3c: PBS volume fraction, ϕ, v. normalized depth profiles for N-asymmetric PS/PBS bilayers near the binodal (N_{PS} = 1370, N_{PBS} = 424, f = 0.22). ϕ v. z, annealed at 225°C, + no anneal, • 30 min.

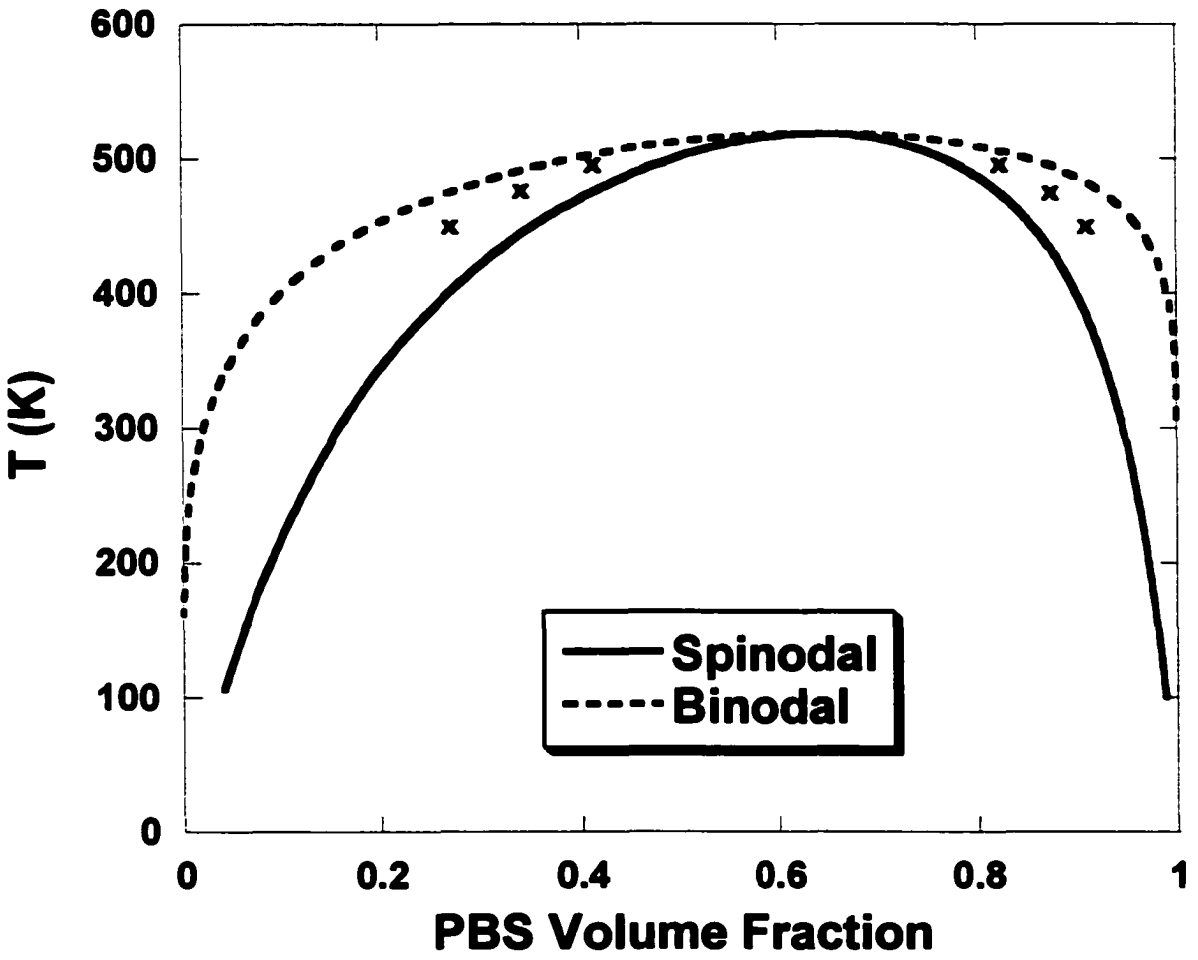

Figure 5.4: Phase diagram for N-asymmetric PS/PBS system (N_{PS} = 1370, N_{PBS} = 424,f = 0.22) predicted from Flory-Huggins theory using χ from SAXS. The **x** points are a guide for the eye to compare to binodal layer compositions from Figures 14a, b, and c.

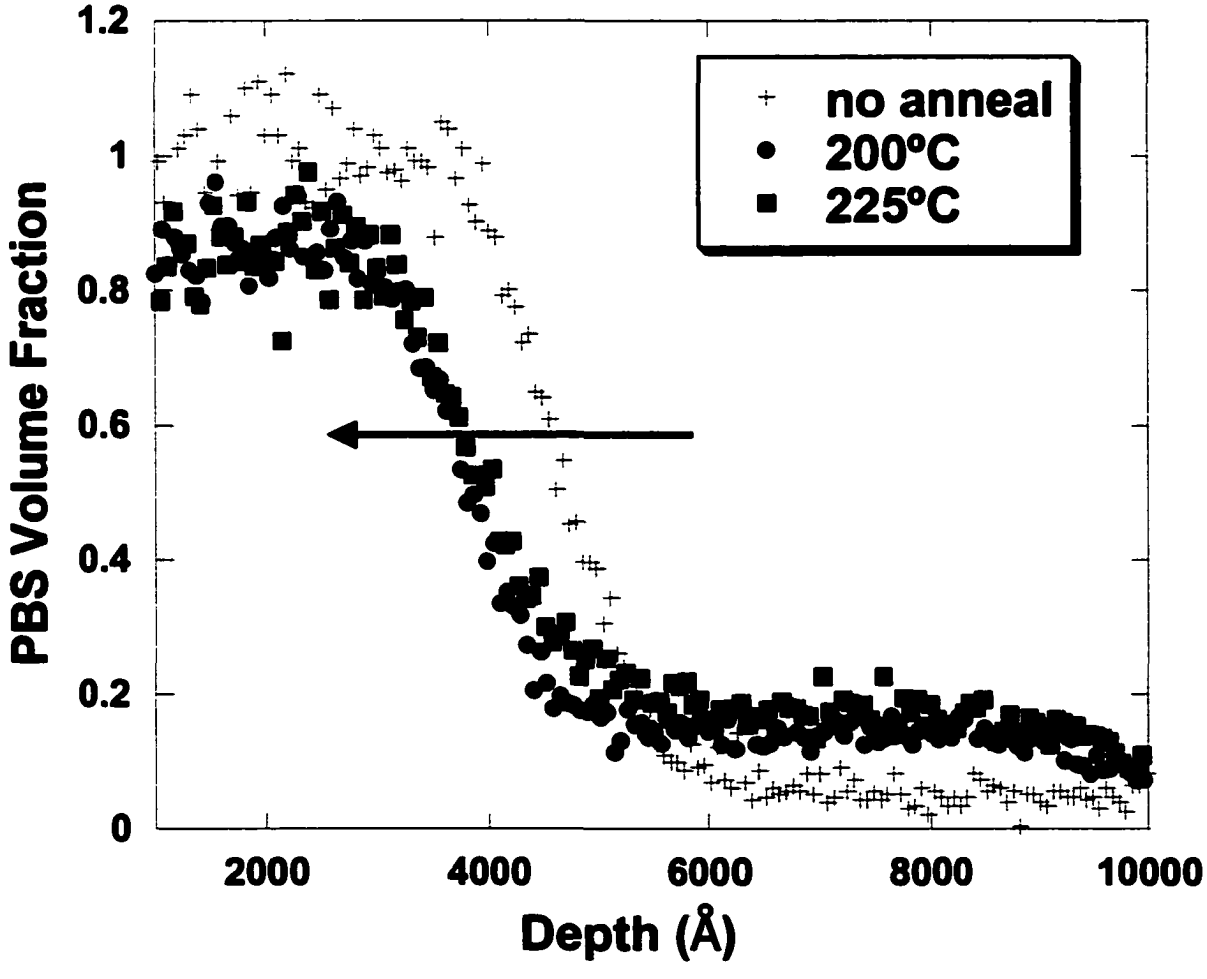

Figure 5.5a: PBS volume fraction, ϕ, v. depth profile for N-asymmetric PS/PBS bilayer near the binodal, $N_{PS} = 7670$, $N_{PBS} = 424$, $f = 0.22$. ϕ v. z, + no anneal, • 200°C 30 min, ■ 225°C 30 min.

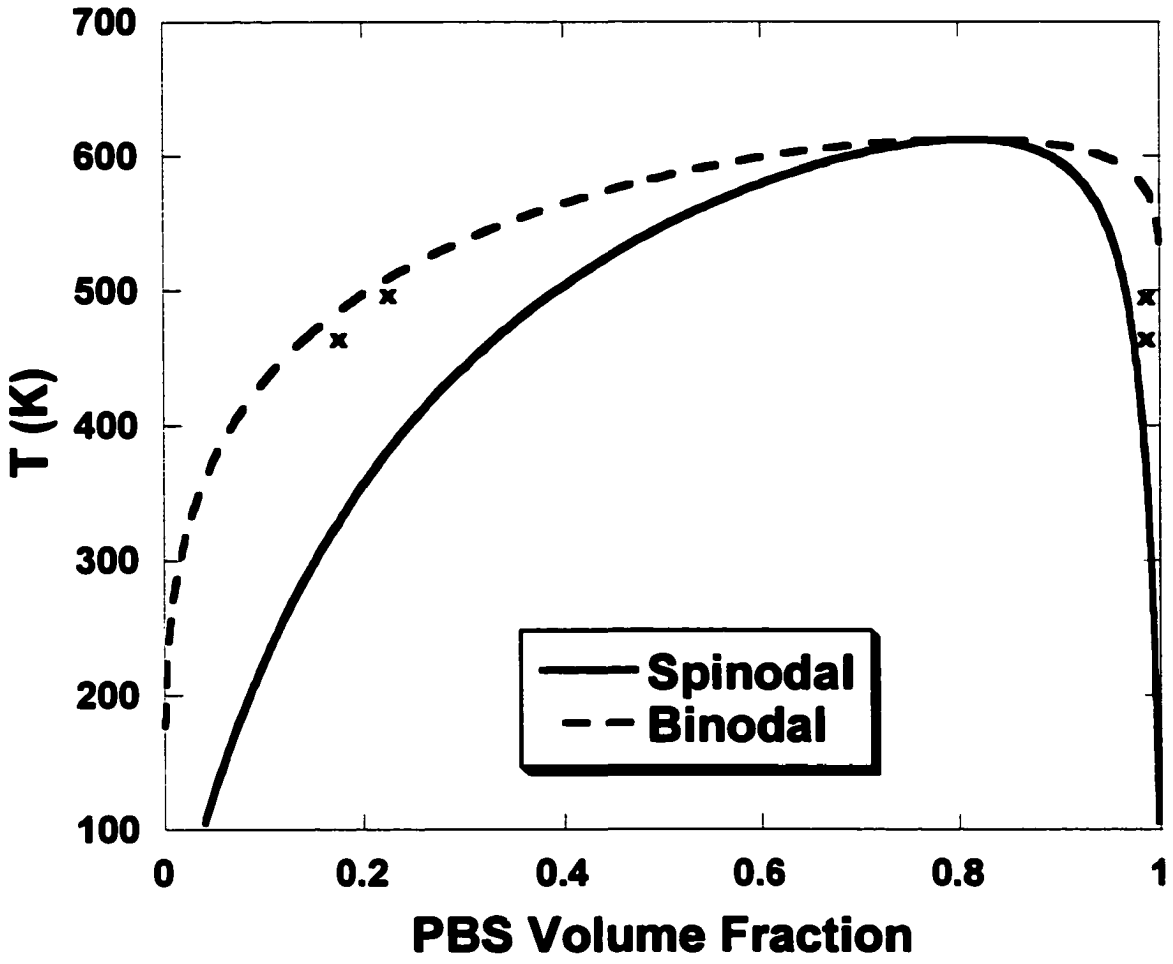

Figure 5.5b: Phase diagram for N-asymmetric PS/PBS bilayer near the binodal, N_{PS} = 7670, N_{PBS} = 424, f = 0.22.

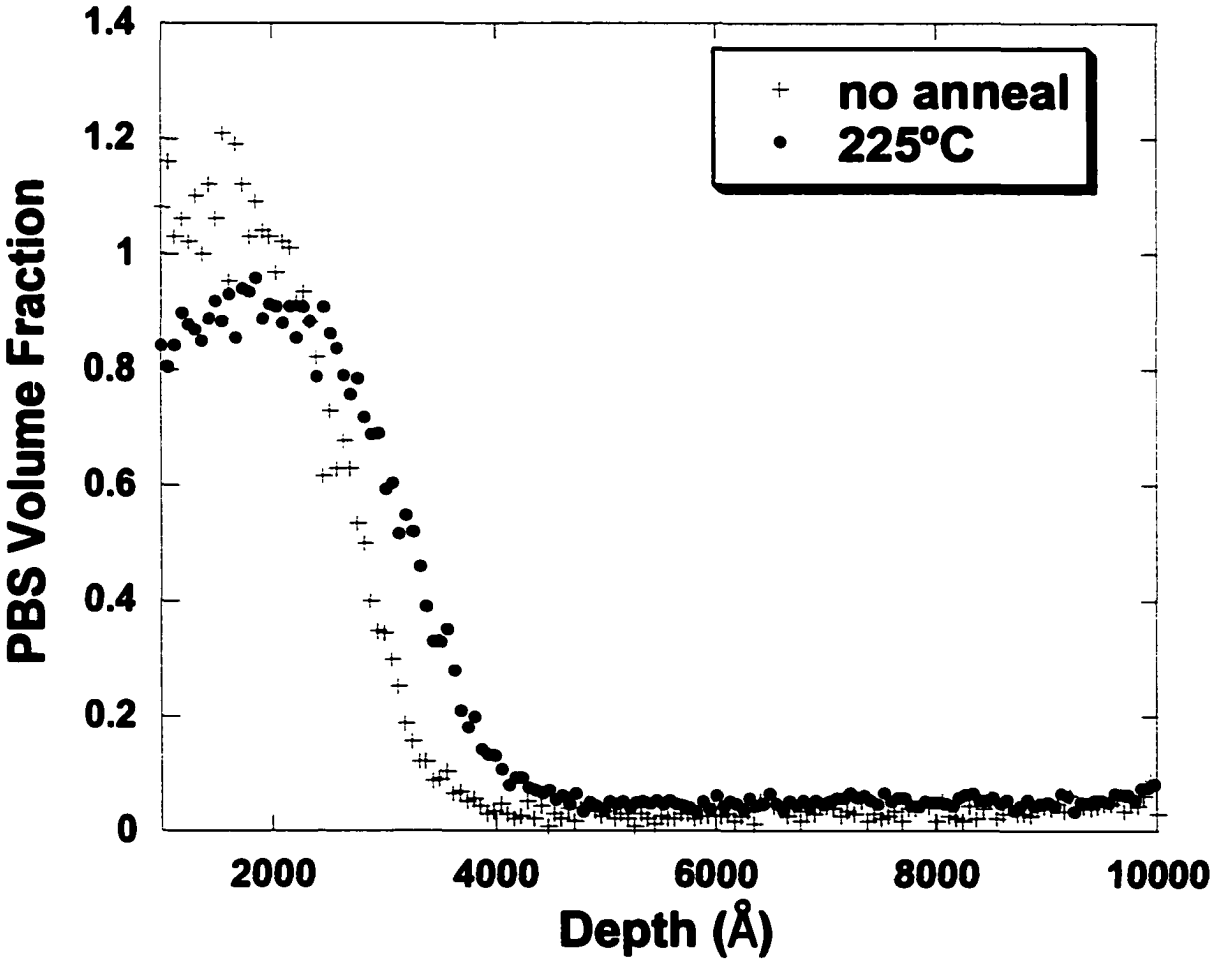

Figure 5.6a: PBS volume fraction, ϕ, v. depth profile for N-asymmetric PS/PBS bilayer near the binodal, $N_{PS} = 424$, $N_{PBS} = 7144$, $f = 0.22$. □ v. z, + no anneal, • 225°C 30 min.

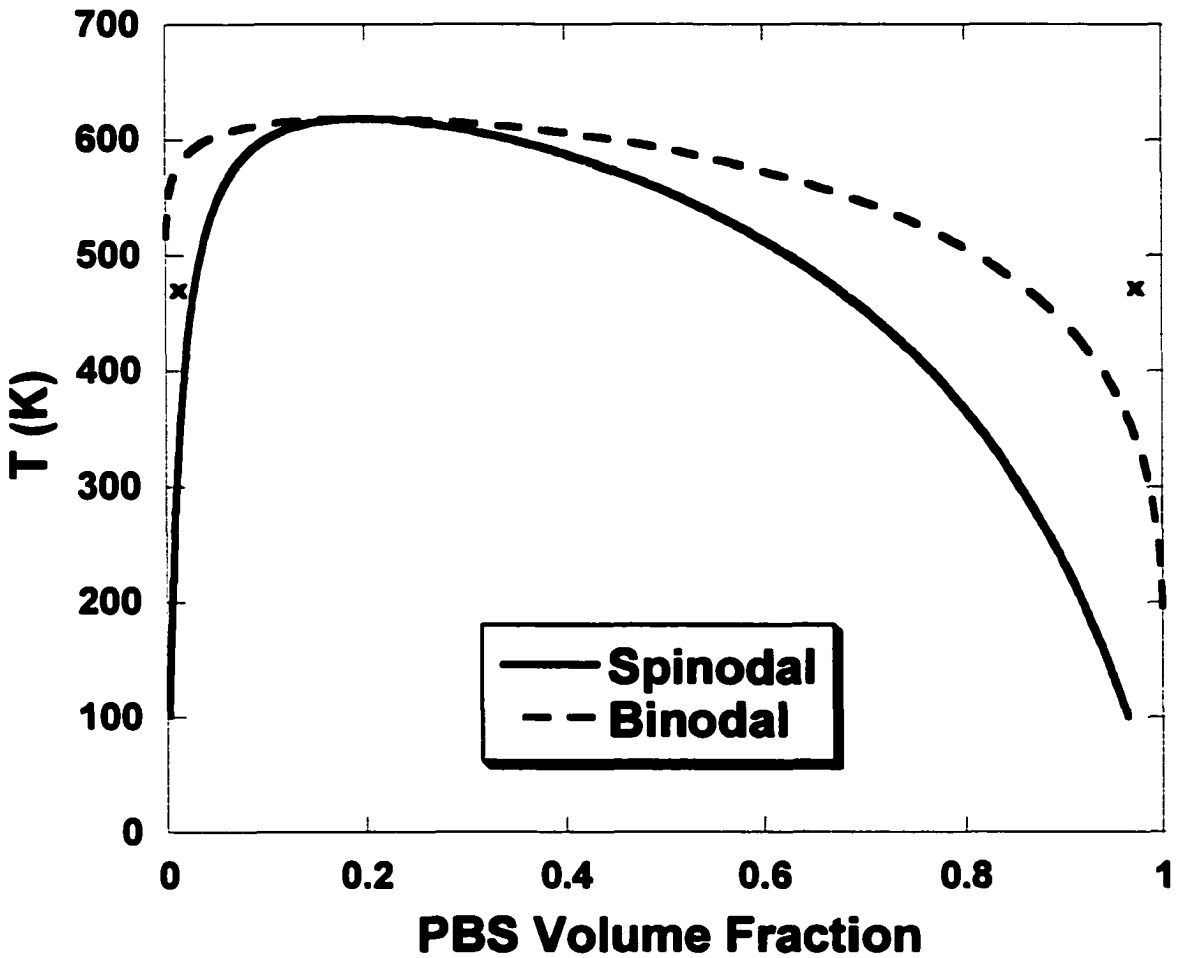

Figure 5.6b: Phase diagram for N-asymmetric PS/PBS bilayer near the binodal, $N_{PS} = 424$, $N_{PBS} = 7144$, $f = 0.22$.

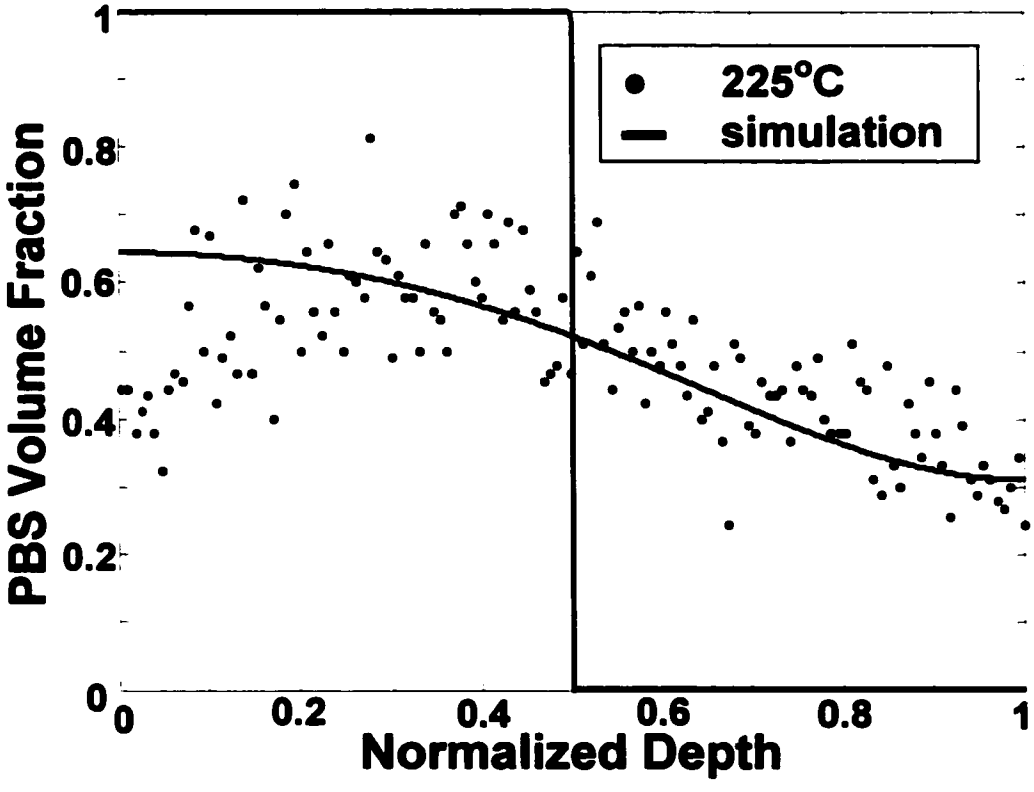

Figure 5.7: PBS volume fraction, ϕ, v. normalized depth (N_{PS} = 4087, N_{PBS} = 7144, f = 0.04) annealed at 225°C, • 30 m, — simulation.

CHAPTER 6

INTERDIFFUSION IN PARTIALLY MISCIBLE POLYMER INTERFACES: EFFECT OF POLYDISPERSITY AND FILM THICKNESS

6.1 Abstract

Interdiffusion and surface segregation in partially miscible polymer bilayers of polystyrene (PS) and the statistically random copolymer poly(styrene-co-4-bromostyrene) (PBS), $(C_8H_{(8-x)}Br_x)_N$, where x is the mole fraction of brominated repeat units in the copolymer and N the degree of polymerization, was studied using Rutherford backscattering spectroscopy (RBS). PS/PBS bilayers with varying x, N, polydispersity, and relative layer thickness were examined. As the phase boundary is approached in partially miscible systems, interdiffusion occurs until layer compositions indicative of binodal conditions are reached; the results for the polydisperse system are compared to those for the analogous monodisperse systems to show the compatibilizing effect of the presence of short chains. For partially miscible bilayers having sufficiently thick PS layer to maintain one-phase blend composition upon interdiffusion of PBS, complete interdiffusion is observed. In immiscible polydisperse bilayers having thin (~1000Å) PBS layers and sufficient difference in surface tension between PS and PBS, the equilibrium state shows encapsulation of PBS by PS. The potential use of thin film interdiffusion and surface encapsulation as means to tailor interfacial properties is discussed.

6.2 Introduction

Compatibilizing partially miscible and immiscible polymer interfaces continues to be a widely researched area. Efforts have investigated the use of compatibilizing agents, such as random copolymers (to reduce interfacial tension between phases and promote interpenetration) [1-5], and demonstrated that interfacial width (and adhesive strength) at the interface can be increased by the addition of such materials [2]. This strengthening of interfaces using random copolymers is facilitated by multiple crossings of the interface and the increased probability of formation of effective entanglements, i.e., entanglements that can support stresses and therefore contribute to the overall fracture energy [6]. Here we investigate the effect of miscibility and molecular weight distribution on interdiffusion and surface phenomena in partially miscible bilayer systems of polystyrene (PS) and the statistically random copolymer poly(styrene-co-4-bromostyrene) (PBS), $(C_8H_{(8-x)}Br_x)_N$, where x is the mole fraction of brominated repeat units in the copolymer and N is the degree of polymerization.

In a partially miscible bilayer with the respective polymers having a polydispersity index (PDI) > 1, the shorter chains of each species are more miscible with each other than longer chains. The quantity $N\chi$, a measure of miscibility, is smaller for chains with lower N. Therefore, short chains can be expected to compatibilize partially miscible interfaces by segregating to the interface and reducing the interfacial tension. Genzer and Composto [7-10], building on the ideas initially developed by Helfand [11], have shown that interfacial stresses in a multi-component (A/B:C blend) system are reduced by having B segregate to the interface when $\chi_{AB} < \chi_{AC}$. In our system, B would represent shorter chains of PS or PBS. In

addition, it has been shown that PS encapsulates PBS in PS/PBS blends in order to reduce the overall surface tension of the system [12,13] (PS has lower surface tension than PBS [13]). Other studies concur; Krausch and co-workers [14] used 50:50 blends of PS/PBS to investigate surface directed spinodal decomposition. They compared behavior in blends to that of multilayered samples at near-binodal compositions. The results show evidence of preferential segregation of the lower surface tension component to the film surface to form a 'wetting layer'. Thus, it has been shown that the surface composition of a blend is determined by respective interfacial and surface tensions. Therefore, when comparing a polydisperse system to a monodisperse system having the same average copolymer composition, it is expected that short chains segregate to the interface and lead to increased interdiffusion for the polydisperse bilayers. Also, in polydisperse immiscible polymer bilayers where the overall surface tension of the system can be reduced by segregation of the lower surface tension constituent to the surface, the result is encapsulation of the higher surface tension constituents. Here we report observations of these phenomena.

6.3 Experimental Techniques

Monodisperse PS and PBS were obtained from Polymer Source, Inc (Dorval, Quebec). PBS was synthesized by the procedure described by Kambour and co-workers [15,16]. Details of the polymer characterization and sample preparation are given elsewhere (see Chapter 4). Table 6.1 lists relevant properties of the polymers used in this study. The bilayers are composed of a bottom layer of PS and a top layer of PBS; both layers vary in thickness and will be reported for each sample. Samples were annealed at pressures less than

10^{-3} Torr for appropriate times at various temperatures ($150 < T < 225^{\circ}C$), above the glass transition temperature of both species, to allow interdiffusion. The samples were then investigated using Rutherford backscattering spectroscopy (RBS) as reported in Chapter 4.

6.4 Results and Discussion

Many polymer/polymer interfaces (and blends) are partially miscible, i.e., they have a Flory-Huggins interaction parameter, χ, near the spinodal interaction parameter, χ_s. Previously (see Chapters 4,5) we discussed interdiffusion in partially miscible bilayers of monodisperse PS/PBS and showed excellent agreement with predicted phase diagrams. Here we discuss I) the effect of polydispersity on interdiffusion in similar systems and II) the effect of film thickness in the same systems.

The PS/PBS system exhibits UCST behavior[15,16] and the interaction parameter $\chi_{S\text{-}BrS}$ between brominated and non-brominated styrene segments has been determined to be [12]

$$\chi_{S\text{-}BrS} = -0.0833 + \frac{73.75}{T} \tag{6.1}$$

Here T is temperature reported in K [17]. The Flory-Huggins interaction parameter, χ, of a homopolymer, A, and a statistically random copolymer, A-B, is expressed as [18]

$$\chi = f^2 \chi_{AB} \tag{6.2}$$

Here f is the volume fraction of B units in the random copolymer. The values of f and x are given in Table 6.1. Table 6.1 also reports the value of $N^{*}\chi$, where N^{*} represents the average N of the system.

I. The effect of polydispersity in partially miscible PS/PBS bilayers

The characteristics of the polymers used are shown in Table 6.1. In Figure 6.1, the effect of polydispersity on the miscibility is shown. Figure 6.1a shows RBS spectra for a monodisperse PS(1.05μm)/PBS(0.8μm) bilayer with N_{MD} = 1370 and f = 0.09 annealed at 225°C. Comparing these to the polydisperse PS(1.19μm)/PBS(0.78μm) bilayer, N_{PD} = 1186 with f = 0.18 also annealed at 225°C shown in Figure 6.1b, we see very similar concentration profiles, but with different time evolution. From these plots it is clear that the presence of short chains in the polydisperse system has a compatibilizing effect at the interface, due to the reduced $N^{*}\chi$ for short chains, but the rate of interdiffusion is hindered by the presence of the long chains. It should be noted that the peak at 15000 corresponds to a contaminant from the gold-coating procedure that has been shown to reside on the surface. Figures 6.1c and 6.1d, having interdiffused to binodal conditions, show the same result; Figure 6.1c is the monodisperse PS(0.8μm)/PBS(0.58μm) bilayer with N_{MD} = 424 and f = 0.28 annealed at 200°C with final composition reaching ϕ_{PBS} ca. 0.8 and Figure 6.1d is the polydisperse PS(1.35μm)/ PBS(0.9μm) bilayer, N_{PD} = 1186 with f = 0.41 annealed at 225°C with a final PBS composition of ca. 0.8. Once again we see striking similarity; the short chains in the polydisperse system increase miscibility, but the time to reach equilibrium is slower due to the presence of long chains in the system. For N_{PD} = 1186, f = 0.56 even the short chains are immiscible (at 225°C) and no interdiffusion is perceptible; the same was observed for N_{MD} = 1370, f = 0.55 under the same annealing conditions (data not shown). Thus, from our studies, we have observed that for immiscible systems with layer thickness greater than 2000Å the

RBS spectra for all the annealing temperatures and times remained unchanged, indicating that there is no interdiffusion. The effect of miscibility and mobility on interdiffusion for all values of T, f, and PDI studied is that as the number of short chains increases ($N^*\chi$ decreases), the system becomes more miscible and the overall interdiffusion is enhanced. However, the time to reach equilibrium is increased by the presence of long chains in the polydisperse systems. Following these results, it is expected that a distribution of both N and f could be used to compatibilize interfaces. For example, in a system such as the one studied here (bilayers of A/AB random copolymer), introducing a distribution of both f and N at the interface could facilitate copolymer having low f, higher N or low N, higher f moving to the A-rich side of the interface and copolymer having higher f, higher N or low f, low N moving to the AB-rich side of the interface, with the distribution compatibilizing the gradient and increasing the interfacial width. It has been shown that the fracture energy of an interface is directly proportional to the interfacial width [19,20]. Thus, by appropriately choosing $N\chi$ (for example, by using various copolymers of different composition (f) and N [11,21]), strategies can be developed to strengthen incompatible interfaces. Hence, understanding miscibility-mediated interdiffusion phenomena might offer an alternative approach to reinforcement of polymer interfaces.

II. The effect of film thickness in partially miscible PS/PBS bilayers

Film thickness has no observed effect on the equilibrium interdiffusion behavior of completely miscible systems. For systems approaching the binodal where the layer thickness ratio is sufficient to maintain one-phase compositions, complete interdiffusion is observed.

For example, if the PS layer is 10μm and the PBS layer is 0.1μm the relative layer thickness allows for a final composition of the completely diffused bilayer (essentially a blend) of ϕ_{PBS} = 0.99, corresponding to a one-phase composition for partially miscible systems (as illustrated in Figure 6.2). Using this strategy, small quantities of additive (polymer or otherwise) may be introduced into a polymer system without the need for blending.

In immiscible polydisperse PS/PBS bilayers with the PBS layer having thickness ≤ 2000Å, we have observed encapsulation of PBS by PS. Concentration v. depth profiles for an encapsulated bilayer is shown in Figure 6.3; this profile is of the polydisperse PS(3μm)/ PBS(1100Å) bilayer with N_{PD} = 1186, f = 0.56 annealed at 175°C. Encapsulation occurs as a result of PS having a lower surface tension than PBS and preferring to wet the polymer/vacuum interface. As mentioned before, several previous efforts [12,13] have shown the encapsulation of PBS by PS in thin film blends. It was shown [12] that the size of the PBS domains was of the order of the film thickness, ca. 1500-2000Å, comparable to the film thickness in this study. Encapsulation is expected to occur in thin film bilayers when the following criteria are met: a) the PBS film is sufficiently thin such that the amplitude of capillary roughness at both the interface and surface facilitates PS movement to the surface, b) the surface tension of PBS is significantly higher than PS such that encapsulation is energetically favored over the layers remaining discreet, c) and the annealing temperature is high enough to facilitate the two previous criteria while low enough that the PS/PBS system remains completely immiscible. It is known that interfacial and surface tension and capillary roughness increase with temperature [22]; however, instabilities in the film can also lead to dewetting of the PBS, or droplet formation [23]. The presence of both the much thicker PS

film and longer chains stabilizes the system and leads to the encapsulation mechanism we propose, illustrated in Figure 6.4. Here the initial bilayer comprises a thin PBS layer ($\leq$~1000Å) on a much thicker PS layer on a substrate. Assuming that the PBS and PS are immiscible, interdiffusion will be negligible (although short chains will migrate to the interface). However, due to the disparity in surface tension, the PBS layer will roughen over time. If the roughness is sufficient to allow penetration of PS through the PBS film, PS will move to the surface and encapsulate the PBS, resulting in a PS-rich surface. We observed this phenomenon in the polydisperse films, but not in any of the monodisperse films. On the contrary, monodisperse films show dewetting. This can be explained by the lack of long chains, which limit the roughening, while short chains lower interfacial tension. We also reported [12] that the relative size of the encapsulated PBS domains decreased with increasing N due to decreased mobility; for the system used in the current work, the presence of short chains may lead to a continuous encapsulated PBS-rich region. The progression of the phase morphology and resulting encapsulated structure has been observed in blend films. As shown by the atomic force micrograph in Figure 6.5a, the surface of blend films roughen to form interconnected and island type phase-separated structures. Figure 6.5b is the proposed morphology of the encapsulated structure, with PS preferentially wetting the surface.

The encapsulation mechanism proposed may be used to strengthen A/C interfaces using a third component, B, such that $\chi_{AB} < \chi_{AC}$. Under the appropriate conditions, B could be encapsulated at the A surface and reduce the interfacial tension between A and C. In this way, excess B would not be present in the A phase and the preparation of the A:B blend

unnecessary. Thus, for situations in which it is undesirable to compromise the bulk properties of A and C, encapsulation offers an alternative.

6.5 Conclusions

Interdiffusion and surface segregation in polydisperse partially miscible PS/PBS bilayers was studied using RBS. The results indicate that interdiffusion is facilitated by a molecular weight distribution due to the presence of short chains in the polydisperse system reducing interfacial tension. For partially miscible bilayers having sufficiently thick PS layer to maintain one-phase blend composition upon interdiffusion of PBS, complete interdiffusion is observed. In immiscible bilayers having thin ($\lesssim$1000Å) PBS layers and sufficient difference in surface tension, the equilibrium state shows encapsulation of PBS by PS. The potential use of thin film interdiffusion and surface encapsulation as means to tailor interfacial properties is discussed.

6.6 References

1. Schaffer, M., et al., *Enhancement of Interfacial Adhesion by Means of Surface Segregation in the Interface between Polycarbonate and SAN blends.* Macromolecules, 1997. **30**: p. 1225-1227.

2. Kulasekere, R., et al., *Homopolymer Interfaces Reinforced with Random Copolymers.* Macromolecules, 1996. **29**: p. 5493-5496.

3. Dai, C.A., et al., *Effect of the Monomer Ratio on the Strengthening of Polymer Phase Boundaries by Random Copolymers.* Macromolecules, 1997. **30**: p. 6727-6736.

4. Dai, C.A., et al., *Reinforcement of Polymer Interfaces with Random Copolymers.* Physical Review Letters, 1994. **73**(18): p. 2472-2475.

5. Edgecombe, B.D., et al., *The Role of Polymer Architecture in Strengthening Polymer-Polymer Interfaces: A comparison of Graft, Block, and Random Copolymers Containing Hydrogen-bonding Moieties.* Macromolecules, 1998. **31**(4): p. 1292-1304.

6. Gorga, R.E. and B. Narasimhan, *Fracture Toughness at Partially Miscible Polymer Interfaces.* J. Polymer Science: Part B: Polymer Physics, 2002, submitted.

7. Faldi, A., J. Genzer, and R.J. Composto, *Segregation at the Interface between a Homopolymer and a Binary Polymer Blend.* Physical Review Letters, 1995. **74**(17): p. 3388-3391.

8. Genzer, J., et al., *Surface Enrichment in a Miscible Polymer Blend: An Experimental Test of Self-Consistent Field and Long-Wavelength Approximation Models.* Macromolecules, 1996. **29**: p. 5438-5445.

9. Genzer, J., A. Faldi, and R.J. Composto, *Mean-field Theory of the Interface Between a Homopolymer and a Binary-polymer Mixture.* J. Chem. Phys., 1996. **105**(22): p. 10135-10144.

10. Genzer, J. and R.J. Composto, *Effect of Molecular Weight on the Interfacial Excess, Tension, and Width in a Homopolymer/Binary Polymer Blend System.* Macromolecules, 1998. **31**: p. 870-878.

11. Helfand, E., *Theory of the Homopolymer, Binary-Polymer-Mixture Interface.* Macromolecules, 1992. **25**: p. 1676-1685.

12. Gorga, R.E., et al., *Quantifying Phase Behavior in Partially Miscible Polystyrene/ Poly (styrene-co-4-bromostyrene) Blends.* Journal of Polymer Science: Part B, Polymer Physics, 2002. **40**(2).

13. Slep, D., et al., *Phase Separation of Polystyrene and Bromo-Polystyrene Mixtures in Equilibrium Structures in Thin Films.* Langmuir, 1998. **14**(17): p. 4860-4864.

14. Krausch, G., et al., *Self-assembly of a Homopolymer Mixture via Phase Separation.* Applied Physics Letters, 1994. **64**(20): p. 2655-2657.

15. Kambour, R.P., J.T. Bendler, and R.C. Bopp, *Phase Behavior of Polystyrene, Poly(2,6-dimethyl-1,4-phenyl oxide) and Their Brominated Derivatives.* Macromolecules, 1983. **16**: p. 753-757.

16. Kambour, R.P. and J.T. Bendler, *Miscibilities in Monodisperse Mixtures of Polystyrene, Poly(p-bromostyrene) and Their Copolymers.* Macromolecules, 1986. **19**: p. 2679-2682.

17. Koch, T. and G.R. Strobl, *Concentration Dependence of the Flory-Huggins Interaction Parameter of a Polymer Blend as Determined by SAXS Experiments.* J. Polymer Science: Part B: Polymer Physics, 1990. **28**: p. 343-353.

18. Bruder, F., et al., *Interdiffusion in the Partially Miscible Polymer Blend of Deuterated Polystyrene and Poly(styrene-co-bromostyrene).* Macromolecules, 1989. **22**: p. 4434-4437.

19. Schnell, R., M. Stamm, and C. Creton, *Direct Correlation between Interfacial Width and Adhesion in Glassy Polymers.* Macromolecules, 1998. **31**: p. 2284-2292.

20. Schnell, R., M. Stamm, and C. Creton, *Mechanical Properties of Homopolymer Interfaces: Transition from Simple Pullout to Crazing with Increasing Interfacial Width.* Macromolecules, 1999. **32**(10): p. 3420-3425.

21. Brochard, F., J. Jouffroy, and P. Levinson, *Polymer-Polymer Diffusion in Melts.* Macromolecules, 1983. **16**: p. 1638-1641.

22. Zhao, W., et al., *Neutron and X-ray Reflectivity Measurements of Polystyrene/ Polybromostyrene (PS/PBrS) Interfaces.* Physica B, 1991. **173**: p. 43-46.

23. Huttenbach, S., et al., *The Interface between Two Strongly Incompatible Polymers: Interfacial Broadening and Roughening near Tg.* Langmuir, 1991. **7**: p. 2438-2442.

Table 6.1: Degree of polymerization, extent of bromination, polydispersity, and miscbility of PS/PBS system. $N^*\chi$ reported at 200°C.

$(C_8H_{(8-x)}Br_x)_N$				
N*	x	f	M_w/M_n	$N^*\chi$
424	0	0	1.03	0
	0.07	0.08		0.20
	0.20	0.22		1.49
	0.25	0.28		2.41
	0.42	0.46		6.51
	0.63	0.66		13.40
1186	0	0	2.28	0
	0.16	0.18		2.79
	0.37	0.41		11.77
	0.52	0.56		26.99
1370	0	0	1.03	0
	0.08	0.09		0.81
	0.22	0.25		6.21
	0.39	0.43		18.38
	0.51	0.55		30.08

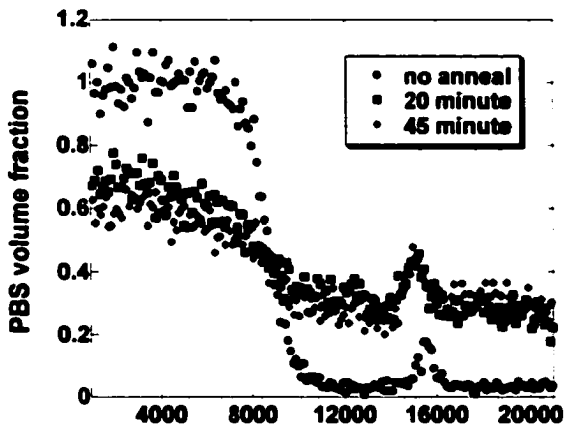

Figure 6.1a: PBS volume fraction, ϕ v. depth for PS/PBS bilayers. Monodisperse PS(1.05μm)/PBS(0.8μm): N_{MD} = 1370, f = 0.09 annealed at 225°C. The peak at 15000 corresponds to a contaminant from the gold-coating procedure that resides on the surface and does not interfere with interdiffusion at the interface.

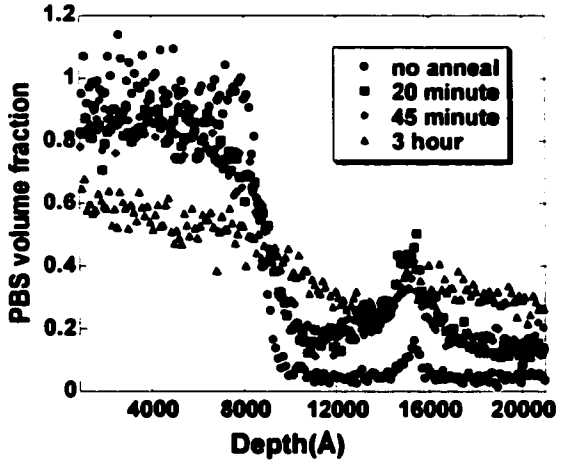

Figure 6.1b: PBS volume fraction, ϕ v. depth for PS/PBS bilayers. Polydisperse PS(1.19μm)/PBS(0.78μm): N_{PD} = 1186, PDI = 2.3, f = 0.18 annealed at 225°C. The peak at 0.75 corresponds to a contaminant from the gold-coating procedure that resides on the surface and does not interfere with interdiffusion at the interface.

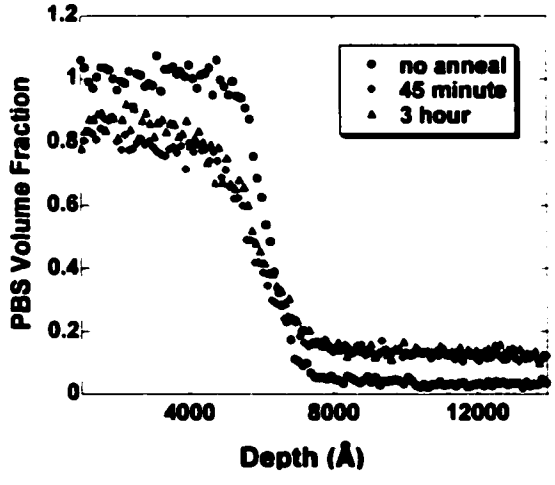

Figure 6.1c: PBS volume fraction, ϕ v. depth for PS/PBS bilayers. Monodisperse PS(0.8μm)/PBS(0.58μm): $N_{MD} = 424$, $f = 0.28$ annealed at 200°C.

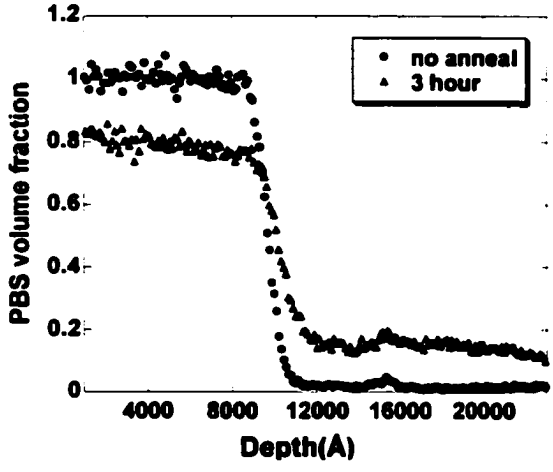

Figure 6.1d: PBS volume fraction, ϕ v. depth for PS/PBS bilayers. Polydisperse PS(1.35μm)/PBS(0.9μm): $N_{PD} = 1186$, $f = 0.41$ annealed at 225°C.

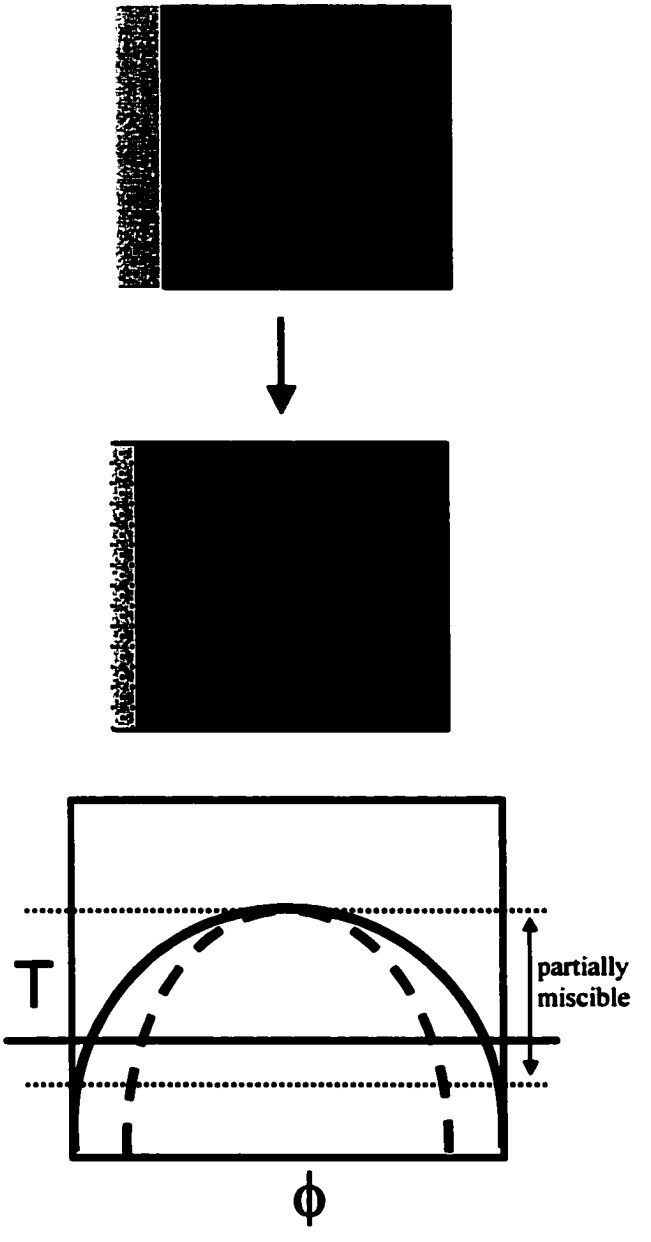

Figure 6.2: Schematic of interdiffusion in partially miscible system, facilitated by layer thickness to maintain one-phase composition.

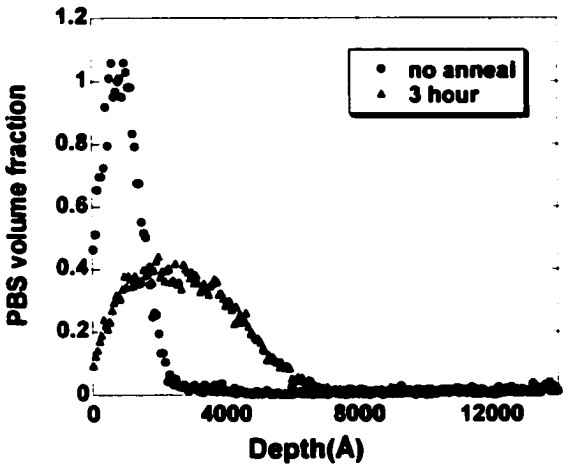

Figure 6.3: PBS volume fraction, ϕ v. depth for PS/PBS bilayers showing encapsulation: Polydisperse PS(3μm)/PBS(1100Å): N_{PD} = 1186, f = 0.56 annealed at 175°C.

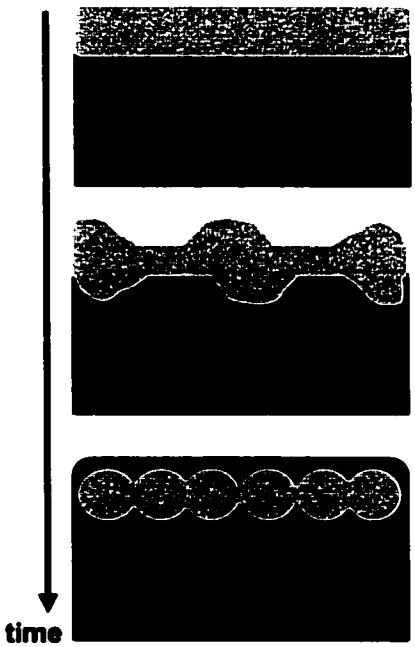

Figure 6.4: Schematic of encapsulation process. The initial bilayer comprises a thin PBS layer (~1000Å) on a much thicker PS layer on a substrate. Assuming that the PBS and PS are immiscible, interdiffusion will be negligible (although short chains will migrate to the interface). However, due to the disparity in surface tension, the PBS layer will roughen over time. If the roughness is sufficient to allow penetration of PS through the PBS film, PS will move to the surface and encapsulate the PBS, resulting in a PS-rich surface.

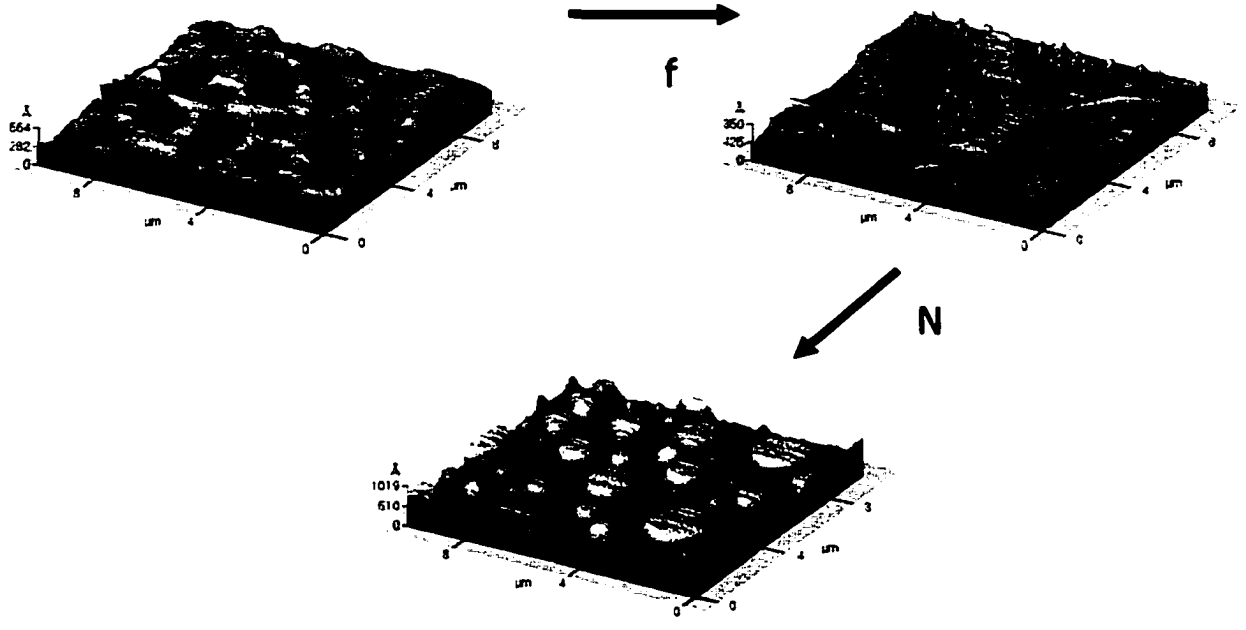

Figure 6.5a: Phase behavior showing encapsulation process. Atomic force micrograph showing the progression of phase morphology as f and N are increased in the PS/PBS system.

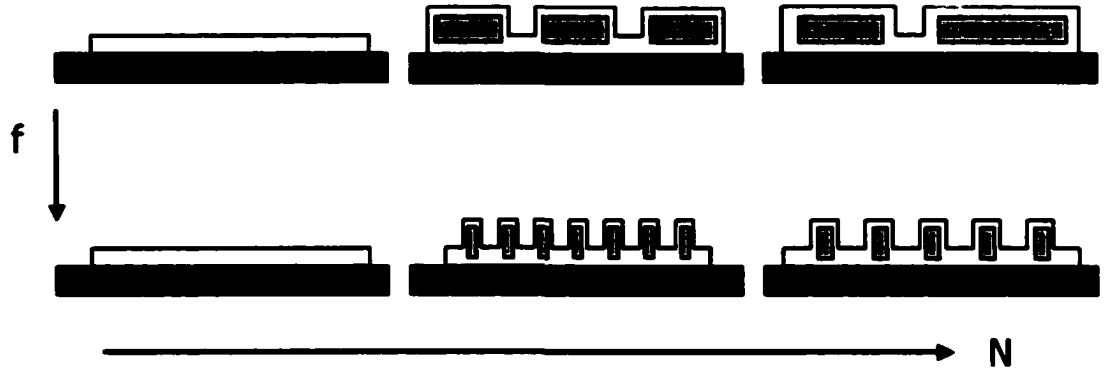

Figure 6.5b: Proposed morphology of encapsulation of PBS by PS from the blend.

CHAPTER 7

QUANTIFYING INTERFACIAL WIDTH AT PARTIALLY MISCIBLE POLYMER INTERFACES

7.1 Abstract

Interfacial widths at partially miscible polymer interfaces of polystyrene (PS) and the statistically random copolymer poly(styrene-*r*-4-bromostyrene) (PBS), $(C_8H_{(8-x)}Br_x)_N$, where x is the mole fraction of brominated repeat units in the copolymer and N the degree of polymerization, were quantified using x-ray reflectivity (XR). In systems where $N_{PS} = N_{PBS}$, it is shown that the interface broadens symmetrically and the equilibrium interface position is unchanged from the original position. For $N_{PS}/N_{PBS} \neq 1$, the interface is shown to move toward the faster diffusing (lower N) component. Interfacial width decreases with increasing degree of polymerization and extent of bromination of the PBS copolymer and increases with annealing temperature, i.e., interfacial width decreases as the system becomes more immiscible. In miscible systems, i.e., those falling in the one-phase region of the phase diagram, interdiffusion proceeds until there is a single layer of constant composition. In partially miscible systems, equilibrium layer compositions are indicative of binodal concentrations; these observations are in agreement with phase diagrams obtained using Flory-Huggins theory and a PS/PBS Flory-Huggins interaction parameter measured using small angle x-ray scattering (SAXS). For immiscible systems, the interfacial widths measured are on the order of tens of Angstroms, consistent with reported values.

7.2 Introduction

Knowledge of the interfacial width in partially miscible polymer systems provides information about the extent to which interpenetration of diffusing chains has taken place, thereby affording a prediction of the fracture strength of the system. The effect of miscibility on interdiffusion, phase, and fracture behavior has already been reported for the partially miscible bilayer systems of polystyrene (PS) and the statistically random copolymer poly(styrene-*r*-4-bromostyrene) (PBS), $(C_8H_{(8-x)}Br_x)_N$, where x is the mole fraction of brominated repeat units in the copolymer and N is the degree of polymerization [1,2](also see Chapters 4-6). In this work we take advantage of the excellent resolution of x-ray reflectivity (XR) to accurately report interfacial widths on the order of Angstroms (for immiscible PS/PBS systems), to quantify interfaces with concentration v. depth profiles which are steeper than what can be detected within the limits of the resolution of Rutherford backscattering spectroscopy (RBS), and to follow the movement of the interface in systems where one species diffuses faster than the interfacing material. The overall goal is to identify molecular attributes that influence interface performance and to obtain quantitative relationships between molecular properties (interdiffusion, interfacial width, interaction parameter, phase behavior, and blend morphology) and macroscopic properties (interfacial fracture energy).

Interfacial widths for the PS/PBS system have been measured for various f, the volume fraction of brominated repeat units in the copolymer, and N_{PS}/N_{PBS}, and the correlation with interdiffusion and phase behavior in this system is demonstrated. Combinations of f and N designed to span a range of miscibility have been chosen; for given

N_{PS} and N_{PBS}, system miscibility is controlled by f. Additionally, systems having the same f were studied at different N_{PS}/N_{PBS}. Phase diagrams for various extents of bromination and molecular weight have already been obtained and χ parameters have been measured using SAXS [1]. The PS/PBS systems, defined in terms of f, N_{PS}, and N_{PBS}, undergo phase transitions within the temperature range considered in this study [1]. In order to directly relate interdiffusion, phase, and fracture behavior identical polymers were used in the respective studies.

7.3 Experimental Techniques

Monodisperse PS and PBS were obtained from Polymer Source, Inc (Dorval, Quebec). PBS was synthesized by the procedure described by Kambour and co-workers [3]. By controlling the amount of bromine added and the reaction time, PBS with varying extents of bromination was synthesized. Characterization of the polymers is described elsewhere (see Chapter 4). Table 7.1 lists relevant properties of the polymers used in this study. N-symmetric interfaces are defined at those with $N_{PS}/N_{PBS} = 1$; N-asymmetric interfaces have $N_{PS}/N_{PBS} \neq 1$.

7.3.1 Preparation of XR bilayers

The bilayers are composed of a bottom layer of PS and a top layer of PBS. For the PS layer, a solution of PS in toluene was prepared and cast onto either a pretreated 3" circular or $1cm^2$ silicon wafer using a spin coater (Headway Research, Garland, TX). The wafers were pretreated for 24h in a solution of chromic/sulfuric acid to remove any organics and residual

polishing silicones, and then cleaned by the RCA method [4]. The films were then dried at room temperature in a controlled atmosphere for 24h followed by in vacuum at 25°C for 6h. Film thickness was measured (on silicon) using an automated film thickness apparatus (Tencor, Mountain View, CA). Film thickness and surface roughness were determined to be 500-1000Å $\pm$ <10Å (confirmed by XR) for the PS layers. For the PBS layer, a solution of PBS in toluene was prepared and cast onto glass slides using a spin coater, then dried in the same manner as the PS layers to yield thickness 500-1000Å with similar roughness. The glass slides used for the PBS films were pretreated in a solution of chromic/sulfuric acid for 24h, then for 10min. in each of the following: acetone, de-ionized water, 2-propanol, and toluene. The PBS films were floated off the slides onto de-ionized water and the corresponding PS film on the silicon wafer was used to pick up the floating PBS film to create the desired bilayer. The bilayer was then dried in a controlled atmosphere at room temperature for 24h and in vacuum at 60°C for 24h. Samples were annealed at $\leq 10^{-4}$ Torr for appropriate times at various temperatures ($150 < T < 250$°C), above the glass transition temperature of both species, to allow interdiffusion. For binodal systems, enough time was allowed to reach equilibrium. Each type of film used as a component of a bilayer was analyzed as a single layer on silicon, for careful determination of thickness, roughness, and electron density. Also, each type of bilayer sample was analyzed as dried (unannealed). The bilayers were annealed in a high vacuum oven ($< 10^{-4}$ Torr) specifically designed and constructed for fast heating/cooling and evacuation. Such an annealing system is necessary to ensure that the films do not dewet and also that the samples can be removed quickly from the heating chamber so that annealing times and temperatures are accurate.

7.3.2 XR Analysis Technique

The X-ray reflectivity (XR) studies were performed at the Advanced Photon Source at Argonne National Laboratory, Argonne, IL. XR provides quantitative density, thickness, and roughness information with 5-15Å resolution [5]. For our studies, the bromine in the PBS copolymer provides the necessary electron density contrast, allowing us to follow the change in the composition of each layer with time. A schematic of the experimental setup is shown in Figure 7.1. Incident x-rays impinge on the 'interfaces' between the materials; some of the x-rays are reflected at a given interface; the remaining are transmitted to the next. If the refractive indices of the respective materials are known, standard optical methods can be used to describe the geometry and the relative intensities of the reflected and refracted x-rays [5-7]. Using x-rays, the reflectivity is determined by the refractive index of the material, n, which is usually less than 1 and given (approximately) by [6,7]:

$$n = 1 - \delta + i\beta \tag{7.1}$$

where dispersion, δ, is dependent on the electron density of the material, ρ_e ($e^-/Å^3$), and the wavelength, λ, of the x-rays:

$$\delta = \frac{\lambda^2 \rho_e r_e}{2\pi} \tag{7.2}$$

Here, r_e is the classical electron radius ($r_e = 2.81 \times 10^{-5}$ Å). Absorption, β, is given by [7]

$$\beta = \frac{\lambda \rho_{abs}}{4\pi} \tag{7.3}$$

Here ρ_{abs} is the absorption coefficient of the material. The reflectivity, R, at interface between arbitrary materials 1 and 2, as shown in Figure 7.1b, is given by the Fresnel equation:

$$R = \left| \frac{k_1 - k_2}{k_1 + k_2} \right| \tag{7.4}$$

Where k_i, the z-component of the wavevector **k**, is given by:

$$k_1 = 2\pi n_1 \frac{\sin\theta_1}{\lambda} \tag{7.5}$$

Here, θ_1 corresponds to the incident angle of the x-ray beam. Snell's law can the be used to relate the angle of incidence of the incoming and transmitted beams:

$$n_1 \cos\theta_1 = n_2 \cos\theta_2 \tag{7.6}$$

Equation 7.6 can be used to calculate the critical angle of total reflection, i.e., when there is no transmitted beam and $\theta_2 = 0$.

$$n_1 \cos\theta_{1c} = n_2 \tag{7.7}$$

To a good approximation:

$$\theta_{1c} = (2\delta_2)^{1/2} \tag{7.8}$$

Hence, for a system having two interfaces with the respective reflective amplitudes being r_1 and r_2,

$$R = \frac{r_t^2 + r_b^2 + 2r_t r_b \cos(2dk_{z,2})}{1 + r_t^2 r_b^2 + 2r_t r_b \cos(2dk_{z,2})} \tag{7.9}$$

The software used to analyze the XR data was Reflek; the input parameters include the number of layers in the sample (including any silicon oxide layer) and the wavelength of the x-rays (experiments were performed at 1.28358Å, 1.02469Å, and 1.26514Å), the footprint on the sample (based on the relative beam and sample sizes), diffractometer

resolution (~0.005°), and the dispersion, absorption, roughness, and thickness of each layer. These parameters are given in Table 7.2.

Results and Discussion

Miscibility in the PS/PBS system is quantified by the product $N^{*}\chi$, where χ is the Flory-Huggins interaction parameter and N^{*} is the effective degree of polymerization; for N-symmetric systems, $N^{*} = N$ and for N-asymmetric bilayers, i.e., for $N_A \neq N_B$, N* is given by:

$$N^{*} = 2N_AN_B/N_A+N_B \tag{7.10}$$

For a homopolymer, A, and a statistically random copolymer, AB [8],

$$\chi = f^2\chi_{AB} \tag{7.11}$$

where f is the volume fraction of B units in the AB copolymer and χ_{AB} corresponds to the segmental interaction parameter between A and B; for our system, the interaction parameter $\chi_{S\text{-}BrS}$ between brominated and non-brominated styrene segments is [1]

$$\chi_{S-BrS} = -0.0833 + \frac{73.75}{T} \tag{7.12}$$

The spinodal interaction parameter, χ_S, is given by:

$$\chi_S = \frac{0.5}{\phi_A N_A} + \frac{0.5}{\phi_B N_B} \tag{7.13}$$

From Eqs. 7.10 and 7.13, with $\phi = 0.5$ (assuming that $\phi_A + \phi_B = 1$ and making the notation change $\phi_B = \phi$ and $\phi_A = 1\text{-}\phi$), the product $N^{*}\chi = 2$ corresponds to the phase boundary. The values of $N^{*}\chi$ for each system studied are given in Tables 7.3 and 7.4. As discussed earlier, bilayer systems having values of $N^{*}\chi < 2$ are considered miscible, while systems with $\sim 3 \geq N^{*}\chi \geq 2$ are "partially miscible", and will interdiffuse until the respective layers reach

equilibrium binodal compositions. Bilayer systems with $N^*\chi > \sim 3$ are considered immiscible and have equilibrium interfacial widths on the order of tens of Angstroms.

Before analyzing PS/PBS bilayers, PS and PBS single layers were first analyzed to get accurate measurement of layer thickness and surface roughness. For the single PS layer shown in Figure 7.2, the thickness is calculated to be 647Å with surface roughness ~13Å. All of the single layers had comparable surface roughness, evidenced by distinguishable oscillations up to $q = 0.45Å^{-1}$. A representation of the electron density profile as $\delta \times 10^6$ v. z, corresponding to the values from the fit of the reflectivity data, is shown in the inset.

The first systems studied were N-symmetric bilayers. For all miscible bilayers ($N^*\chi < 2$), complete interdiffusion occurs and the equilibrium interfacial width is equal to the total thickness of the original bilayer, however, in both partially miscible and immiscible systems, the bilayers retain features of 2 layers, indicative of binodal compositions and small interpenetration depths, respectively. The two partially miscible systems of interest are N = 24, f = 0.28 and N = 1370, f = 0.25. The XR data of these bilayers were fit using binodal compositions calculated from equations 7.11 and 7.13. As shown in Table 7.3, the interfacial width in these systems decreases with $N\chi$. Shown in Figure 7.3 is the case where N = 1370, f = 0.25, which falls in the partially miscible region of the phase diagram. Figure 7.3a shows the unannealed bilayer, with roughness at the interface of the order of 12Å. However, Figure 7.3b shows the bilayer annealed for 3 hours at 225°C. Here, the oscillations are dampened due to the interdiffusion to binodal conditions, giving an interfacial width of 311Å and corresponding changes in electron density, as shown in the inset. For an example of an immiscible system, Figure 7.4 shows an XR spectrum for an unannealed PS/PBS bilayer (N_{PS}

$= N_{PBS} = 1370$, $f = 0.43$). This spectrum was fit to determine the thickness and corresponding roughness of each layer. For the example considered in Figure 7.4, the PS and PBS layers are 571Å and 654Å thick, respectively, and the interfacial roughness is on the order of 15Å. After annealing a bilayer of this system at 145°C for 3 hours, the interfacial width is calculated to be 40 ± 2.5Å. For this same system annealed at 160°C for only 10 minutes, the interfacial width is 38 ± 2 Å. This marked affect of temperature is due to an increase in both miscibility and mobility at elevated temperatures.

For N-asymmetric interfaces, shown in Table 7.4, all bilayers showed the interface moving toward the faster diffusion component, in agreement with results previously reported (see Chapter 5). For partially miscible bilayers, the interfacial widths were of the order of 300Å.

Conclusions

Interfacial widths, w_I, at PS/PBS interfaces were measured using XR. It is shown that w_I increases with temperature and decreases with increasing degree of polymerization and extent of bromination in the PBS copolymer. For miscible systems, i.e., $N^{\bullet}\chi < 2$, the equilibrium state is a single layer of constant composition, indicating complete interdiffusion and w_I equal to the thickness of the initial bilayer. In systems approaching binodal conditions, i.e., $N^{\bullet}\chi \sim 2$, w_I approaches a plateau and equilibrium layer compositions from the XR data agree with those expected from the binodal curve of the phase diagrams predicted using Flory-Huggins theory and an interaction parameter measured using SAXS[1].

For immiscible systems, i.e., $N^{\bullet}\chi >> 2$, w_I reaches only tens of Angstroms at equilibrium, consistent with expected values.

References

1. Gorga, R.E., et al., *Quantifying Phase Behavior in Partially Miscible Polystyrene/ Poly (styrene-co-4-bromostyrene) Blends.* Journal of Polymer Science: Part B, Polymer Physics, 2002. **40**: p. 255-271.
2. Gorga, R.E. and B. Narasimhan, *Fracture Toughness at Partially Miscible Polymer Interfaces.* Journal of Polymer Science, Part B: Polymer Physics, 2002. **Submitted**.
3. Kambour, R.P. and J.T. Bendler, *Miscibilities in Monodisperse Mixtures of Polystyrene, Poly(p-bromostyrene) and Their Copolymers.* Macromolecules, 1986. **19**: p. 2679-2682.
4. Kern, W. and D.A. Puotinen, *Cleaning Solution Based on Hydrogen Peroxide for use in Silicon Semiconductor Technology.* RCA Review, 1970. **31**: p. 187-206.
5. Zhao, W., et al., *Neutron and X-ray Reflectivity Measurements of Polystyrene / Polybromostyrene (PS/PBrS) Interfaces.* Physica B, 1991. **173**: p. 43-46.
6. Huttenbach, S., et al., *The Interface between Two Strongly Incompatible Polymers: Interfacial Broadening and Roughening near Tg.* Langmuir, 1991. **7**: p. 2438-2442.
7. Roe, R.-J., *Methods of X-ray and Neutron Scattering in Polymer Science.* Topics in Polymer Science, A Series of Advanced Textbooks and Monographs, ed. J.E. Mark. 2000, New York: Oxford University Press.

8. Bruder, F. and R. Brenn, *Measuring the Binodal by Interdiffusion in Blends of Deuterated Polystyrene and Poly (styrene-co-4-bromostyrene).* Macromolecules, 1991. **24**: p. 5552-5557.

Table 7.1: Degree of polymerization, extent of bromination, and polydispersity of PS/PBS system.

$(C_8H_{(8-x)}Br_x)_N$			
N	x	f	M_w/M
424	0	0	1.03
	0.07	0.08	
	0.20	0.22	
	0.25	0.28	
	0.42	0.46	
1370	0	0	1.03
	0.08	0.09	
	0.22	0.25	
	0.39	0.43	
7670	0	0	1.05
7144	0.04	0.04	1.1
	0.20	0.22	

Table 7.2: Fitting parameters dispersion, δ, and absorption, β, at λ = 1.26514Å for PS/PBS bilayers on silicon. Using Equations 7.2 and 7.3, these parameters may be calculated for different wavelengths.

Material	dispersion, δ (x 10^6)	absorption, β (x 10^6)
Silicon	5.0212	0.16
SiO_2	4.3868	0.17
PS	2.2474	0.0041
PBS, f = 0.04	2.2771	0.0056
PBS, f = 0.08	2.2996	0.0067
PBS, f = 0.09	2.3072	0.0071
PBS, f = 0.22	2.3988	0.011
PBS, f = 0.25	2.4143	0.012
PBS, f = 0.28	2.4376	0.013
PBS, f = 0.43	2.5501	0.018
PBS, f = 0.46	2.5716	0.020

Table 7.3: Interfacial width, w_I, for N-symmetric PS/PBS systems. $N\chi$ evaluated at the temperature shown. For miscible systems ($N\chi < 2$), the equilibrium interfacial width is equivalent to the total thickness of the bilayer.

N	f	$N\chi$	T (°C)	w_I(Å)
424	0	0	200	--
	0.08	0.20	200	--
	0.22	1.49	200	--
	0.28	3.02	150	140
		2.41	200	230
1370	0	0	200	--
	0.09	0.81	200	--
	0.25	5.54	175	143
		6.96	225	93
	0.43	21.06	145	40
7670	0	0	200	--
7144	0.04	0.86	200	--

Table 7.4: Interfacial width, w_I, for N-asymmetric PS/PBS systems: $N^*\chi$ evaluated at the temperature shown. For miscible systems ($N^*\chi < 2$), the equilibrium interfacial width is equivalent to the total thickness of the bilayer.

N_{PS}	N_{PBS}	f	T (°C)	$N^*\chi$	w_I(Å)
1370	424	0.08	200	0.30	--
7670	424	0.08	200	0.37	--
1370	424	0.22	200	2.27	304
7670	424	0.22	200	2.82	300
424	1370	0.09	200	0.38	--
7670	1370	0.09	200	1.37	--
424	7144	0.04	200	0.093	--
1370	7144	0.04	200	0.27	--
424	7144	0.22	200	2.81	293

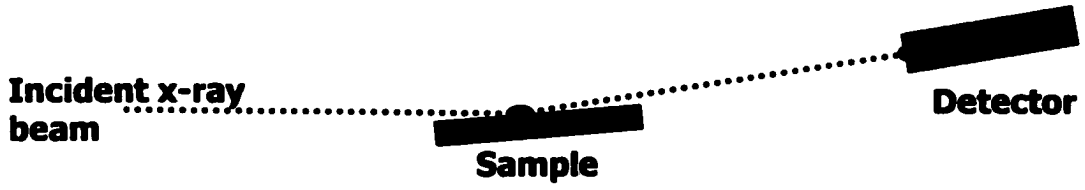

Figure 7.1a: Schematic of XR experimental setup.

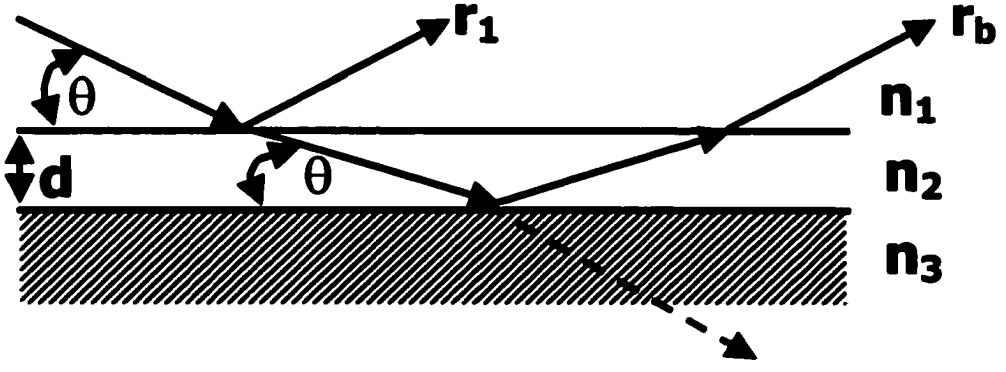

Figure 7.1b: Schematic of reflection in a single layer sample. X-rays are reflected from the surface of the film and from the substrate surface; n_i are the respective refractive indices.

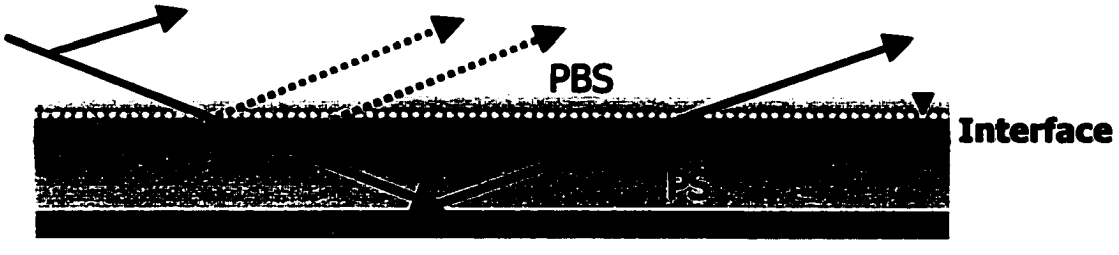

Figure 7.1c: Schematic of reflection in an annealed bilayer sample. X-rays are reflected from each layer of the sample that has sufficient electron density contrast.

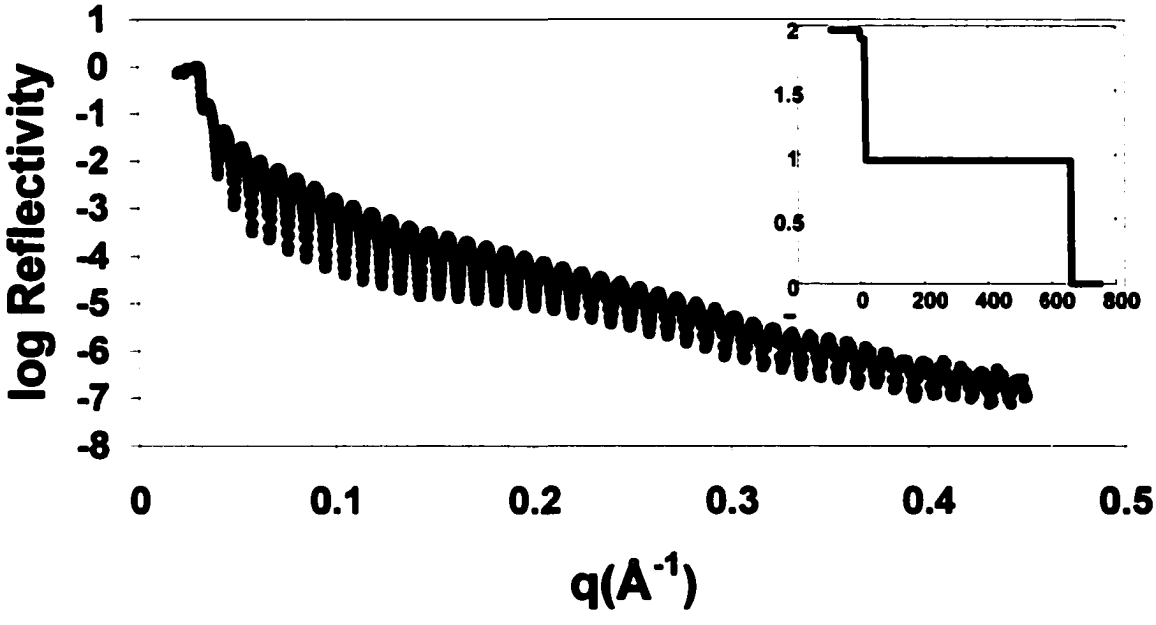

Figure 7.2: XR data of unannealed PS single layer, N = 424. The PS layer is 647Å thick and the surface roughness is on the order of 13Å; this low value of surface roughness is evidenced by the distinct oscillations even at q = 0.45. A representation of the electron density profile (as $\delta \times 10^6$ v. z) is shown in the inset.

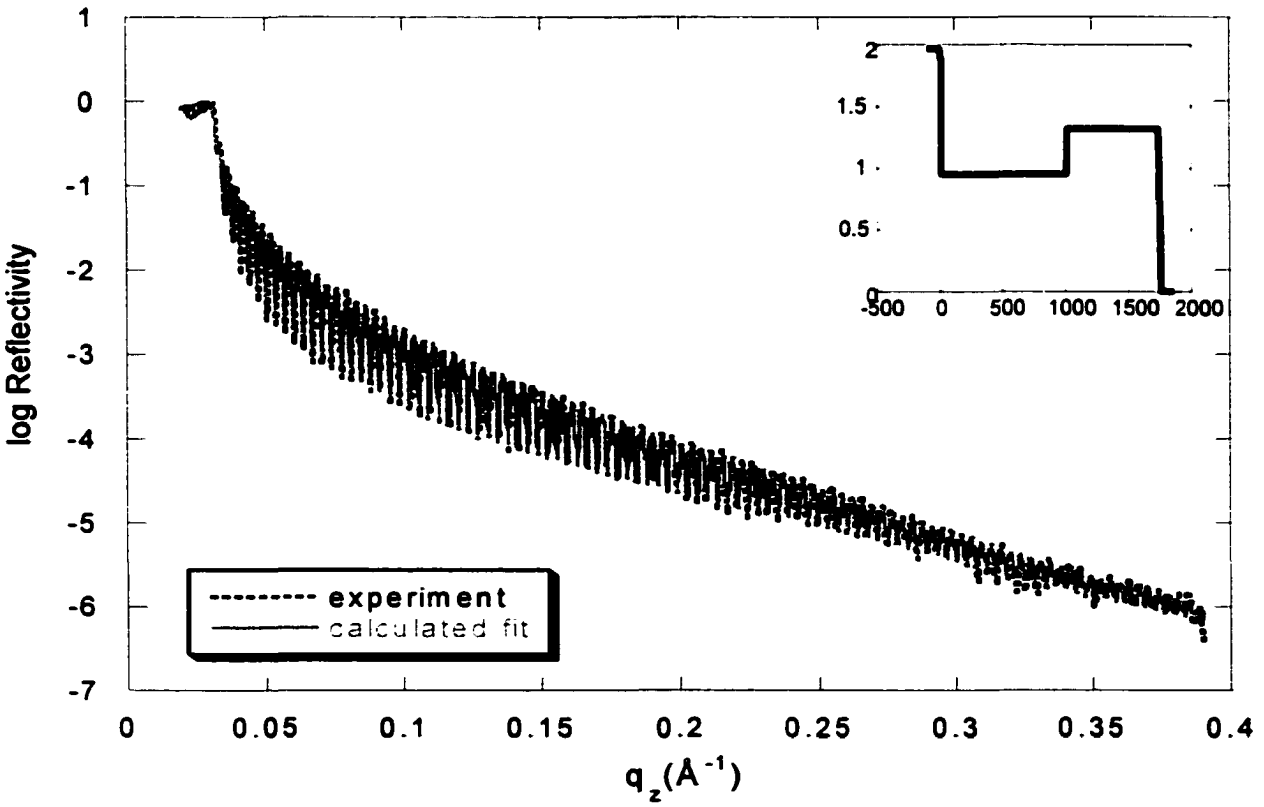

Figure 7.3a: XR data of unannealed N-symmetric bilayer. N = 1370, f = 0.25. PS and PBS layers are 1005Å and 729Å thick, respectively, and the interfacial roughness is on the order of 12Å. A representation of the electron density profile (as $\delta \times 10^6$ v. z) is shown in the inset.

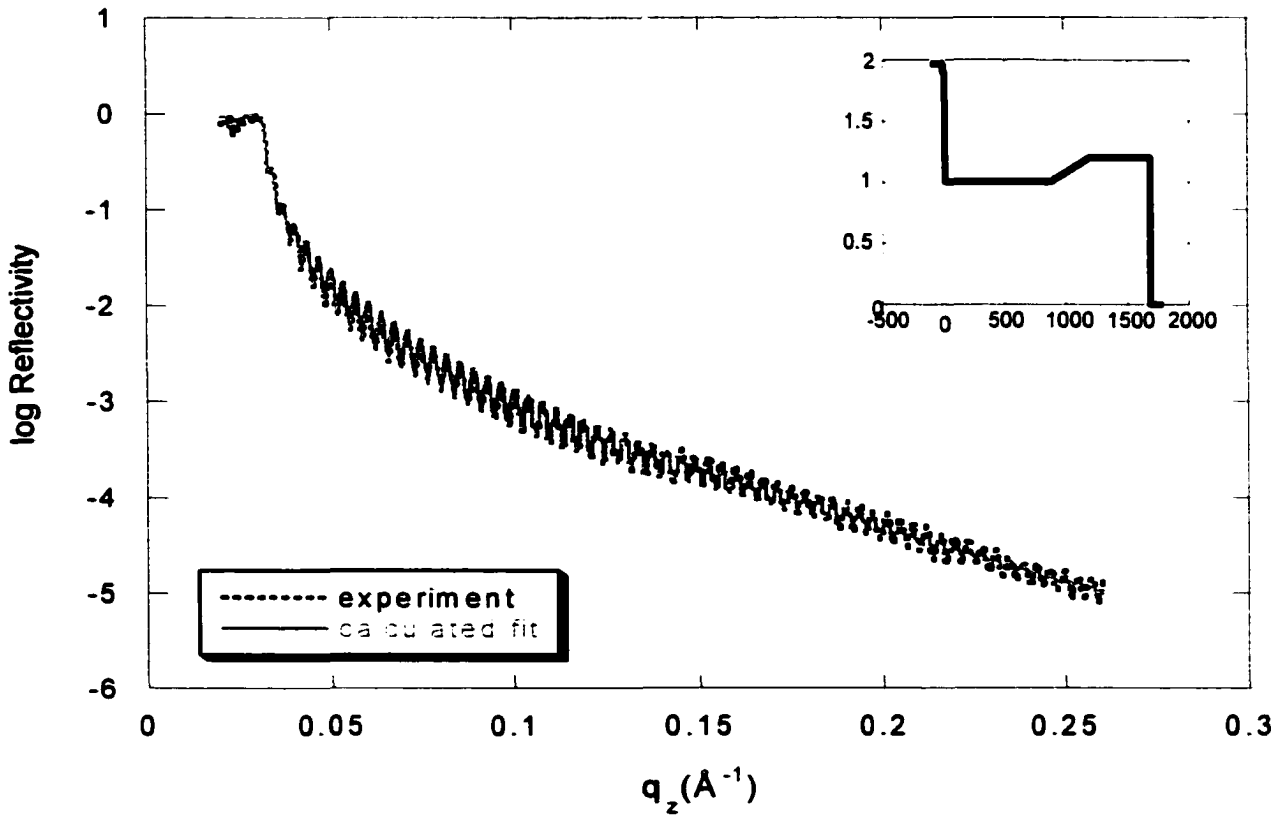

Figure 7.3b: XR data of unannealed N-symmetric bilayer. N = 1370, f = 0.25. PS and PBS layers are 1018Å and 652Å thick, respectively, and the interfacial width is of the order of 311Å. A representation of the electron density profile (as $\delta \times 10^6$ v. z) is shown in the inset.

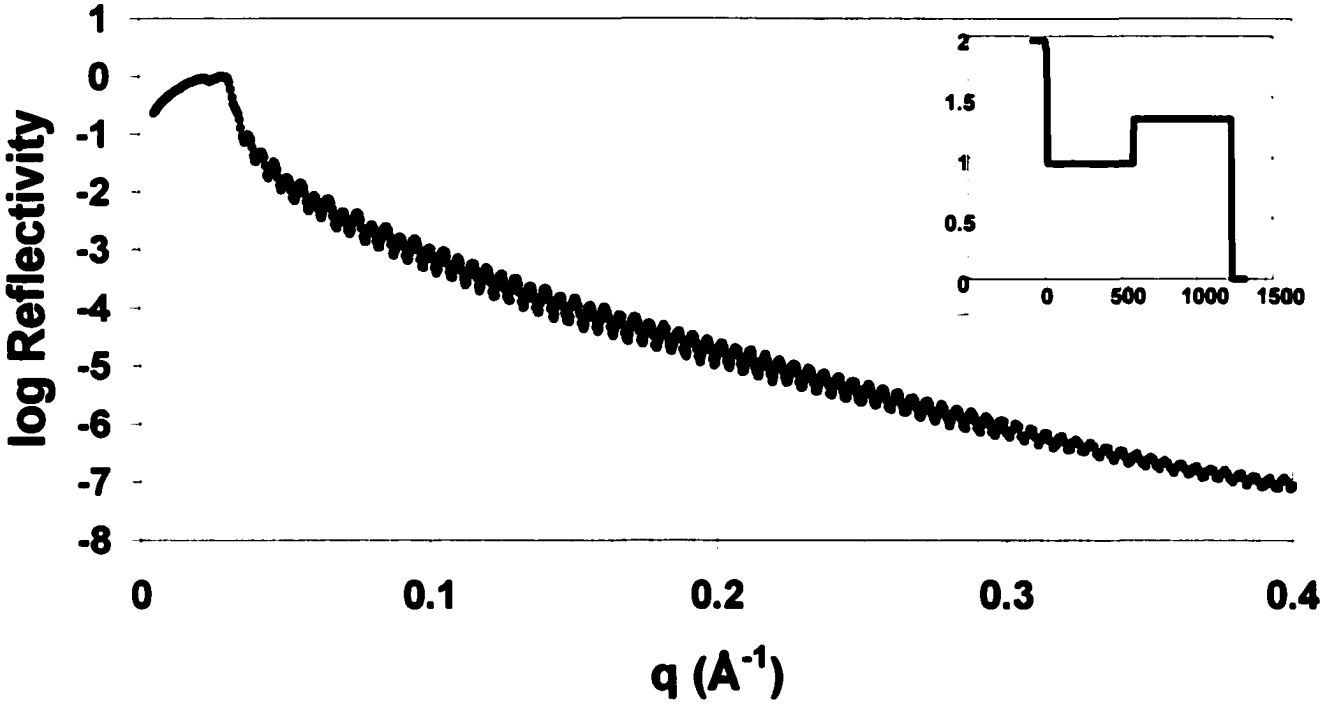

Figure 7.4: XR data of unannealed N-symmetric bilayer. N = 1370, f = 0.43. PS and PBS layers are 571Å and 654Å thick, respectively, and the interfacial roughness is on the order of 15Å. A representation of the electron density profile (as $\delta \times 10^6$ v. z) is shown in the inset.

CHAPTER 8

CONCLUSIONS

The research reported in this dissertation has contributed to a fundamental understanding of interdiffusion phenomena at homopolymer/copolymer interfaces. It has been shown that both interdiffusion dynamics and interfacial width can be quantified in partially miscible systems as a function of degree of polymerization, copolymer composition, and temperature through measurement of concentration v. depth profiles. The experimental studies investigated interdiffusion phenomena in bilayers of polystyrene (PS) and the statistically random copolymer poly(styrene-*r*-4-bromostyrene) (PBS), $(C_8H_{(8-x)}Br_x)_N$, where x is the mole fraction of brominated repeat units in the copolymer and N the degree of polymerization. Rutherford backscattering spectroscopy (RBS) was used to examine PS/PBS bilayers; PBS volume fraction v. depth profiles were obtained from the evolution of the bromine peak in the RBS spectra. Mutual diffusion coefficients were determined by comparison of the RBS data to a mean-field interdiffusion model. The effect of the thermodynamic component of the mutual diffusion coefficient was demonstrated using N-symmetric systems. For partially miscible systems it was shown that incorporating the square-gradient modification in the diffusion equation derived from the Flory-Huggins expression for free energy fit the concentration v. depth profiles. In N-asymmetric systems, both kinetic and thermodynamic effects were investigated and agreement with the fast-mode expression for mobility was demonstrated. The mutual diffusion coefficient was shown to decrease with increasing degree of polymerization and extent of bromination of the PBS copolymer and increase with temperature. It was also shown that as spinodal conditions are

approached, interdiffusion occurred until layer compositions indicative of the phase boundary are reached. These observations were in agreement with phase diagrams obtained using Flory-Huggins theory and a PS/PBS Flory-Huggins interaction parameter measured using small angle x-ray scattering (SAXS). The implications of this miscibility dependence of the mutual diffusion coefficient, based on both composition of the copolymer and degree of polymerization, were discussed. For bilayers of PS/PBS with a great disparity in thickness, the effect of interfacial tension and the resulting "interphase" formation and preferential segregation to the surface were investigated. For polydisperse systems, it was shown that short chains present behave as surfactants and ultimately increase the extent of interdiffusion. For immiscible polydisperse systems, the phenomenon of surface encapsulation from the bilayer was demonstrated.

X-ray reflectivity (XR) was used to measure interfacial width in bilayers comparable to those used in both the N-symmetric and N-asymmetric RBS studies. XR experiments were performed on the synchrotron beamline at the Advanced Photon Source, Argonne National Laboratory. In agreement with the results of the RBS studies, interfacial width increases over time, but is limited by miscibility at equilibrium and the equilibrium interfacial width plateau is reached significantly faster in more miscible systems. These results are in qualitative agreement with our RBS studies on measurement concentration v. depth profiles, which show decreasing interdiffusion with increase in the extent of bromination. The XR studies have demonstrated that a) for the lower extents of bromination considered (N = 424: f = 0.08, f = 0.22, N = 1370: f = 0.09, N = 7144, f = 0.04) the synchrotron beam is sensitive to the electron density difference, thus rendering X-ray reflectivity feasible for the proposed studies; b) for systems where extensive interdiffusion

was observed using RBS, the reflectivity data showed loss of distinguishable layers; c) for systems where no interdiffusion or interdiffusion until binodal compositions was observed in the RBS studies, the reflectivity data indicate that the bilayers remain discreet and interfacial widths can be measured.

In conclusion, the fundamental understanding of the role of miscibility in the interfacial characteristics of homopolymer/copolymer systems obtained in this dissertation will aid in the molecular design of tailored interfaces for specific applications. The results of this work, specifically the quantification of the transition from miscible to partially miscible to immiscible, will assist in characterization of the molecular behavior at the growing interface as interdiffusion progresses. Also, it was demonstrated that interdiffusion (RBS), interfacial width (XR), fracture energy (MDCB), phase diagram predictions (using χ from SAXS), and phase morphology (AFM), are consistent with each other.

CHAPTER 9

FUTURE DIRECTIONS

9.1 Introduction

This dissertation discussed interdiffusion phenomena, including measurements of interfacial width, in a partially miscible homopolymer/copolymer system and the correlation with phase behavior and fracture energy for the same system. This chapter discusses possibilities for future research in areas that are a direct extension of the knowledge of the miscibility and mobility effects in partially miscible polymer systems gained from the work described in this dissertation.

9.2 Investigation of compositional dispersion in partially miscible homopolymer/ copolymer systems

A more complete description of the interdiffusion behavior at a partially miscible polymer interface A/AB, where A is a homopolymer and AB a statistically random copolymer of A and B, must allow for the two species to have different a) degree of polymerization (N_i), b) polydispersity (PDI), and c) mobility (D_i), while also allowing for the possibility of a distribution of copolymer composition in the AB layer. As mentioned previously, the effect of miscibility in the system must be taken into account, as quantified by the Flory-Huggins (FH) interaction parameter, χ. For a homopolymer, A, and a statistically random copolymer, AB,

$$\chi = f^2 \chi_{AB} \tag{9.1}$$

where f is the volume fraction of B units in the AB copolymer and χ_{AB} corresponds to the segmental interaction parameter between A and B. The spinodal interaction parameter, χ_S, is given by

$$\chi_S = \frac{0.5}{\phi_A N_A} + \frac{0.5}{\phi_B N_B} \tag{9.2}$$

For N-asymmetric bilayers, i.e., when $N_A \neq N_B$, the average N of the system, N^*, is given by $N^* = 2N_AN_B/N_A+N_B$. From Eq. 9.2, with $\phi = 0.5$ (assuming that $\phi_A + \phi_B = 1$ and making the notation change $\phi_B = \phi$ and $\phi_A = 1-\phi$), the product $N^*\chi = 2$ corresponds to the phase boundary. As discussed earlier, bilayer systems having values of $N^*\chi < 2$ are considered miscible, while systems with $\sim 3 \geq N^*\chi \geq 2$ are "partially miscible", and will interdiffuse until the respective layers reach equilibrium binodal compositions.

In general, it is possible to have both a distribution of N (in A or AB) and a distribution of f in the AB copolymer. In a partially miscible bilayer with the respective polymers having PDI > 1, the shorter chains of each species are more miscible with each other than the longer chains, i.e., the quantity $N^*\chi$ is smaller for chains with lower N. Therefore, short chains can be expected to compatibilize partially miscible interfaces, dominating the effect of the presence of longer chains. When comparing a polydisperse system to a monodisperse system having the same f, it is expected that short chains will segregate to the interface and lead to increased interdiffusion for the polydisperse bilayers. To capture this behavior, a normalized N_i^* for polydisperse systems could be defined as

$$\frac{1}{N_i^*} = \frac{\sum_j \frac{n_j}{N_j}}{\sum_j n_j} \tag{9.3}$$

Here, N_j is the degree of polymerization of chain j and n_j is the number of such chains. This normalization is only necessary when polydisperse systems are considered. For the case when there is a composition "drift" in the AB copolymer, the same idea holds, i.e., chains with lower f will contribute to lower $N^*\chi$ values and therefore have a compatibilizing role at the interface. Because miscibility is dependent on f^2, a normalized composition may be proposed as:

$$\frac{1}{f} = \frac{\sqrt{\sum_k \frac{m_k}{f_k^2}}}{\sqrt{\sum_k m_k}} \tag{9.4}$$

Here f_k is the composition of chain k and m_k is the number of chains with composition f_k. Again, this normalization is only necessary when there is a distribution of f in the AB copolymer.

The results of Chapter 6 indicate that interdiffusion is facilitated by a molecular weight distribution due to the presence of short chains in the polydisperse system reducing interfacial tension. Following from this, an investigation of the effect of introducing a dispersion of copolymer composition may also be a way to compatibilize interfaces without using short chains, which may actually weaken interfaces due to their limited ability to form significant entanglements across the interface that can support stresses. Research in this area has only recently begun [1], and new theories may need to be developed to describe interdiffusion in such systems.

9.3 Applications in semi-crystalline polymer interfaces

Although amorphous polymers were used in all of the studies in this dissertation, there is an opportunity to study the same phenomena, i.e., to relate microscopic characteristics (including molecular architecture) to the macroscopic properties in semi-crystalline polymer systems. The crystalline phases near the interface have the ability to act as a hindrance to formation of entanglements that can support stresses by essentially blocking diffusion of chains of the interfacing material from entering the layer, but they may also provide additional fracture strength by acting as anchors for "tie molecules" bridging the interface. Exploring the effect of copolymer composition, degree of polymerization, and dispersions in either or both as well as any disparity in glass transition temperature would provide valuable insight for molecularly tailoring semi-crystalline interfaces.

9.4 Applications in photoresist research

The discussion of miscibility-limited diffusion, the effect of introducing dispersions of copolymer composition and degree of polymerization, and the correlation with surface phenomena and phase behavior can be directly extended to the area of photoresist materials. The following is a proposed research plan that is a direct extension of the work described in this dissertation.

The continued decrease of feature sizes in microelectronic devices will soon require critical dimensions (CD) less than 100nm. However, the allowable variation in CD is approaching the size scale of the constituent polymer molecules (< 20nm) used to fabricate them. Efforts to achieve the required CD while controlling its variation, or line edge roughness (LER), have resulted in investigations into the source of this roughness. LER has

been attributed to variables such as the feature size, exposure technique, development process, and the intrinsic properties of the photoresist materials. The goal of the proposed research is to investigate and understand the contribution of fundamental material variables (miscibility, phase morphology, surface/interfacial energy) on LER in photoresist materials.

A schematic of the photolithographic process with chemically amplified photoresists used in current semiconductor production lines is shown in Figure 9.1 [2]. A silicon substrate is coated with a polymer photoresist film loaded with a photoacid generator (PAG) and other additives and subjected to a post apply bake (PAB). The photoresist is then patterned by exposure to radiation through a mask (aerial image). Upon exposure, the PAG is converted into an acid species and a post-exposure bake (PEB) is used both to enhance acid diffusion and to catalyze a deprotection reaction on the polymer, altering its solubility to an aqueous base solution. In negative-tone resists, the exposed regions are insoluble in the developer while in positive-tone resists the exposed regions are soluble in the developer. An etching process, typically reactive ion etching, is used to transfer the pattern from the photoresist material to the underlying substrate; consequently, any defect in the photoresist pattern is also transferred.

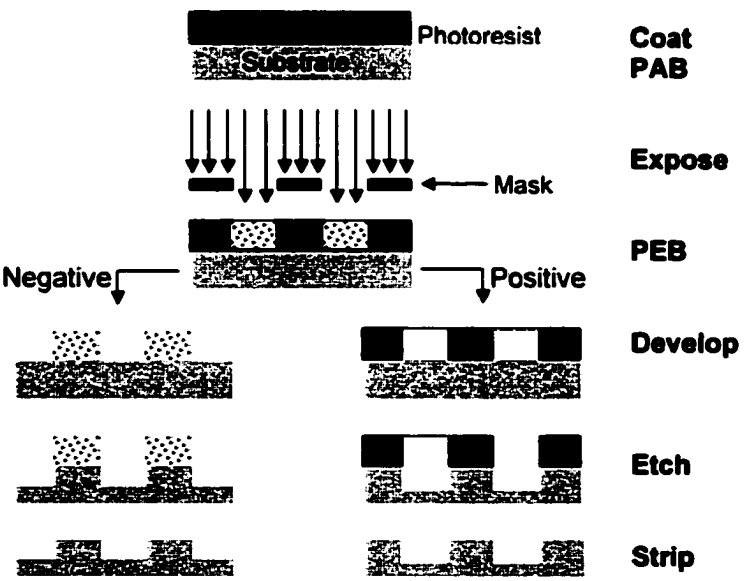

Figure 9.1. The photolithographic process[2]

The effects of processing parameters, aerial image quality, development, and etching on LER have been studied with both experiments and models [3-8]. These effects are currently optimized without reference to the material properties of the system. However, at the smaller length scales anticipated for the future, the LER limits due to the intrinsic properties and behavior of the systems comprise larger fractions of the available error budget and may control the ultimate limitations in the use of these photoresists to pattern device structures.

Some work has begun to address the materials contributions to LER, but few studies have identified or quantified fundamental physical parameters and mechanisms needed to understand the performance of these complex formulations. For example, it has been shown that LER can be reduced by the promotion of uniform dissolution during development [5]. This is important in regions of variable solubility, located at the edges of the patterned structures (line-edge), due to the physical processes in lithography. Figure 9.2 [9] schematically shows the material components in the line-edge region. At the line-edge, the exposure dose does not have sharply defined edges. Edges are created from a threshold dose leading to varying levels of deprotection in the photoresist polymer. Consequently, a composition gradient is present between the

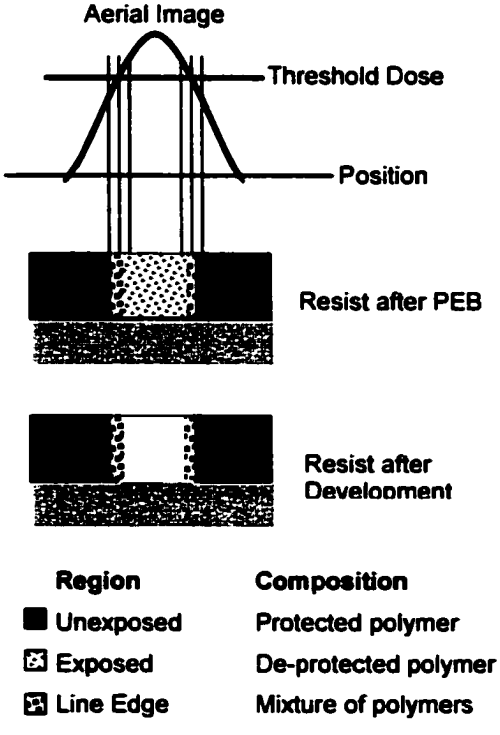

Figure 9.2. Analysis of resist composition in line edge region of a chemically amplified positive tone resist under an imaging dose[11]

exposed and unexposed areas of the resist leading to varying solubility and dissolution rate. Prior investigations have shown that polymer aggregates are formed in the line edge region, leading to non-uniform dissolution [10-12]. The location, breadth, and composition of the line-edge region controls both CD and LER.

Fundamental materials science studies of the line-edge region have only recently begun. Lin and co-workers [9] performed the first experiments investigating the effects of the phase behavior of mixtures of protected and deprotected polymers on LER. Using blends of protected polymer with copolymers having varying extents of de-protection, they showed that heterogeneous composition along the line-edge may lead to the formation of phase separated domains that result in increased surface roughness after development. By probing the surface roughness of these blends following standard resist processing steps, they define a temperature for which minimal surface roughness is achieved. Also, the depth-dependence of LER was investigated using AFM [13]. It was observed that roughness decreases near the photoresist/substrate interface suggesting possible surface/interfacial energy effects and warranting further investigation.

Although the mechanisms of the sources of LER have been qualitatively identified, they have not been investigated using fundamental polymer physics concepts and formalism. This research will focus on the effect of phase behavior between the deprotected and protected polymer in the line-edge region. As an example, the degree of miscibility between the two polymers consisting of varying fractions of the same monomers (as in the line-edge region) strongly affects both the kinetics and interfacial characteristics [14, 15]. This work will first measure important bulk thermodynamic parameters, and then develop a theoretical construct relating the thermodynamic and kinetic behavior to predict the behavior of a

material system under defined conditions. The theoretical predictions can be tested with experiments measuring the topography and surface composition using atomic force microscopy (AFM), scanning electron microscopy (SEM), and x-ray photoelectron spectroscopy (XPS) and the length scale of transitions from one distinct phase to another (interfacial width) using neutron reflectivity(NR).

An evident first step would be to quantify the Flory-Huggins interaction parameter in these partially miscible polymer systems. The Flory-Huggins interaction parameter, χ, is a segmental interaction parameter that quantifies the compatibility of a polymer system and has both enthalpic and entropic contributions. As illustrated in Figure 9.3, due to competing thermodynamic (segregation) and kinetic (interdiffusion) effects in partially miscible polymer systems, an optimal temperature can be determined for a given blend of homopolymer/ copolymer if the Flory-Huggins interaction parameter and copolymer composition(s) are known. Initial investigations to determine χ between various species in a positive-tone chemically amplified photoresist, i.e., between protected and de-protected polymer, $\chi_{P\text{-}DP}$, and between protected or de-protected polymer and any additives that may be present, $\chi_{P\text{-}A}$ and $\chi_{DP\text{-}A}$, will use the model 248nm system of the protected polymers poly(t-butyloxycarbonyl-oxystyrene) (PBOCSt) and poly(hydroxy-styrene) (PHS) with the PAG bis(p-tert-butylphenyl) iodonium perfluorooctane-sulfonate (PFOS).

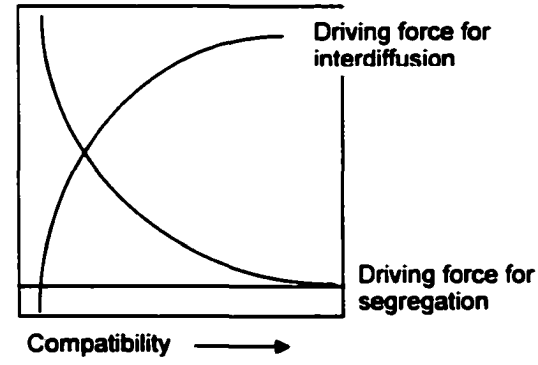

Figure 9.3: In partially miscible polymer systems, there are competing effects of thermodynamic and kinetic origin. Because of this intrinsic material property, minimal roughness can be achieved.

Small angle neutron scattering (SANS) could be used to quantify the interaction parameter between protected and de-protected molecules deuterated accordingly. Traditional SANS techniques to measure the interaction parameter using elevated temperatures to achieve a one-phase system are not straightforward in positive-tone resists with protected and de-protected polymers due to the de-protection reaction that occurs at elevated temperatures. To overcome this difficulty, a ternary system using a common solvent can be employed and χ determined from the respective interactions of the protected and de-protected polymers with the solvent.

To confirm that the interaction parameters determined from bulk measurements are applicable to thin films, it would be necessary to examine the phase morphology in thin films of these materials using AFM. AFM has been used extensively to give both qualitative and quantitative information about the phase morphology of photoresist systems [5, 8, 9, 12, 13, 16-21]. The lateral dimension and height of phase domains and the dependence of the morphology on various parameters including molecular weight, copolymer composition, and content of additives will be quantified using AFM. The effect of these parameters on the solubility will also be investigated, knowing that evenly distributed solubility reduces LER, as mentioned above. Due to differences in surface energy of the protected and de-protected polymers, there may be a surface enrichment of the lower surface energy material. To complement the AFM studies, XPS will be used to determine the surface composition in the line-edge region.

Neutron reflectivity (NR) will be used to verify whether exposure creates discrete layers of copolymers with varying extents of de-protection and to measure interfacial widths in bilayers of the fully protected polymer and the partially de-protected copolymers. Once

the thermodynamic parameters are known, they can be used to predict the kinetic behavior of the system.

Results of this research would provide information about the material properties that control the success of a particular material in a microlithographic application. With knowledge of the thermodynamic parameters of the system, the kinetic behavior and performance of a photoresist material with given process conditions can be predicted. For photoresist systems including positive-tone, negative-tone, and top-surface imaging 248, 193, and 157nm materials, knowledge of the fundamental material properties such as χ, phase morphology, surface energy, and solubility will allow processing conditions to be tailored accordingly to achieve minimum CD and LER.

9.5 References

1. Benkoski, J.J., G.H. Fredrickson, and E.J. Kramer, *Effects of Coposition Drift on the effectiveness of Random Copolymer Reinforcement at Polymer-Polymer Interfaces.* Journal of Polymer Science, Part B: Polymer Physics, 2001. **39**: p. 2363-2377.
2. Stewart, M.D., et al., *Organic imaging materials: a view of the future.* Journal of Physical Organic Chemistry, 2000. **13**: p. 767-774.
3. Koh, H.P., et al., *Effects of process parameters on pattern-edge roughness of chemically amplified resists.* Proc. SPIE-Int. Soc. Opt. Eng., 2000. **3999**(Pt. 1, Advances in Resist Technology and Processing XVIII): p. 240-251.
4. Schmid, G.M., et al., *Understanding molecular-level effects during post-exposure processing.* Proc. SPIE-Int. Soc. Opt. Eng., 2001. **4345**(Part 2, Advances in Resist Technology and Processing XVIII): p. 1037-1047.

5. Ryoo, M., et al., *Control of line edge roughness of ultrathin resist films subjected to EUV exposure.* Proc. SPIE-Int. Soc. Opt. Eng., 2001. **4345**(Part 2, Advances in Resist Technology and Processing XVIII): p. 903-911.

6. Hasko, D.G., S. Yasin, and A. Mumtaz, *Influence of developer and development conditions on the behavior of high molecular weight electron-beam resists.* Journal of Vacuum Science Technology B, 2000. **18**(6): p. 3441-3444.

7. Palmateer, S.C., et al., *Line edge roughness in sub-0.18-μm resist patterns.* Proc. SPIE-Int. Soc. Opt. Eng., 1998. **3333**(Part 1, Advances in Resist Technology and Processing XV): p. 634-642.

8. He, D. and F. Cerrina, *Process dependence of roughness in a positive-tone chemically amplified resist.* Journal of Vacuum Science Technology B, 1998. **16**(6): p. 3748-3751.

9. Lin, Q., R. Sooriyakumaran, and W.-S. Huang, *Toward controlled resist line edge roughness: material origin of line edge roughness in chemically amplified positive-tone resists.* Proc. SPIE-Int. Soc. Opt. Eng., 2000. **3999**(Part 1, Advances in Resist Technology and Processing XVII): p. 230-239.

10. Namatsu, H., et al., *Influence of edge roughness in resist patterns on etched patterns.* Journal of Vacuum Science Technology B, 1998. **16**(6): p. 3315-3321.

11. Namatsu, H., T. Yamaguchi, and K. Kurihara, *Resist materials providing small line-edge roughness.* Materials Research Society Symposium Proceedings, 2000. **584**(Materials Issues and Modeling for Device Nanofabrication): p. 135-146.

12. Yamaguchi, T., et al., *Line-edge roughness characterized by polymer aggregates in photoresists.* Proc. SPIE-Int. Soc. Opt. Eng., 1999. **3678**(Part 1, Advances in Resist Technology and Processing XVI): p. 617-624.

13. Reynolds, G.W. and J.W. Taylor, *Correlation of atomic force microscopy sidewall roughness measurements with scanning electron microscopy line-edge roughness measurements on chemically amplified resists exposed by x-ray lithography.* Journal of Vacuum Science Technology B, 1999. **17**(6): p. 2723-2729.

14. Gorga, R.E., et al., *Quantifying Phase Behavior in Partially Miscible Polystyrene/Poly(styrene-co-4-bromostyrene) Blends.* Journal of Polymer Science: Part B: Polymer Physics, 2002. **40**: p. 255-271.

15. Jablonski, E.L., et al., *Miscibility-Mediated Interdiffusion Dynamics at Polymer Interfaces.* Macromolecules, 2001. **submitted**.

16. Lin, Q., R. Sooriyakumaran, and W.-S. Huang, *AFM study of positive chemically amplified resists.* Polymer Preprints (American Chemical Society, Division of Polymer Chemistry), 2000. **41**(2): p. 1460-1461.

17. Lin, Q., et al., *Line-edge roughness in positive-tone chemically amplified resists: effect of additives and processing conditions.* Proc. SPIE-Int. Soc. Opt. Eng., 2001. **4345**(Part 1, Advances in Resist Technology and Processing XVIII): p. 78-86.

18. Nelson, C., et al., *Comparison of metrology methods for quantifying the line edge roughness of patterned features.* Journal of Vacuum Science Technology B, 1999. **17**(6): p. 2488-2498.

19. Nelson, C.M., et al., *Metrology methods for quantifying edge roughness: II.* Proc. SPIE-Int. Soc. Opt. Eng., 1999. **3677**(Part 1, Metrology, Inspection, and Process Control for Microlithography XIII): p. 53-61.

20. Kant, A., G. Talor, and N. Samarakone, *Quantitative line edge roughness characterization for sub-0.25-μm DUV lithography.* Proc. SPIE-Int. Soc. Opt. Eng., 1999. **3677**(Part 1, Metrology, Inspection, and Process Control for Microlithography XIII): p. 35-42.

21. Sugihara, T., et al., *Resist surface investigations for reduction of line-edge-roughness in top surface imaging technology.* Microelectronic Engineering, 1999. **46**(1-4): p. 339-343.

APPENDIX 1

CONVERSION OF RBS DATA TO CONCENTRATION V. DEPTH

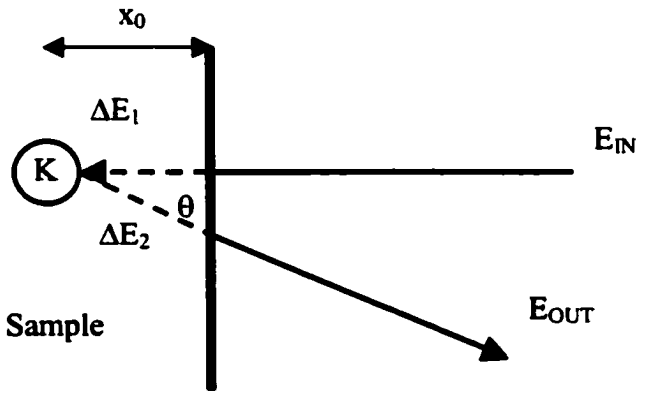

The initial ion energy impinging on the sample from the accelerator is given by E_{IN}. All the RBS studies shown here were carried out at an energy of 2.06MeV. The energy lost entering the sample is given by ΔE_1, and can be determined from the stopping range of ions in matter (SRIM). K is the kinematic factor, essentially a measure of the energy lost upon colliding with an element. Values of K are tabulated for common elements[1]. For a perfectly elastic collision, K would equal unity. The heavier the element, the larger the magnitude of the kinematic factor. For bromine, this factor is 0.8185. ΔE_2 is the energy lost by the ion while exiting the sample and can also be determined using SRIM. E_{OUT} is the energy of the ion leaving the sample, which is the energy that the detector records. The angle between the incident beam and the detector is θ and was equal to 165° for all the studies discussed in this thesis.

The stopping range of ions in this sample are given in the units of dE/dx. Using[1]

$$\Delta E_1 \approx x_0 \left(\frac{dE}{dx}\right)\Big|_{E_{IN}} \text{ as an approximation to } \int_0^{x_0} \frac{dE}{dx} dx \text{ and} \qquad \text{(A1.1)}$$

[1] (http:/www.research.ibm/ionbeams/SRIM)

$$\Delta E_2 \approx \frac{x_0}{\cos\theta}\left(\frac{dE}{dx}\right)\Big|_{K(E_{IN}-\Delta E_1)} \text{ to approximate } \frac{1}{\cos\theta}\int_{x_0}^{0}\frac{dE}{dx}dx \qquad \text{(A1.2)}$$

and assuming ΔE_1 to be negligible compared to E_{IN}, the following can be derived:

$$E_{OUT} = K\left(E_{IN} - x_0\left(\frac{dE}{dx}\right)\Big|_{E_{IN}}\right) - \frac{x_0}{\cos\theta}\left(\frac{dE}{dx}\right)\Big|_{KE_{IN}} \qquad \text{(A1.3)}$$

The values for dE/dx at both E_{IN} and KE_{IN} can be found using SRIM and are reported in the units of eV/Angstrom. E_{OUT} is given by the channel to energy conversion provided by RUMP. RUMP is a software package developed by Doolittle and, in addition to providing data conversion parameters, can be used to simulate and perform preliminary analysis on the RBS spectra. Typical RBS data is obtained as counts (normalized yield) v. channel (energy). Energy is converted to depth by solving for x_0 in Equation A1.3. Counts are normalized with respect to the bromine peak to obtain volume fraction.

APPENDIX 2

DERIVATION OF DIFFUSION EQUATION

The Flory-Huggins expression for free energy of mixing, modified by the square-gradient term, for two polymers A and B is given by:

$$f_{FH} = \frac{\phi}{N_B}\ln\phi + \frac{1-\phi}{N_A}\ln(1-\phi) + \chi\phi(1-\phi) + \frac{b^2}{36\phi(1-\phi)}\left(\frac{\partial\phi}{\partial x}\right)^2 \qquad \text{(A2.1)}$$

Here $\phi = \phi_B = 1-\phi_A$, represent the volume fractions of polymers A and B, b is the average monomer segment length, χ is the Flory-Huggins segmental interaction parameter, and N_A and N_B are the degrees of polymerization of A and B. The chemical potential is the derivative of the free energy expression with respect to ϕ, given by:

$$\mu = \frac{\partial f_{FH}}{\partial\phi} = \frac{1+\ln\phi}{N_B} - \frac{1+\ln(1-\phi)}{N_A} + \chi(1-2\phi) - \frac{b^2}{18\phi(1-\phi)}\left(\frac{\partial^2\phi}{\partial x^2}\right) - \frac{b^2(1-2\phi)}{36\phi^2(1-\phi)^2}\left(\frac{\partial\phi}{\partial x}\right)^2 \qquad \text{(A2.2)}$$

The spatial derivative of the chemical potential is given by:

$$\frac{\partial\mu}{\partial x} = \left(\frac{1}{\phi N_B} + \frac{1}{(1-\phi)N_A} - 2\chi\right)\frac{\partial\phi}{\partial x} - \frac{b^2}{18\phi(1-\phi)}\left(\frac{\partial^3\phi}{\partial x^3}\right) + \frac{b^2(1-2\phi)}{18\phi^2(1-\phi)^2}\left(\frac{\partial^2\phi}{\partial x^2}\right)\left(\frac{\partial\phi}{\partial x}\right) - \frac{b^2(1-2\phi)}{18\phi^2(1-\phi)^2}\left(\frac{\partial^2\phi}{\partial x^2}\right)\left(\frac{\partial\phi}{\partial x}\right) + \frac{b^2\left(\phi(1-\phi)+(1-2\phi)^2\right)}{18\phi^3(1-\phi)^3}\left(\frac{\partial\phi}{\partial x}\right)^3 \qquad \text{(A2.3)}$$

Incorporating the fast-mode expression for mobility, the flux is given by:

$$-J = mobility\left(\frac{\partial \mu}{\partial x}\right) =$$

$$\phi(1-\phi)\left(\phi N_A D_A + (1-\phi)N_B D_B\right)\left[\begin{array}{l}\left(\frac{1}{\phi N_B}+\frac{1}{(1-\phi)N_A}-2\chi\right)\frac{\partial \phi}{\partial x}-\frac{b^2}{18\phi(1-\phi)}\left(\frac{\partial^3 \phi}{\partial x^3}\right) \\ +\frac{b^2\left(\phi(1-\phi)+(1-2\phi)^2\right)}{18\phi^3(1-\phi)^3}\left(\frac{\partial \phi}{\partial x}\right)^3\end{array}\right] \tag{A2.4}$$

The following two steps expand the flux expression.

$$-J = \left(\phi N_A D_A + (1-\phi)N_B D_B\right)\left[\begin{array}{l}\left(\frac{(1-\phi)}{N_B}+\frac{\phi}{N_A}-2\chi\phi(1-\phi)\right)\frac{\partial \phi}{\partial x}- \\ \frac{b^2}{18}\left(\frac{\partial^3 \phi}{\partial x^3}\right)+\frac{b^2\left(\phi(1-\phi)+(1-2\phi)^2\right)}{18\phi^2(1-\phi)^2}\left(\frac{\partial \phi}{\partial x}\right)^3\end{array}\right] \tag{A2.5}$$

$$\begin{aligned}-J = & \left(\begin{array}{l}\frac{\phi(1-\phi)N_A D_A}{N_B}+(1-\phi)^2 D_B+\phi^2 D_A+\frac{\phi(1-\phi)N_B D_B}{N_A}- \\ 2\chi\phi^2(1-\phi)N_A D_A-2\chi\phi(1-\phi)^2 N_B D_B\end{array}\right)\frac{\partial \phi}{\partial x} \\ & -\frac{b^2\phi N_A D_A}{18}\left(\frac{\partial^3 \phi}{\partial x^3}\right)-\frac{b^2(1-\phi)N_B D_B}{18}\left(\frac{\partial^3 \phi}{\partial x^3}\right)+\frac{b^2 N_A D_A\left(\phi(1-\phi)+(1-2\phi)^2\right)}{18\phi(1-\phi)^2}\left(\frac{\partial \phi}{\partial x}\right)^3 \\ & +\frac{b^2 N_B D_B\left(\phi(1-\phi)+(1-2\phi)^2\right)}{18\phi^2(1-\phi)}\left(\frac{\partial \phi}{\partial x}\right)^3\end{aligned} \tag{A2.6}$$

Using the mass balance $\frac{\partial \phi}{\partial t}+\frac{\partial J}{\partial x}=0$, the overall diffusion equation with the square-gradient modification and the fast-mode expression for mobility is given by:

$$\frac{\partial \phi}{\partial t}=-\frac{\partial J}{\partial x}=\left(\begin{array}{l}\frac{\phi(1-\phi)N_A D_A}{N_B}+(1-\phi)^2 D_B+\phi^2 D_A+\frac{\phi(1-\phi)N_B D_B}{N_A}- \\ 2\chi\phi^2(1-\phi)N_A D_A-2\chi\phi(1-\phi)^2 N_B D_B\end{array}\right)\frac{\partial^2\phi}{\partial x^2}+$$
$$\left(\begin{array}{l}\frac{(1-2\phi)N_A D_A}{N_B}-2(1-\phi)D_B+2\phi D_A+\frac{(1-2\phi)N_B D_B}{N_A}- \\ 2\chi(2\phi-3\phi^2)N_A D_A-2\chi(1-4\phi+3\phi^2)N_B D_B\end{array}\right)\left(\frac{\partial\phi}{\partial x}\right)^2-$$
$$\frac{b^2\phi N_A D_A}{18}\left(\frac{\partial^4\phi}{\partial x^4}\right)-\frac{b^2(1-\phi)N_B D_B}{18}\left(\frac{\partial^4\phi}{\partial x^4}\right)+\frac{b^2 N_A D_A\left(\phi(1-\phi)+(1-2\phi)^2\right)}{18\phi(1-\phi)^2}\left(3\left(\frac{\partial\phi}{\partial x}\right)^2\left(\frac{\partial^2\phi}{\partial x^2}\right)\right)+$$
$$\frac{b^2 N_B D_B\left(\phi(1-\phi)+(1-2\phi)^2\right)}{18\phi^2(1-\phi)}\left(3\left(\frac{\partial\phi}{\partial x}\right)^2\left(\frac{\partial^2\phi}{\partial x^2}\right)\right)-\frac{b^2 N_A D_A}{18}\left(\frac{\partial^3\phi}{\partial x^3}\right)\left(\frac{\partial\phi}{\partial x}\right)+\frac{b^2 N_B D_B}{18}\left(\frac{\partial^3\phi}{\partial x^3}\right)\left(\frac{\partial\phi}{\partial x}\right)+$$
$$\frac{b^2 N_A D_A\left(\phi(1-\phi)(-3(1-2\phi))-\left(\phi(1-\phi)+(1-2\phi)^2\right)(1-3\phi)\right)}{18\phi^2(1-\phi)^3}\left(\frac{\partial\phi}{\partial x}\right)^4+$$
$$\frac{b^2 N_B D_B\left(\phi(1-\phi)(-3(1-2\phi))-\left(\phi(1-\phi)+(1-2\phi)^2\right)(2-3\phi)\right)}{18\phi^3(1-\phi)^2}\left(\frac{\partial\phi}{\partial x}\right)^4 \qquad \text{(A2.7)}$$

For N-asymmetric, miscible systems, the square-gradient modification is unnecessary; the diffusion equation is given by:

$$\frac{\partial \phi}{\partial t}=-\frac{\partial J}{\partial x}=\left(\begin{array}{l}\frac{\phi(1-\phi)N_A D_A}{N_B}+(1-\phi)^2 D_B+\phi^2 D_A+\frac{\phi(1-\phi)N_B D_B}{N_A}- \\ 2\chi\phi^2(1-\phi)N_A D_A-2\chi\phi(1-\phi)^2 N_B D_B\end{array}\right)\frac{\partial^2\phi}{\partial x^2}+$$
$$\left(\begin{array}{l}\frac{(1-2\phi)N_A D_A}{N_B}-2(1-\phi)D_B+2\phi D_A+\frac{(1-2\phi)N_B D_B}{N_A}- \\ 2\chi(2\phi-3\phi^2)N_A D_A-2\chi(1-4\phi+3\phi^2)N_B D_B\end{array}\right)\left(\frac{\partial\phi}{\partial x}\right)^2 \qquad \text{(A2.8)}$$

For N-symmetric systems, $N_A = N_B = N$

$$\frac{\partial\phi}{\partial t} = -\frac{\partial J}{\partial x} = \left(\phi(1-\phi)\left(D_A + D_B\right) + (1-\phi)^2 D_B + \phi^2 D_A - 2N\chi\phi(1-\phi)\left(\phi D_A + (1-\phi)D_B\right)\right)\frac{\partial^2\phi}{\partial x^2} +$$
$$\left(D_A - D_B - 2\chi N\left(\left(2\phi - 3\phi^2\right)D_A + \left(1 - 4\phi + 3\phi^2\right)D_B\right)\right)\left(\frac{\partial\phi}{\partial x}\right)^2 - \frac{b^2 N\left(\phi D_A + (1-\phi)D_B\right)}{18}\left(\frac{\partial^4\phi}{\partial x^4}\right) +$$
$$\frac{b^2 N\left(D_A\phi + D_B(1-\phi)\right)\left(\phi(1-\phi) + (1-2\phi)^2\right)}{18\phi^2(1-\phi)^2}\left(3\left(\frac{\partial\phi}{\partial x}\right)^2\left(\frac{\partial^2\phi}{\partial x^2}\right)\right) - \frac{b^2 N\left(D_A - D_B\right)}{18}\left(\frac{\partial^3\phi}{\partial x^3}\right)\left(\frac{\partial\phi}{\partial x}\right) +$$
$$\frac{b^2 N D_A\left(\phi(1-\phi)\left(-3(1-2\phi)\right) - \left(\phi(1-\phi) + (1-2\phi)^2\right)(1-3\phi)\right)}{18\phi^2(1-\phi)^3}\left(\frac{\partial\phi}{\partial x}\right)^4 +$$
$$\frac{b^2 N D_B\left(\phi(1-\phi)\left(-3(1-2\phi)\right) - \left(\phi(1-\phi) + (1-2\phi)^2\right)(2-3\phi)\right)}{18\phi^3(1-\phi)^2}\left(\frac{\partial\phi}{\partial x}\right)^4 \qquad \text{(A2.9)}$$

Assuming $D_A \sim D_B$, the previous expression simplifies to:

$$\frac{\partial\phi}{\partial t} = -\frac{\partial J}{\partial x} = \left(\phi(1-\phi)(2D_0) + D_0 - 2N\chi\phi(1-\phi)(D_0)\right)\frac{\partial^2\phi}{\partial x^2} +$$
$$\left(-2\chi N\left((1-2\phi)D_0\right)\right)\left(\frac{\partial\phi}{\partial x}\right)^2 - \frac{b^2 N(D_0)}{18}\left(\frac{\partial^4\phi}{\partial x^4}\right) +$$
$$\frac{b^2 N(D_0)\left(\phi(1-\phi) + (1-2\phi)^2\right)}{18\phi^2(1-\phi)^2}\left(3\left(\frac{\partial\phi}{\partial x}\right)^2\left(\frac{\partial^2\phi}{\partial x^2}\right)\right) + \qquad \text{(A2.10)}$$
$$\frac{b^2 N D_0\left(\phi(1-\phi)\left(-3(1-2\phi)\right) - \left(\phi(1-\phi) + (1-2\phi)^2\right)(1-3\phi)\right)}{18\phi^2(1-\phi)^3}\left(\frac{\partial\phi}{\partial x}\right)^4 +$$
$$\frac{b^2 N D_0\left(\phi(1-\phi)\left(-3(1-2\phi)\right) - \left(\phi(1-\phi) + (1-2\phi)^2\right)(2-3\phi)\right)}{18\phi^3(1-\phi)^2}\left(\frac{\partial\phi}{\partial x}\right)^4$$

For N-symmetric, miscible systems, the expression further reduces to:

$$\frac{\partial\phi}{\partial t} = -\frac{\partial J}{\partial x} = \left(\phi(1-\phi)(2D_0) + D_0 - 2N\chi\phi(1-\phi)(D_0)\right)\frac{\partial^2\phi}{\partial x^2} +$$
$$\left(-2\chi N\left((1-2\phi)D_0\right)\right)\left(\frac{\partial\phi}{\partial x}\right)^2 \qquad \text{(A2.11)}$$

APPENDIX 3

MATLAB PROGRAMS USED TO MODEL INTERDIFFUSION

This is an example of the full model for N-asymmetric systems using the fast-mode expression for mobility and including the square-gradient modification. The input parameters are the tracer diffusion coefficients and respective degrees of polymerization, total thickness of the bilayer, temperature (T), composition of the copolymer (f), and statistical segment length (a). All simulations were performed in Matlab.

```
clear
clc

DA = 7e-18;
DB = 4e-16;
L = 0.92e-6;
DPA = 7670;
DPB = 424;
T = 473.15;
f = 0.22;
chi = f^2*(-.0833+73.75/T);
N = 500;
delx = 1/N;
a = 7.4e-10;

[T,y]=ode15s('NASGfullcode',[],[],[],DA,DB,L,DPA,DPB,T,chi,N,a,delx);
```

```
function varargout = NASGfullcode(t,y,flag,DA,DB,L,DPA,DPB,T,chi,N,a,delx)
%
switch flag
case ''                          % Return dy/dt = f(t,y).
  varargout{1} = f(t,y,DA,DB,L,DPA,DPB,T,chi,N,a,delx);
case 'init'                      % Return default [tspan,y0,options].
  [varargout{1:3}] = init(N);
%case 'jacobian'                 % Return Jacobian matrix df/dy.
%  varargout{1} = jacobian(t,y,p1,p2);
%case 'jpattern'                 % Return sparsity pattern matrix S.
%  varargout{1} = jpattern(t,y,p1,p2);
%case 'mass   '                  % Return mass matrix.
%  varargout{1} = mass(t,y,p1,p2);
%case 'events'                   % Return [value,isterminal,direction].
%  [varargout{1:3}] = events(t,y,p1,p2);
```

```
%otherwise
%  error(['Unknown flag ''' flag '''.']);
end
%
%% ------------------------------------------------------------------------
%
function dydt = f(t,y,DA,DB,L,DPA,DPB,T,chi,N,a,delx)

dydt = zeros(N,size(y,2));

i = 1;
dydt(i,:) = 1/L^2*((y(i,:).*DPA*DA+(1-y(i,:)).*DPB*DB).*(y(i,:)./DPA+(1-y(i,:))./DPB...
   -2*chi.*y(i,:).*(1-y(i,:))).*...
   (y(i+1,:)-y(i,:))./(delx^2)...
   +(2.*y(i,:).*DA-2.*(1-y(i,:)).*DB+DPA*DA.*(1-2.*y(i,:))./DPB+DPB*DB.*(1-
2.*y(i,:))./DPA...
   +2*chi.*y(i,:).*(3.*y(i,:)-2).*DPA*DA+2*chi.*(1-y(i,:)).*(3.*y(i,:)-1).*DPB*DB).*...
   ((y(i+1,:)-y(i,:))./(2*delx)).^2)...
   -a^2/(18*L^4).*((y(i,:).*DPA*DA+(1-y(i,:)).*DPB*DB).*...
   (y(i+2,:)-4.*y(i+1,:)+3.*y(i,:))./(delx^4)...
   -(DPB*DB-DPA*DA).*...
   (y(i+1,:)-y(i,:))./(2*delx).*...
   (y(i+2,:)-2.*y(i+1,:)+y(i,:))./(2*delx^3)...
  -(DPA*DA.*(3.*y(i,:).^3-3.*y(i,:).^2+y(i,:))+...
   DPB*DB.*(-3.*y(i,:).^3+6.*y(i,:).^2-4.*y(i,:)+1))./((y(i,:).*(1-y(i,:))).^2).*...
   ((y(i+1,:)-y(i,:))./(delx^2)).*...
   ((y(i+1,:)-y(i,:))./(2*delx)).^2 ...
   -(DPB*DB.*(-3.*y(i,:).^4+9.*y(i,:).^3-12.*y(i,:).^2+8.*y(i,:)-2)+...
   DPA*DA.*(3.*y(i,:).^4-3.*y(i,:).^3+3.*y(i,:).^2-y(i,:)))./((y(i,:).*(1-y(i,:))).^3).*...
   ((y(i+1,:)-y(i,:))./(2.*delx)).^4);

i = 2;
dydt(i,:) = 1/L^2*((y(i,:).*DPA*DA+(1-y(i,:)).*DPB*DB).*(y(i,:)./DPA+(1-y(i,:))./DPB...
   -2*chi.*y(i,:).*(1-y(i,:))).*...
   (y(i+1,:)-2.*y(i,:)+y(i-1,:))./(delx^2)...
   +(2.*y(i,:).*DA-2.*(1-y(i,:)).*DB+DPA*DA.*(1-2.*y(i,:))./DPB+DPB*DB.*(1-
2.*y(i,:))./DPA...
   +2*chi.*y(i,:).*(3.*y(i,:)-2).*DPA*DA+2*chi.*(1-y(i,:)).*(3.*y(i,:)-1).*DPB*DB).*...
   ((y(i+1,:)-y(i-1,:))./(2*delx)).^2)...
   -a^2/(18*L^4).*((y(i,:).*DPA*DA+(1-y(i,:)).*DPB*DB).*...
   (y(i+2,:)-4.*y(i+1,:)+6.*y(i,:)-3.*y(i-1,:))./(delx^4)...
   -(DPB*DB-DPA*DA).*...
   (y(i+1,:)-y(i-1,:))./(2*delx).*...
   (y(i+2,:)-2.*y(i+1,:)+y(i-1,:))./(2*delx^3)...
   -(DPA*DA.*(3.*y(i,:).^3-3.*y(i,:).^2+y(i,:))+...
```

```
   DPB*DB.*(-3.*y(i,:).^3+6.*y(i,:).^2-4.*y(i,:)+1))./((y(i,:).*(1-y(i,:))).^2).*...
   ((y(i+1,:)-2.*y(i,:)+y(i-1,:))./(delx^2)).*...
   ((y(i+1,:)-y(i-1,:))./(2*delx)).^2 ...
   -(DPB*DB.*(-3.*y(i,:).^4+9.*y(i,:).^3-12.*y(i,:).^2+8.*y(i,:)-2)+...
   DPA*DA.*(3.*y(i,:).^4-3.*y(i,:).^3+3.*y(i,:).^2-y(i,:)))./((y(i,:).*(1-y(i,:))).^3).*...
   ((y(i+1,:)-y(i-1,:))./(2*delx)).^4);

i = 3:N-2;
dydt(i,:) = 1/L^2*((y(i,:).*DPA*DA+(1-y(i,:)).*DPB*DB).*(y(i,:)./DPA+(1-y(i,:))./DPB...
   -2*chi.*y(i,:).*(1-y(i,:))).*...
   (y(i+1,:)-2.*y(i,:)+y(i-1,:))./(delx^2)...
   +(2.*y(i,:).*DA-2.*(1-y(i,:)).*DB+DPA*DA.*(1-2.*y(i,:))./DPB+DPB*DB.*(1-
2.*y(i,:))./DPA...
   +2*chi.*y(i,:).*(3.*y(i,:)-2).*DPA*DA+2*chi.*(1-y(i,:)).*(3.*y(i,:)-1).*DPB*DB).*...
   ((y(i+1,:)-y(i-1,:))./(2*delx)).^2)...
   -a^2/(18*L^4).*((y(i,:).*DPA*DA+(1-y(i,:)).*DPB*DB).*...
   (y(i+2,:)-4.*y(i+1,:)+6.*y(i,:)-4.*y(i-1,:)+y(i-2,:))./(delx^4)...
   -(DPB*DB-DPA*DA).*...
   (y(i+1,:)-y(i-1,:))./(2*delx).*...
   (y(i+2,:)-2.*y(i+1,:)+2.*y(i-1,:)-y(i-2,:))./(2*delx^3)...
   -(DPA*DA.*(3.*y(i,:).^3-3.*y(i,:).^2+y(i,:))+...
   DPB*DB.*(-3.*y(i,:).^3+6.*y(i,:).^2-4.*y(i,:)+1))./((y(i,:).*(1-y(i,:))).^2).*...
   ((y(i+1,:)-2.*y(i,:)+y(i-1,:))./(delx^2)).*...
   ((y(i+1,:)-y(i-1,:))./(2*delx)).^2 ...
   -(DPB*DB.*(-3.*y(i,:).^4+9.*y(i,:).^3-12.*y(i,:).^2+8.*y(i,:)-2)+...
   DPA*DA.*(3.*y(i,:).^4-3.*y(i,:).^3+3.*y(i,:).^2-y(i,:)))./((y(i,:).*(1-y(i,:))).^3).*...
   ((y(i+1,:)-y(i-1,:))./(2*delx)).^4);

i = N-1;
dydt(i,:) = 1/L^2*((y(i,:).*DPA*DA+(1-y(i,:)).*DPB*DB).*(y(i,:)./DPA+(1-y(i,:))./DPB...
   -2*chi.*y(i,:).*(1-y(i,:))).*...
   (y(i+1,:)-2.*y(i,:)+y(i-1,:))./(delx^2)...
   +(2.*y(i,:).*DA-2.*(1-y(i,:)).*DB+DPA*DA.*(1-2.*y(i,:))./DPB+DPB*DB.*(1-
2.*y(i,:))./DPA...
   +2*chi.*y(i,:).*(3.*y(i,:)-2).*DPA*DA+2*chi.*(1-y(i,:)).*(3.*y(i,:)-1).*DPB*DB).*...
   ((y(i+1,:)-y(i-1,:))./(2*delx)).^2)...
   -a^2/(18*L^4).*((y(i,:).*DPA*DA+(1-y(i,:)).*DPB*DB).*...
   (-3.*y(i+1,:)+6.*y(i,:)-4.*y(i-1,:)+y(i-2,:))./(delx^4)...
   -(DPB*DB-DPA*DA).*...
   (y(i+1,:)-y(i-1))./(2*delx).*...
   (-y(i+1,:)+2.*y(i-1,:)-y(i-2,:))./(2*delx^3)...
   -(DPA*DA.*(3.*y(i,:).^3-3.*y(i,:).^2+y(i,:))+...
   DPB*DB.*(-3.*y(i,:).^3+6.*y(i,:).^2-4.*y(i,:)+1))./((y(i,:).*(1-y(i,:))).^2).*...
   ((y(i+1,:)-2.*y(i,:)+y(i-1,:))./(delx^2)).*...
   ((y(i+1,:)-y(i-1,:))./(2*delx)).^2 ...
```

```
   -(DPB*DB.*(-3.*y(i,:).^4+9.*y(i,:).^3-12.*y(i,:).^2+8.*y(i,:)-2)+...
   DPA*DA.*(3.*y(i,:).^4-3.*y(i,:).^3+3.*y(i,:).^2-y(i,:)))./((y(i,:).*(1-y(i,:))).^3).*...
   ((y(i+1,:)-y(i-1,:))./(2*delx)).^4);

i = N;
dydt(i,:) = 1/L^2*((y(i,:).*DPA*DA+(1-y(i,:)).*DPB*DB).*(y(i,:)./DPA+(1-y(i,:))./DPB...
   -2*chi.*y(i,:).*(1-y(i,:))).*...
   (-y(i,:)+y(i-1,:))./(delx^2)...
   +(2.*y(i,:).*DA-2.*(1-y(i,:)).*DB+DPA*DA.*(1-2.*y(i,:))./DPB+DPB*DB.*(1-
2.*y(i,:))./DPA...
   +2*chi.*y(i,:).*(3.*y(i,:)-2).*DPA*DA+2*chi.*(1-y(i,:)).*(3.*y(i,:)-1).*DPB*DB).*...
   ((y(i,:)-y(i-1,:))./(2*delx)).^2)...
  -a^2/(18*L^4).*((y(i,:).*DPA*DA+(1-y(i,:)).*DPB*DB).*...
   (3.*y(i,:)-4.*y(i-1,:)+y(i-2,:))./(delx^4)...
   -(DPB*DB-DPA*DA).*...
   (-y(i-1,:)+y(i,:))./(2*delx).*...
   (-y(i,:)+2.*y(i-1,:)-y(i-2,:))./(2*delx^3)...
   -(DPA*DA.*(3.*y(i,:).^3-3.*y(i,:).^2+y(i,:))+...
   DPB*DB.*(-3.*y(i,:).^3+6.*y(i,:).^2-4.*y(i,:)+1))./((y(i,:).*(1-y(i,:))).^2).*...
   ((-y(i,:)+y(i-1,:))./(delx^2)).*...
   ((y(i,:)-y(i-1,:))./(2*delx)).^2 ...
   -(DPB*DB.*(-3.*y(i,:).^4+9.*y(i,:).^3-12.*y(i,:).^2+8.*y(i,:)-2)+...
   DPA*DA.*(3.*y(i,:).^4-3.*y(i,:).^3+3.*y(i,:).^2-y(i,:)))./((y(i,:).*(1-y(i,:))).^3).*...
   ((y(i,:)-y(i-1,:))./(2*delx)).^4);


%% ------------------------------------------------------------------------
%
function [tspan,y0,options] = init(N)
tspan = [0,10];
y0 = [ones(250,1)*0.9999; ones(250,1)*0.0001];
options = odeset('reltol',.09,'abstol',.05);
%
```

VITA

NAME OF AUTHOR: Erin Lynne Jablonski

DATE AND PLACE OF BIRTH: July 31, 1979, Ft. Leonardwood, MO.

DEGREES AWARDED:

- Ph.D. in Chemical Engineering, Iowa State University, 2002
- M.S. in Chemical Engineering, Rutgers, the State University of New Jersey, 2001
- B.S. in Chemical Engineering, Biochemical Engineering Option, Rutgers, the State University of New Jersey, 1999

HONORS AND AWARDS:

- National Research Council Research Associateship Program, 2002
- National Science Foundation Graduate Research Fellowship, 1999-2002
- Invited to the U.S. X-Ray and Neutron Scattering School, Argonne National Laboratory, 2000

PROFESSIONAL EXPERIENCE:

- Research Assistant, Department of Chemical and Biochemical Engineering, Rutgers, the State University of New Jersey, 1997-1999
- Research Fellow, Department of Chemical and Biochemical Engineering, Rutgers, the State University of New Jersey, 1999-2000
- Research Fellow, Department of Chemical Engineering, Iowa State University, 2001-2002
- Instructor, Topics in Engineering, Office of Precollegiate Programs for Talented and Gifted, Iowa State University, 2002
- Faculty Intern, Transport Phenomena I, Department of Chemical Engineering, Iowa State University, 2001

PROFESSIONAL PUBLICATIONS:

- R.E. Gorga, E.L. Jablonski, P. Thiyagarajan, S. Seifert, and B. Narasimhan, "Quantifying Phase Behavior in Partially Miscible Polystyrene and Poly (styrene-co-4-bromostyrene) blends" (J. Polymer Science: Part B: Polymer Physics, 2002, 40, p. 255-271).
- E.L. Jablonski, R.E. Gorga, and B. Narasimhan, "Interdiffusion and Phase Behavior at Homopolymer/Random Copolymer Interfaces" (submitted to Polymer, 2002).
- E. L. Jablonski and B. Narasimhan, "Interdiffusion in Partially Miscible Polymer Bilayers: Effect of Film Thickness and Polydispersity" (submitted to Macromolecules, 2002).
- E.L. Jablonski and B. Narasimhan, "Quantifying Interfacial Width at Partially Miscible Polystyrene and Poly (styrene-co-4-bromostyrene) Interfaces" (in preparation).